Asynchronous Magnetic Bead Rotation (AMBR) Microfluidic Biosensor Platform for Rapid Microbial Growth and Susceptibility Studies

by

Irene Sinn

A dissertation submitted in partial fulfillment
of the requirements for the degree of
Doctor of Philosophy
(Biomedical Engineering)
in The University of Michigan
2012

Doctoral Committee:

Professor Raoul Kopelman, Co-Chair
Professor Mark A. Burns, Co-Chair
Professor Joseph L. Bull
Professor Nina Lin
Professor Shuichi Takayama

2012

For the Sinn Family
[Mom, Dad, Robin, Phoebe, Pig (Doots), Bobo, and Rakey]

Table of Contents

LIST OF FIGURES

ABSTRACT

The emergence and spread of antimicrobial resistance is one of the world's most pressing health problems. The methicillin-resistant *S. aureus* (MRSA) kills more Americans (approximately 19,000 persons) annually than emphysema, HIV/AID, Parkinson's and homicide combined. To address this concern, antimicrobial susceptibility tests (AST) that can more rapidly determine the antibiotic susceptibility of infectious organisms are being developed, enabling prompt and most appropriate therapies. In this dissertation, we present an asynchronous magnetic bead rotation (AMBR) droplet microfluidic platform that can measure the growth of a single or small population of bacteria and rapidly determine the minimum inhibitory concentration (MIC) of antibiotics.

By compartmentalizing individual 2–20 μm magnetic beads in 1 nL aqueous droplets, we enhance the sensitivity and parallelization capabilities of the AMBR system. When placed within a rotating magnetic field, at driving field frequencies above the critical frequency (20–800 Hz), the AMBR sensor rotates asynchronously. The rotational rate of the sensor provides insight into the system's physical (e.g. shape and volume) and environmental (e.g. viscosity) properties. With this platform, we monitored the growth of individual bacteria by measuring the elongation (e.g. 80 $\pm$ 38 nm length change) of *E. coli*, corresponding to the sensor volumetric change of 0.1 μm^3. By increasing the bead

size and modifying its surface functionalization, we measured the growth of a small population of *E. coli* within an order of magnitude of a single division time.

For AST applications, we applied three approaches: (1) volumetric single bacterium approach, (2) volumetric small population approach, and (3) viscosity based small population approach. Bacteria were treated with ampicillin or gentamicin, at concentrations above and below the reported MIC values, and we were able to differentiate between growing and non-growing *E. coli* within 100 minutes. We envision that this platform may reduce the turnaround time for AST by 80 % when compared to commercial systems, which take an average of 6 hours for *E. coli*. Development of more rapid AST system can improve patient lives, reduce the use of wide-spectrum antibiotics and slow the spread of antimicrobial resistance.

CHAPTER 1:

Introduction

1.1 Project Overview

The integration of magnetic beads and microfluidics has introduced a new avenue of analysis for biomedical applications. The ability to functionalize, manipulate, and detect magnetic beads and the high-throughput, low-volumes, and fast-reaction times of microfluidics make magnetic bead microfluidic systems increasingly powerful biosensing tools.[1,2] In this dissertation, we present a novel microfluidic biosensor platform that uses a sensitive asynchronous magnetic bead rotation (AMBR) biosensor to monitor microbial cell growth. We demonstrate proof-of-concept studies and the feasibility of the platform system for rapid microbial growth studies, specifically towards antimicrobial susceptibility testing applications.

1.1.1 AMBR Microfluidic Droplet Platform

The time-dependent rotational response of the AMBR biosensor provides information regarding the environmental conditions (e.g. viscosity) surrounding the magnetic bead, the physical properties of the bead (e.g. magnetic moment, bead complex shape, and bead complex volume), and external magnetic field properties (e.g. magnetic field strength and field frequency).[3,4] The AMBR biosensor has been demonstrated to be extremely sensitive towards system changes; as a result, for biosensing applications, it is

imperative that the incidence of false positives, such as inherent time-dependent responses in the system, is negligible. To address this concern, individual AMBR biosensors are compartmentalized within individual nanoliter water-in-oil droplets and arrayed within a microfluidic chamber. The subsequent AMBR microfluidic biosensor platform is, therefore, a highly sensitive biosensing platform that can be applied towards real-time, long-term studies, and with higher-throughputs.[5] We apply this platform towards microbial growth studies, specifically for antimicrobial susceptibility testing; however, the versatility of the AMBR microfluidic platform may allow it to be extended towards a variety of biomedical and biosensing applications.

1.1.2 Application for Antimicrobial Susceptibility Testing (AST)

The U.S. Centers for Disease Control and Prevention (CDC) calls antibiotic resistance one of its "top concerns" and "one of the world's most pressing health problems."[6] Nearly 2 million patients in the United States develop hospital-acquired bacterial infections each year, with approximately 90,000 of these infections resulting in death.[7] Furthermore, 70% of these bacterial infections are caused by bacteria resistant to at least one of the commonly used antibiotics.[7] Infections from resistant organisms are linked to increased mortality rates.[8] Patients infected with MRSA (methicillin-resistant *Staphylococcus aureus*) were reported to have almost a 100% increase in mortality as compared with patients infected with MSSA (methicillin-susceptible *S. aureus*).[9] In fact, MRSA alone causes more deaths in the US than AIDS/HIV.[10,11] An effective way to limit the emergence and spread of antimicrobial resistance is through accurate diagnosis and rapid treatment of the offending pathogen.[6] Faster diagnostic tests can reduce inappropriate antibiotic use,[12] health care costs,[9] prevalence of antimicrobial resistance,

[9,13,14] as well as mortality rates. In addition to the health burden, infections caused by antibiotic resistant bacteria are responsible for nearly $20 billion per year in excess healthcare costs, $35 billion in societal costs and $8 billion in additional hospital days in the US.[6] Antibiotic resistance and susceptibility are, of course, two sides of the same coin. The combination of the emergence and spread of antimicrobial resistance, the limited availability of new antibiotics, and the longer patient hospitalization times, has been described as a "perfect storm."[15] Rapid detection of resistance, so that proper therapy can be initiated earlier, is extremely important in tackling this worldwide problem. New innovative approaches aimed at reducing the time to determine antimicrobial resistance are needed.

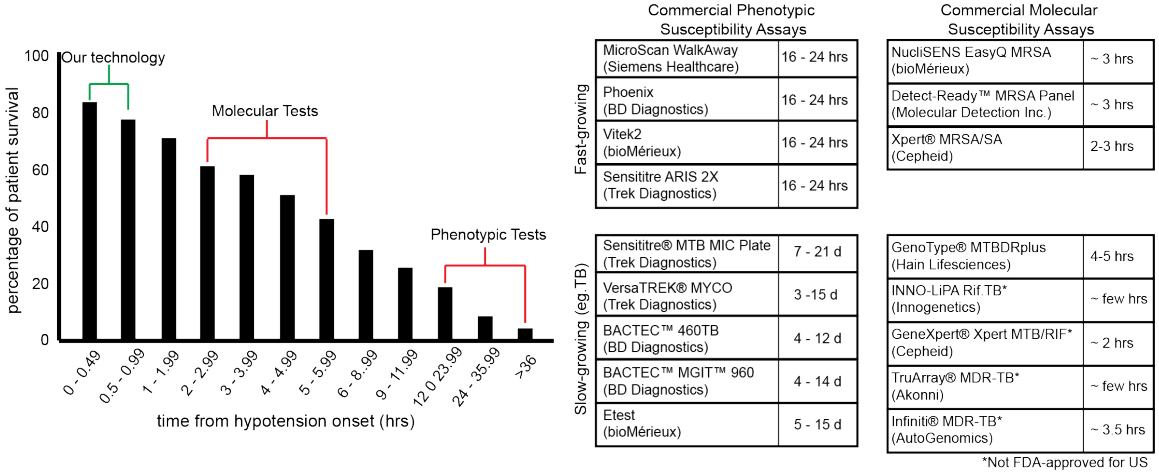

Figure 1-1. Patient survival percentage upon initiation of antibiotics treatment, following onset of septic-shock associated hypotension.[16] [Right] Current commercial phenotypic and molecular susceptibility assay systems with their corresponding turnaround time (TAT). The corresponding survival rate for each assay's TAT is shown on graph. Compared to phenotypic and molecular tests, our technology has the potential to provide results in a time frame where initiation of appropriate antibiotics will have the greatest impact on survival. Molecular methods cannot determine a "MIC" value, and thus are not useful towards detecting new mutants and resistant organisms.

Clinical antimicrobial susceptibility testing (AST) to determine the *minimum inhibitory concentration* (MIC) of antibiotics currently takes up to 24 hours for fast

growing bacteria and up to 14 days for slow growing bacteria (e.g. *Mycobacterium tuberculosis).*[17–19] As management of bacterial infections is highly time-sensitive, patients are prescribed empiric therapies.[14] Ineffective therapies result not only in delays of appropriate treatment, but also contribute to the development of antimicrobial resistance. Studies report that a delay in appropriate antibiotic administration corresponds with significant incremental increases in fatality rate.[16,20] In particular, for septic-shock patients, *each hour* of delay in effective antimicrobial treatment was associated with an average decrease in survival of 7.6% [Figure 1-1].[16] Bacterial meningitis patients have a 740% increased risk of death when antibiotic administration is delayed by just 6 hours.[19] There is still a lack of rapid, effective diagnostic tests to identify the infecting agents and determine the corresponding antimicrobial susceptibilities.[21] Through the improvement and development of sensitive growth-based AST methods, bacterial resistance to antibiotics would be more rapidly detected,[22] which may enable patients to receive appropriate and effective therapies more quickly.[12] Making order-of-magnitude faster methods available, new workflows may emerge and replace the current system in which patient samples are batched for processing; this may consequently improve further the efficiency of the AST and thus the treatment process.

Commercial automated AST systems can now determine the MIC values of a *fast-growing* bacterial species within 6 – 24 hours.[22,23] It has been suggested that faster AST results may be achieved through the development of new approaches to detect bacterial proliferation, such as by improving optical detection.[22] We have developed a rapid, off-microscope, asynchronous magnetorotation-based microfluidic platform that reduces the turnaround time for fast-growing bacteria by 80 %. We anticipate that the platform is

faster than standard systems that require long incubation times (at least 6 hours) in order to culture a sufficiently large population of bacteria for their resistance to be detected. In contrast, the AMBR platform developed, as described in subsequent chapters, was able to detect growth within minutes to hours, with a nanoliter-scale culture (nL culture).[24] In fact, the growth of nL culture may be measured within a fraction of a bacterial division cycle (i.e. on the order of minutes for uropathogenic *E. coli*), when the sensitivity of the sensor was enhanced by modifying bead size.[24] This large reduction in AST time will have the greatest impact for *slow-growing* bacteria, such as *Mycobacterium tuberculosis*, which traditionally can take 14 days to detect resistance.[17,18] As a result, considering a TB doubling time of 24 hours,[25] our magnetorotation microfluidic platform may reduce the time to detect TB growth to 9-12 hours. We note that the magnetorotation sensor is based on measuring changes in a magnetic bead's rotational period upon a change in the bead's environment, such as bacterial cell growth events.[24,26] As the magnetic bead's rotation can be monitored without a microscope,[24,27] this simplicity will keep down costs, as well as improving patient care and public health.

Aside from the automation of the antimicrobial susceptibility testing (AST) process, there had previously been few technical developments towards improving AST methods. Analysis had been based on simple optical measurements by measuring the absorbance/transmission of bacterial suspension, e.g. bacteria scatter more and more light as they multiply. In these systems, specimen collection, pathogen isolation and AST analysis takes well over 24 hours, even for fast growing bacteria [Figure 1-2]. Towards addressing this problem, in order to reduce the AST time, we integrated the AMBR biosensor with microfluidics to create a robust, sensitive platform.[3,5,24,28] AMBR is also

highly sensitive to the growth of a bacterial nanoliter (nL) culture.[5,29] This high sensitivity results from the ability to detect small time changes in volumetric growth and/or viscosity, changes that are associated with bacterial growth. An effective antibiotic inhibits growth, of course. Using this technology, we have built a simple and robust prototype using off-the-shelf electronic components. The AMBR can be performed using any magnetic microparticles or nanoparticles, whether commercial or fabricated in-house, which makes the platform extremely versatile.

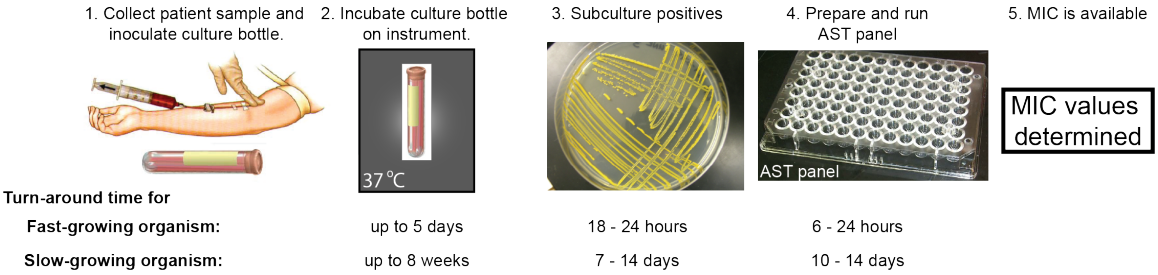

Figure 1-2. Flow chart of antimicrobial susceptibility testing (AST) procedure and corresponding turn-around time (TAT) for fast-growing and slow-growing organisms. (1) Patient sample is obtained and inoculated into a culture bottle. (2) The culture bottle is incubated on an instrument. (3) Upon a positive result, the sample is subcultured to obtain pure isolates. (4) The isolate is loaded onto the AST test panel and the panel is run on a commercial AST system, and (5) the MIC values are available upon test completion.

Presently, there are 4 automated AST instruments in clinical use within the US that generate AST results within 6 - 24 hrs.[22,23] These systems measure bacterial growth through turbidometric or colorimetric readings. The main limiting factor of these commercial systems is the need to culture large concentrations of bacteria for a sufficiently long time in order to detect antibiotic effects on bacterial growth. In contrast, we report on a technique that can measure bacterial growth within a bacteria's doubling time – Chapter 2.[5,24,29] Resulting from this sensitive detection method is the order of magnitude reduction in the culturing time, and therefore AST time; the impact of this is potentially most significant for slower growing bacteria.

1.2 Asynchronous Magnetic Bead Rotation (AMBR) Sensors

1.2.1 History

Magnetic particles are increasingly used in biomedical applications, as life science and clinical tools. Their widespread use stems from the ability to functionalize magnetic particles and subsequently manipulate these particles without disturbing the sample with an external magnetic field. As a result, magnetic particles have naturally found use in biomolecule/analyte target and detection, sample enrichment, and micro mixing, in addition to, a plethora of other bioapplications.[30] Recently, the emergence of an asynchronous magnetic bead rotation (AMBR) biosensor extends upon these magnetic particle capabilities, imparting on the ability to not only manipulate the magnetic particle, as described previously, but also utilize the magnetic particle as the biosensor system.

1.2.2 AMBR Rotational Theory

The AMBR biosensor can be comprised of either a ferromagnetic or superparamagnetic particle; these magnetic properties govern the underlying rotational response of the sensor. As a result, it is important to identify whether the AMBR biosensor behaves ferromagnetically or superparamagnetically when torqued (i.e. rotated) by an externally rotating magnetic field.

Traditionally, ferromagnetic materials are defined as materials that retain a permanent magnetic moment when an external magnetic field is removed (e.g. kitchen magnets). In contrast, superparamagnetic materials are defined as materials that do not retain a magnetic moment when an external magnetic field is removed; in fact, superparamagnetic materials are considered to have an induced magnetic moment, possessing a magnetic moment only when an external field is present. This traditional

definition of ferromagnetism and superparamagnetism is widely accepted, and helps define commercially available magnetic particles: upon magnetic field removal, ferromagnetic particles remain aggregated and superparamagnetic particles disperse. It is important to note that the magnetic behavior (i.e. dispersal) has a time-scale factor, as the magnetism of a material is dependent on the time required for a magnet to lose its magnetic dipole, which is known as the relaxation time. Therefore, in actuality, whether a magnetic particle is considered to be ferromagnetic or superparamagnetic depends on an understanding of the time-scale factor (i.e. the relationship between the instrument measurement time and the relaxation time).

The magnetic moment and magnetic dipole of superparamagnetic particles decay to zero magnetization when the external magnetic field is removed. The time required for the magnetic particle to have no magnetization is dependent on the magnetic material and its magnetization. The accepted time-scale that is used to differentiate between commercial superparamagnetic or ferromagnetic particles is generally on the order of 100 s.[30] The traditional method to determine ferromagnetism or superparamagnetism is to generate a hysteresis loop with a superconducting quantum interfering device (SQUID). The presence of an open hysteresis loop suggests that the material is ferromagnetic and a closed hysteresis loop suggests that the material is superparamagnetic [Figure 1-3].

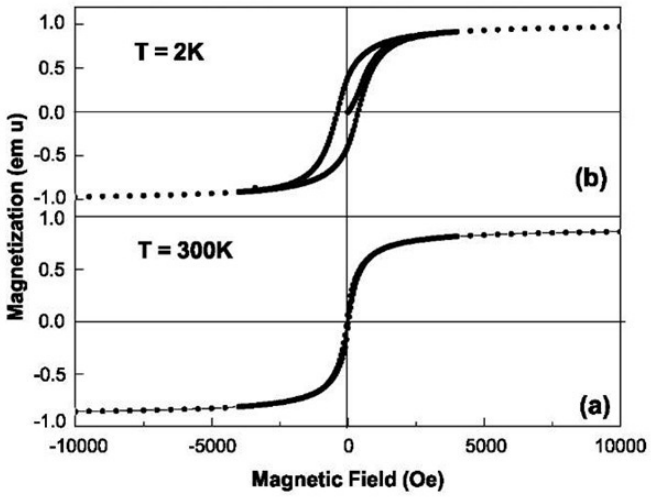

Figure 1-3. Hysteresis loop of a ferromagnetic (top) and superparamagnetic (bottom) material.[31]

With the presented AMBR, a constant rotating magnetic field is applied on the particle and a torque is continuously exerted on a magnetic bead. In this case, the time-scale of measurement is smaller than the relaxation time of commercially available superparamagnetic and ferromagnetic magnetic particles; as a result, both bead types rotate within an externally rotating magnetic field. However, as mentioned previously, the magnetic particle's underlying rotational behavior is unique to its magnetism. To identify its behavior, it is necessary to measure the frequency-dependent rotational behavior of the bead.

Permanent-Dipole (Ferromagnetic) Rotational Response

At driving frequencies for which the permanent dipole dominates (i.e. ferromagnetic beads), the rotational equation can be expressed by,

$$\langle \dot{\theta} \rangle = \begin{cases} \Omega & \Omega < \Omega_c \\ \Omega - \sqrt{\Omega^2 - \Omega_c^2}; & \Omega > \Omega_c \end{cases}, \qquad [1\text{-}1]$$

where $\langle\dot{\theta}\rangle$ is the average rotational frequency of the bead, Ω is the external magnetic field driving frequency, and Ω_c is the critical external driving frequency.[3,32,33] At driving frequencies below the critical frequency, $\Omega < \Omega_c$, the magnetic particle's rotational rate is linearly dependent on the external field frequency. At driving frequencies above the critical frequency, $\Omega > \Omega_c$, the particle rotates asynchronously with the external field frequency. Within the asynchronous regime, the AMBR system can function as a biosensor, as information about the magnetic bead complex and its external environment can be deduced from the bead's rotation. For a given particle's rotation, at a constant driving field frequency, the critical frequency can be determined by

$$\Omega_c = \sqrt{\Omega^2 - \left(\Omega - \langle\dot{\theta}\rangle\right)^2}. \quad [1\text{-}2]$$

The critical frequency is defined as,

$$\Omega_c = \frac{mB}{\kappa\eta V} \quad [1\text{-}3]$$

where *m* is the magnetic moment of the bead, *B* is the magnetic field amplitude, κ is the shape factor, η is the dynamic viscosity, and *V* is the volume of the bead complex.[3,33] As a result, by keeping certain parameters constant, it is possible to extrapolate field, magnetic particle, or environmental information from a ferromagnetic bead's rotation.

Induced-Dipole (Superparamagnetic) Rotational Response

At driving frequencies for which the induced-dipole dominates (i.e. superparamagnetic beads), the simplified version of the rotational equation can be expressed by

$$\dot{\theta}_{SPM} = \frac{\chi'' V_m B^2}{\kappa\eta V \mu_0}, \quad [1\text{-}4]$$

where χ'' is the total imaginary susceptibility of the bead, V_m is the volume of the magnetic content of the bead, B is the magnetic field amplitude, κ is the shape factor, η is dynamic viscosity, μ_0 is the permeability of free space, and V is the volume of the bead complex.[24,28,30] In contrast to the beads whose rotation is governed by its permanent dipole, the frequency dependent rotational response for beads governed by its induced dipole is not as pronounced. This results from the fact that the frequency-dependence is a factor of the imaginary susceptibility term. Using **Equation 1-4**, it is possible to extract information regarding the field, bead, and environmental properties from the rotation of superparamagnetic beads.

1.2.3 Applications

As illustrated in the previous section, a magnetic bead's rotation is dependent on the following factors: m (magnetic moment), B (magnetic field amplitude), κ (shape factor), η (dynamic viscosity), and V (volume of the bead complex). As a result, we can apply the AMBR sensor for probing or biosensing assay applications by monitoring changes to these listed parameters.

Viscometer

By measuring the rotational rate of the AMBR sensor in solution, the viscosity can be calculated with the following equations,

$$\eta = \frac{mB}{\kappa V \Omega_c} \text{ [permanent dipole] OR } \eta = \frac{\chi'' V_m B^2}{\kappa V \mu_0 \dot{\theta}_{SPM}} \text{ [induced dipole],}^{4,29} \qquad [1\text{-}5]$$

assuming the magnetic field strength and the physical and magnetic properties of the particle are known. Until recently, see Chapter 5, absolute viscosity measurements were unable to be determined because of the inherent heterogeneity of commercial magnetic particles, and hence, variability in magnetic moment. As a result, applications of the

AMBR sensor as a viscometer have been limited to measuring relative changes in viscosity. McNaughton et al. (2007) demonstrated proof-of-concept studies indicating the potential of the AMBR viscometer by accurately monitoring the temperature-dependent viscosity changes of a 90% glycerol solution.[4] As the temperature increased, the measured rotational rate increased, which corresponds with a decrease in the suspension viscosity [Figure 1-4].[4]

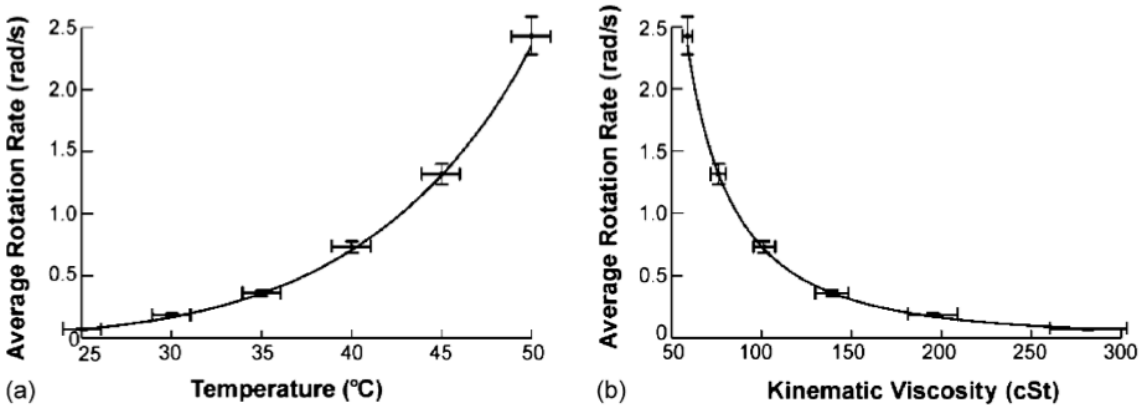

Figure 1-4. (a) Temperature-dependent, and (b) corresponding viscosity-dependent rotational response of the AMBR biosensor in a 90% glycerin solution.[4]

Analyte Detection

The AMBR biosensor can be extended towards analyte detection applications, by taking advantage of the sensor's rotational-rate dependence on volumetric, shape, and magnetic moment [**Equation 1-3** and **Equation 1-4**]. In fact, the volume and shape factors are nearly co-dependent, i.e. if an analyte binds, the volume of the complex increases and the shape factor changes; as a result, this will be considered as the effective volume, $V_{eff} = \kappa V$. Analyte binding to the AMBR sensor changes the effective volume or the magnetic moment of the AMBR complex, which translates to a measurable change in the bead's rotation, as shown below

$$\Omega_c = \frac{mB}{\eta V_{eff}} \text{ OR } \dot{\theta}_{SPM} = \frac{\chi'' V_m B^2}{\eta \mu_0 V_{eff}}.^{26,34,35} \quad [1\text{-}6]$$

Using the approach described above, individual and sequential bacteria binding events have been detected. The sensitivity of this method is dependent on the size of the magnetic bead used. For instance, if a magnetic bead that is on the order of magnitude of a bacterium were used, bacteria binding would significantly alter the shape factor and dramatically increase the effective volume. If a larger magnetic bead is used, many bacteria may be required to bind before it results in a sufficient change in the effective volume and measurable change in the bead's rotation. Preliminary studies have been demonstrated to detect single and sequential bacteria-binding event can be detected, as each binding event shifts the bead's average rotational frequency [Figure 1-5].[26] As a result, by measuring these stepwise changes in the rotational rate, the AMBR sensor may find biomedical applications for targeted bacterial detection studies.

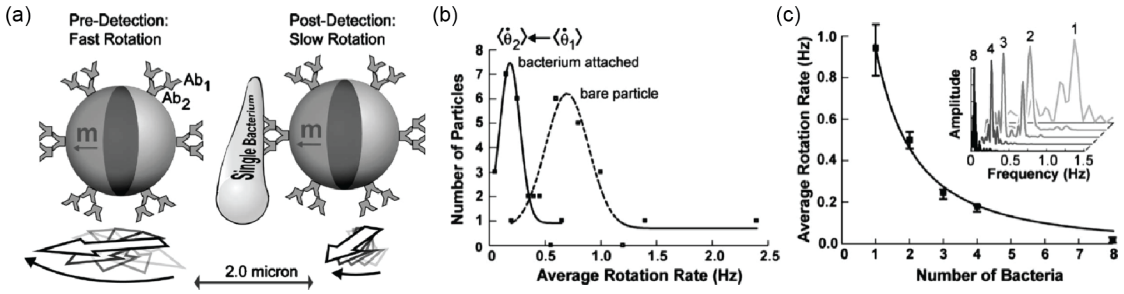

Figure 1-5. (a) Schematic of the rotational response of the magnetic bead upon a single bacterium binding events. (b) The rotational rate of a particle with a bacterium attached is significantly lower than a bare particle. (c) Rotational response of a magnetic particle upon sequential bacteria binding events.[26]

A modified version of the AMBR sensor, known as label-acquired magnetorotation (LAM), has been applied towards analyte detection and concentration estimations.[34,35] LAM is based on a sandwich assay, in which the analyte is bound to a substrate surface, and detection is enhanced through secondary binding. For preliminary analyte detection studies, large functionalized non-magnetic particles are introduced into a suspension with a target analyte of interest, and after sufficient binding time,

functionalized non-magnetic particle labels are introduced into the suspension that will target the analyte [Figure 1-6].[34] In the presence of analyte, the non-magnetic particles would be essentially bound to the larger non-magnetic particle, and the complex would therefore be magnetic and can be torqued by an external rotating magnetic field. The magnetic moment of the complex would be dependent on the amount of magnetic particles bound, which correlates with the amount of analyte present. As a result, the presence of analyte would result in the magnetic bead rotating with the external field and the degree of rotation is dependent on analyte concentration, i.e. the higher the analyte concentration, the faster the bead will rotate. This system can be extended towards detecting a low concentration of a target analyte in a suspension. Recently, the LAM biosensor has been applied towards measuring bioanalyte (i.e. thrombin) concentrations.[35]

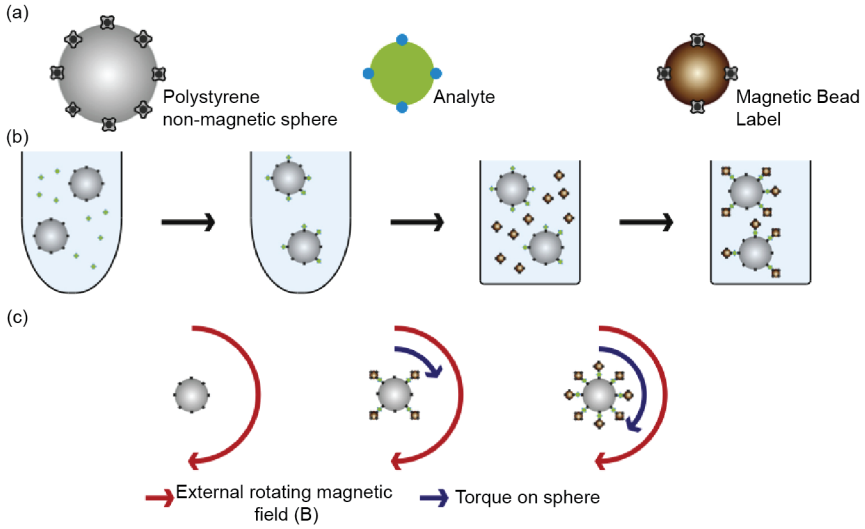

Figure 1-6. Schematic of the label-acquired magnetorotation (LAM) sensor, with the following components (a) polystyrene non-magnetic beads, analyte, and magnetic bead label. (b) The non-magnetic beads are introduced into a suspension and allowed to capture the target analyte. The magnetic bead labels are then introduced into the

suspension and attaches to the analyte. (c) If analyte is present, the magnetic bead label will bind to the sphere complex, introducing a magnetic moment to the system. The more analyte present, more magnetic bead labels will attach to the bead, and the system will have an increasingly larger magnetic moment. The rotation of the complex will correlate with the magnetic moment system.[34]

Cellular Growth

The high sensitivity of the AMBR biosensor in observing environmental and volumetric changes naturally lends itself towards cell growth measurements. The cells must be magnetically modified, whether through cellular ingestion of magnetic beads or cellular attachment to the bead surface. As cells grow and divide, the effective volume of the complex changes, translating to a change in the bead's rotation [Figure 1-7].[24,27]

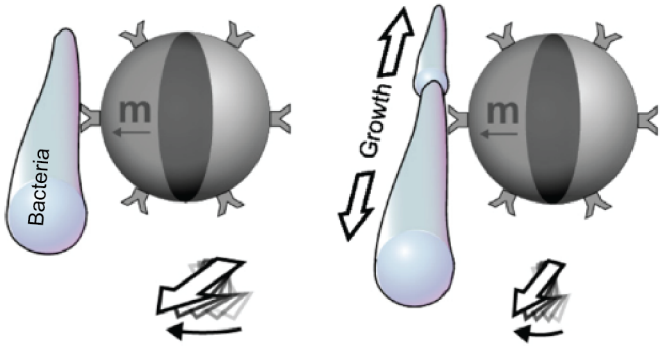

Figure 1-7. Schematic of bacterial growth. As the bacteria elongates, the bead's rotation slows.[27]

Cellular Growth - Ingestion

A cell can be magnetically modified through cellular ingestion of magnetic nanoparticles, rendering the whole cell magnetic. Within a rotating magnetic field, the whole cell rotates and growth can be detected by measuring changes in the complex's effective volume; this approach is referred to as cell magnetorotation (CM). With CM, real-time measurements of mammalian cell death and growth have been observed by monitoring the bead's rotational rate.[36] When cellular health is jeopardized, vesicles within and on the surface of the cell began to swell, commonly referred to as "cellular

blebbing," resulting in a rapid increase in the complex's effective volume, which consequently, causes a rapid increase in the complex's rotational period. This rapid increase in rotational period contrasts the incremental increase that is observed from a slow-growing, healthy cell.[36] Therefore, it is possible to differentiate between a healthy and distressed mammalian cell by observing the degree, i.e. rate, of increase in the rotational period of the cell complex.

Cellular Growth - Surface Attachment

Cells are commonly magnetically labeled, through non-specific and targeted binding techniques, for applications involving binding assays or sample enrichment [Figure 1-8]. After the initial binding event, cellular growth can be detected by

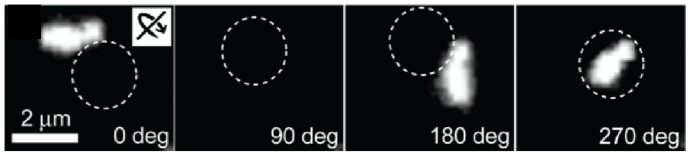

Figure 1-8. Fluorescent image of a fluorescently labeled-bacterium bound to a 2 µm magnetic microsphere; the magnetic microsphere is outlined by the dotted circle.[26]

monitoring the increases in the complex volume, which translates to incremental increase in the rotational period [**Equation 1-5**]. This technique of applying the AMBR sensor towards growth measurements has been applied towards monitoring the growth of yeast cells and bacterial cells [see Chapters 3 and 4].[5,24,30] For yeast cell growth measurements, single yeast cells were attached to magnetic particle dimer complex, and the rotation was monitored.[30] A 3-fold increase in the rotational period of the AMBR sensor was observed within 60 minutes, which corresponded to yeast cell growth and budding events, as verified by light microscopy images. Using a similar approach, bacterial growth can be measured by monitoring the rotation of the AMBR sensor – detailed in Chapter 3 and Chapter 4. The sensitivity of the system towards growth can be tuned by adjusting the

size of the magnetic bead. If the magnetic bead is comparable in size with a bacterium, the AMBR sensor possesses the sensitivity to measure single bacterium elongation events [see Chapter 3].[24] If the magnetic bead is sufficiently larger than the size of a bacterium, the sensitivity may be reduced comparatively; however, the system benefits in that more bacteria are able to bind to the bead surface because of the larger surface area [see Chapter 4].[5] Therefore, the AMBR sensor has the versatility and sensitivity to measure the growth and division of cells that are bound to the magnetic bead.

Cellular Growth – Label-free approach

A label-free AMBR approach to monitor cell growth is through monitoring environmental viscosity changes that result from cell growth and cellular metabolism. At the present time, there are contrasting views as to whether bacterial growth increases or decreases a suspension's viscosity. For instance, a sufficiently high concentration of motile bacteria known as 'pullers' decreases suspension viscosity, whereas 'pushers' increases suspension viscosity.[37,38] Studies have also reported that suspension viscosity decreases as bacteria proliferate because the bacteria ingest the larger, more viscous macromolecules present in growth medium.[39] In contrasting reports, suspension viscosity increases as bacteria proliferate because the bacteria may excrete high molecular weight, sticky exopolysaccharides.[40,41] In summary, the exact mechanism and effect on solution viscosity is still unknown, and likely to be highly dependent on the bacteria species and its internal and external environment. However, bacteria proliferation is known to change bacterial viscosity; as a result, it is possible to utilize the AMBR sensor as a label-free method to detect growth [see Chapter 5].

1.2.4 System Advancement

Sensitivity

There are numerous techniques to improve the AMBR sensor's sensitivity. One method towards reducing the size of the magnetic bead complex was described earlier, as changes on the surface of the magnetic bead will have a more drastic effect on the bead's volumetric properties. A second approach to enhance AMBR sensitivity is to rotate the magnetic beads faster; for instance, if the bead's rotation (i.e. revolutions per minutes) were sufficiently increased, each measurement would require shorter amounts of time. As a result, changes in the effective volume or viscosity would be more rapidly detectable.[42]

Another technique to increase AMBR sensitivity is to apply a group of magnetic particles, i.e. an agglomerate of microparticles clusters.[30] By increasing the complex size, the rotation can be more easily detectable and monitored. Furthermore, with this cluster configuration, the signal, and hence the ease of detection, is accentuated; for instance, if bacteria are bound to the magnetic bead within the cluster system, bacterial growth results in an expansion in the group conformation, which can be more rapidly observed with the biosensing system.[30] By continually enhancing the system sensitivity, the AMBR biosensor may find novel applications (i.e. virus detection) that may revolutionize biosensing technologies.[42]

Off-Microscope Sensor

In its current state, the AMBR sensor is a microscopy-based system, as light microscopy is used to capture the bead's rotation and image analysis software is used to determine the rotational rate. As microscopy systems are expensive and often require trained technicians, there is a need to develop an off-microscope sensor if the AMBR

biosensing technology is to find application outside of centralized laboratories. Developing an off-microscopy detection system is straightforward if there exists a sufficiently sensitive detection system that can monitor and measure the bead's rotation.

Potential detection systems for the AMBR system are magnetoresistive sensors, photo detectors, or CMOS sensors. Significant advancements have been made in magnetoresistive sensing; however, magnetoresistive sensors still lack the ability to monitor the rotation of a single magnetic bead. Applying a photo detector towards monitoring the magnetic bead's rotation has been previously demonstrated. In this technique, a photodiode or laser is applied on the magnetic bead, generating a light scattering pattern. The light-scattering pattern is captured and monitored with a photo detector and the rotational value can be extracted by applying a Fourier transform to the raw light-scatter signal.[27] Another method of detection is using a CMOS sensor; this CMOS approach is similar to the photo detector approach. The AMBR sensor's rotation is monitored with a highly pixelated CMOS sensor; when light shines on the AMBR sensor, a pattern arises on the CMOS sensor that resembles a light scatter. By analyzing individual pixels on the CMOS sensor, a rotational pattern and rate can be identified. At the current state, in order for the CMOS sensor to function, asymmetry must be first introduced to the magnetic bead complex (i.e. optically or physically asymmetrical particles). By achieving an off-microscope detection technique, the AMBR biosensor system will be one step closer towards being a tool that may be implemented in clinical or point-of-care systems.

Although significant advances have been made towards improving the AMBR biosensor system, there remains a critical flaw - the system is largely limited in

throughput. In proof-of-concept studies demonstrating system feasibility, only a single AMBR sensor could be continuously monitored for a short time period. This results from two factors: (1) Magnetic interactions between the AMBR sensor results in the need to sufficiently isolate the sensors from one another and (2) Surface interactions, such as particle stiction to the substrate surface, may result in false results. Towards reducing magnetic interactions, the magnetic bead suspension must be sufficiently dilute or the magnetic beads should be physically separated from one another.

When suspensions are sufficiently dilute, only single magnetic beads may be monitored in a single field-of-view of the microscopy or sensor system. Furthermore, when the magnetic beads were physically separated using a NUNC cell plate, all AMBR sensors resided in the same solution; therefore, cell-cell interactions or solubilized signals or compounds may affect the system. In addition, surface interactions between the AMBR sensor and the substrate surface limited the system towards detection studies, as these surface interactions naturally led to inherent time-dependent rotational periods. To address these concerns, the AMBR sensor has been integrated with a novel microfluidic droplet technology that encapsulates individual AMBR sensors in nanoliter volume droplets. As a result, these droplets may be densely arrayed, enabling higher-throughput studies; the AMBR sensors are isolated in nanoliter droplets, forming isolated experimental conditions; and the encapsulation of AMBR biosensors in suspended water-in-oil droplets precludes surface stiction effects.

1.3 Microfluidic Droplets

1.3.1 History

Microfluidics is the science and technology of systems that manipulate small amounts of fluids, liquids and gases, in channels at length scales of tens to hundreds of micrometers.[43] The design and utilization of microfluidic devices for fluid transport have found many applications from the life sciences, pharmaceuticals, biomedicine and fundamental science, to chemical syntheses and screenings and environmental testing. Passive or actively controlled microfluidic devices have been designed for transport processes, which include mixing, reactions, separations, and particle manipulations, or for fluid control, which include valves, pumps, actuators, mixers, reactors, and sensors.[44] The strength of microfluidic systems lies in its ability for integration; this has lead to the rapid expansion of the field and development towards micro-total analysis system (μTAS), commonly known as 'lab-on-a-chip' systems.[45] These idealized integrative systems incorporate sample preparation, handling, detection, and analysis,[46] which enables high-throughput screening studies; these systems are all incorporated on a user-friendly, automated device.[47] Furthermore, the parallel analysis capabilities, which make higher throughput analysis possible, and the reduced quantities of reagents and materials required, which reduces reaction and analysis times, make possible for microfluidic technologies to have a revolutionizing impact on biological and chemical assays.[48]

1.3.2 Fluid Flow Concepts at the Microscale

The physical properties of microsystems are governed by scaling laws, which express the variation of physical quantities with length scale, l, of a given system or object, provided that other external quantities, such as time (t), pressure (p) and

temperature (T), remain constant.[49] For instance, a general scaling law frequently used for microfluidic systems examines the ratio of the surface forces, such as surface tension and viscosity, to volume forces, such as gravity and inertia, as a system's dimensions are reduced. This scaling law can be expressed by

$$\frac{surface\ forces}{volume\ forces} \propto \frac{l^2}{l^3} \propto l^{-1} \overset{l \to 0}{\rightarrow} \infty \qquad [1\text{-}7]$$

indicating the importance of surface forces in these micron-based systems.[44] The governing Navier-Stokes equation will be reduced to

$$\rho \frac{d\underline{u}}{dt} = -\nabla p + \eta \nabla^2 \underline{u} + \underline{f} \qquad [1\text{-}8]$$

where ρ is the fluid density, $\underline{u}$ is the fluid velocity vector, η is the viscosity, and $\underline{f}$ represents the body force densities, as the nonlinear term is neglected.[50] Important scaling laws as a function of a typical length scale, l, for a number of physical quantities are presented in **Table 1-1**.

Table 1. Scaling Laws

Linear flow rate	reduced		l^1
Volumetric flow rate	reduced	on the	l^3
Diffusive rate	increased	order	l^2
Driving Pressure	increased	of	l^4
Gravity effects	reduced		l^3

Table 1-1. Scaling Laws at the Microscale.

In addition to scaling laws, dimensionless numbers provide further insight into the physical phenomena occurring in microfluidic devices, as it expresses the ratio between two fluid properties and provides a sense for how a system behaves at a particular fluidic parameter space.[50] For instance, the most commonly referred dimensionless parameter in microfluidic systems is the Reynolds number,

$$Re = \frac{\rho U_0 L_0}{\eta}, \qquad [1\text{-}9]$$

where U_0 is the initial flow speed, and L_0 is the characteristic length. The Reynolds number compares the relative importance of inertial effects and viscous effects; at the dimensions employed by microfluidic devices, the Reynolds number is sufficiently low ($Re << 2000$); in this regime, viscous forces are dominant and flow conditions are governed by laminar flow.[50,51] The Peclet number is another important dimensionless number, which compares the convective and diffusive effects in channels. This value governs the degree and form of mixing in fluid samples, which are important parameters when designing devices for sensing and separating flow sources and ingredients.[50] Dimensionless number provides insight to the microscopic flow properties, and therefore, these values influence the design and dimensions of microfluidic systems.

Microfluidic systems have increasingly been applied towards applications in the development and improvement of current large-scale chemical assays and analytical systems. Microfluidics provides the user with a high degree of fluid control in transport and manipulation. When dimensions are reduced to the micron scale, physical processes, such as surface effects, that are not apparent on the macroscale are more easily observed and harnessed.[52] The incorporation of liquid handling, temperature and detection components into a single device allows for analysis and screening procedures to be completed at higher speeds, higher throughput, greater yield, and improved selectivity.[52] For instance, the rapid heat exchange due to downscaling and the incorporation of temperature controllers makes DNA analysis methods more efficient, as PCR operations can be completed rapidly with thermal cycling.[52] In addition to the reduced sample volume, the ability to efficiently mix fluid and samples in the laminar flow systems, through manipulating the channel geometries, dimensions or using active mixing

techniques, help speed up chemical reactions or enzyme assays.[53] Furthermore, the small size and ability to densely pack microfluidic channels and devices allow for highly parallelized reactions, enabling higher-throughput analytical studies.[53] Significant technological advances have been made in the burgeoning field of microfluidics; however, the technology still remains predominantly proof-of-concept.[43] As a result, the full potential of microfluidics will remain unknown until its transition to a widely commercialized system. The end goal is often to develop a lab-on-chip device for biomedicine applications; although highly integrative systems have been developed on a device, the fully integrated and automated lab-on-chip platforms are limited in production and use. In subsequent sections, we review a variety of concepts that contribute towards the construction of a highly integrative microfluidic system and how these concepts have been applied towards chemical analysis applications.

1.3.3 Droplet Microfluidics Control

Droplet-based microfluidic systems enable the miniaturization and compartmentalization of reactions into femtoliter to microliter volume droplets that remain mobile in closed-conduit and open-conduit microfluidic channels. Unlike continuous flow systems, droplets enable isolated reactions to be performed in parallel without cross-contamination or sample dilution. Furthermore, reactions are not required to be stationary as in array chips. As a result, microfluidic droplet-based systems present a high-throughput platform for biological and chemical research.

Continuous flow analysis (CFA), also known as gas-segmented flow analysis (SFA), is a flow technique in which a continuous aqueous stream is segmented with air bubbles, forming liquid slugs. The AutoAnalyzer, the first CFA-based analyzer, was

developed by Skeggs in the 1950s and was commercialized by Technicon Corporation in the 1970s.[54] This technological advance significantly increased the number and rate of sample processing events as each slug acts as a distinct reaction microchamber. Slugs were isolated from one another with air pockets in order to prevent sample interaction, carryover, and dilution by reducing longitudinal dispersion effects.[55,56] Although air provides a barrier between liquid slugs, the inherent compressibility of air results in stream pulsation; therefore, the movement of the liquid slug is uncontrolled.

Flow injection analysis (FIA), an unsegmented flow technique, was developed later in the 1970s to address the issues involved with air-liquid systems, namely, the pulsation in the flow. Rather, discrete sample solutions are inserted directly into a continuously flowing liquid stream, mixed with other continuously flowing solution, and detected downstream. With the elimination of air plugs, dispersion effects are more readily and precisely controlled by adjusting the sample volume, tube length and pumping rate.[56] Furthermore, mixing occurs from diffusion and convective diffusion effects. To ensure reproducibility of the experimental method, physical and chemical equilibrium must not be attained by the time the signal is detected; as a result FIA is often labeled as a fixed-time kinetic methodology.[57] For simple reactions, FIA is the preferred method because of its relative ease and simplicity of automation and the faster analysis times compared to CFA techniques.[55] However, FIA is limited in that detection must occur fairly rapidly after sample introduction in order to reduce signal dilution. Therefore, for experiments that require multiple reagent additions or where reaction times exceed 30 seconds, CFA is preferred method.

1.3.4 Isolation and Compartmentalization

Droplets are useful for isolating solutions, reagents, or cells, and for compartmentalizing reactions into picoliter (pL) to nanoliter (nL) volumes. The formation of droplets can be done with passive mechanisms, such as with co-flowing streams, cross-flowing streams in a T-shaped junction, and elongation flow in a flow focusing geometry,[58] with active electrohydrodynamic (EHD) mechanisms,[59] such as dielectrophoresis (DEP)[60] and electrowetting on dielectric (EWOD),[61] or with surface acoustic waves (SAW),[62] which will not be discussed in this chapter. For closed conduit systems, droplets are typically formed with passive methods as nonlinearity and instability are introduced into laminar two-phase flow microfluidic systems.[63] Two or more streams of immiscible fluids are combined at a rate in which the shear force at the fluid interface is sufficiently large to cause the continuous phase to break the aqueous phase into discrete droplets.[64] The fluids, typically comprised of an oil and an aqueous phase, are incompressible and do not suffer from compression effects. In addition, the immiscibility of the two-phases ensures the isolation and compartmentalization of each phase.

Droplet formation is governed by the capillary number, $Ca = \frac{\eta U_0}{\gamma}$, where η [Pa-s] and U_0 [m/s] is the viscosity and velocity of the continuous phase, respectively, and γ [N/m] is the interfacial tension between the immiscible phases.[65] At low capillary numbers, $Ca < 10^{-2}$, the interfacial force dominates the shear stress forces and the droplet formation dynamics is governed by the ratio of the volumetric flow rates between the two immiscible fluids.[66] When $Ca > 10^{-2}$, the shear stresses dominate and the channel dimensions and geometries and the fluid and flow properties all influence the droplet

break-up process.[66] Passive droplet generation techniques are ideal for experimental conditions where a large number of droplets are desired, namely for high-throughput or parallel analysis applications, such as large-scale PCR[67] or culturing techniques.[68] Furthermore, the composition of the neighboring droplets can be controlled by adjusting the relative concentration of the upstream aqueous solution.[69] This is especially useful for chemical analysis applications, such as enzymatic assays,[69,70] drug discovery assays,[70] and protein crystallization techniques,[69] in which various concentrations of initial analyte or solutions must be tested to optimize a procedure.[69]

Recently, EHD droplet formation mechanisms have gained interest, as these processes are commonly performed in open conduits and do not require any external pumps. Droplets are formed by electrically manipulating the fluid properties; this concept relies on the fact that the surface tension is a function of electric potential across an interface.[59] The distinction between DEP and EWOD lies in their energy transduction mechanism and their electric origin.

DEP is based on electromechanical forces exerted on electrically neutral liquids when the fluid is exposed to non-uniform electric fields; this results in the attraction of polarizable fluid towards regions with higher electric field intensity.[69] In this case, the liquid must be of higher dielectric permittivity than the surrounding fluid. The primary forces involved with DEP concerns the wetting force on the interfacial line between the droplet, surrounding medium, and the contact surface, the force on the fluid interface, and the body force due to the pressure gradient in the fluid.[64] The liquid profile is dependent on the frequency of the applied field. Below the critical frequency, $f_c = \frac{G_w}{2\pi\left(\frac{C_d}{2}+C_w\right)}$, where G_w is the conductance, C_d is the dielectric coating and C_w is the capacitance, the entire

voltage drop occurs across the dielectric layer and the liquid becomes equipotential and wets the entire electrode surface; above the critical frequency, only some portion of the total applied voltage drop occurs in the water; as a result, the liquid remains in drop form.[71] By manipulating the frequency and magnitude of the applied voltage, the size and uniformity of the droplets can be controlled.

In contrast, EWOD-based droplet platforms are based on the presence of free charge at the liquid interface. The application of an electric field reduces the liquid-surface interfacial energy, which renders the surface hydrophilic and enhances fluid wettability. This correspondence between the solid-liquid interfacial tension, γ_{SL}^0, and the applied voltage, *V*, is shown from Lippmann's equation, $\gamma_{SL} = \gamma_{SL}^0 - \frac{\varepsilon V^2}{2d}$, where γ_{SL}^0 is the interfacial tension at zero applied potential, and ε and *d* is the dielectric constant and thickness of the insulating film, respectively.[61] The droplet formation process is initiated as a path of adjacent electrodes are actuated and a liquid protrusion is formed; when intermediate electrodes are sequentially grounded, these surfaces revert back to its hydrophobic state, consequently, forming a droplet. With this mechanism, the electric strength, frequency of the applied field, and the width of the channel control determine the resultant droplet size.

Chemical Assays: Reagent Addition and Mixing

Conducting a chemical assay in a microfluidic droplet often requires multiple steps for completion. Picoliter to nanoliter volumes of reagents must first be combined or sequentially introduced to a droplet in order to instigate reactions. The mechanism for passive droplet fusion involves three steps: (1) particle collision, (2) film drainage, and (3) film rupture. The rate and efficiency of coalescence depends on the fluid drainage

dynamics near contact regions between two droplet interfaces[72] and surfactants that stabilize emulsions by increasing deformation and introducing surface tension gradients.[73] The drainage dynamics can be controlled by adjusting the fluid flow rate, particle generation frequency, and channel design, as higher rates of film drainage and droplet interaction time increases coalescence events.[74] Furthermore, the rate of film drainage is dependent on the viscosity ratio of the two fluids and the surfactant at the fluid interface.[75] Higher viscosity ratios render the interfaces less mobile and surfactants stabilize droplets, thereby reducing coalescence events.[76] Surfactant effects are determined by the Marangoni number, which is the ratio of the surface tension forces versus viscous forces. When the Marangoni number, $Mg = E/Ca$, where E is the Gibbs-Marangoni elasticity, exceeds a critical value, further increase in surfactant concentration has no influence on coalesecence.[75] Therefore, it is important to take into account fluid and flow properties in addition to surfactant effects when initiating droplet fusion processes.

Droplets can also be fused actively with electric, magnetic, thermal, or optical mechanisms. In DEP fusion, the droplet composition must be dielectrically distinct from its carrier fluid; therefore, when the electrode adjacent to the target droplets is activated, neighboring droplets will be guided towards a central region with higher electric field until coalescence occurs, under similar mechanisms as described in passive fusion techniques.[64] Droplets that have not been stabilized will spontaneously fuse, as this fused configuration reduces the system's entropy. Stabilized droplets, on the other hand, may not spontaneously fuse; therefore, electrical pulses or larger voltages are implemented to induce coalescence.[77] Non-electrical means, with magnetic beads[78] or optical tweezers,[79]

have also been demonstrated as fusion mechanisms. Magnetic particles can be used to transport two droplets together until fusion occurs.[78] Optical tweezers also offer precise control and accuracy for fusion events, but its limitations lies in the complicated and expensive set-up.[79]

Upon droplet fusion events, the inherently slow mixing times in laminar flow systems require that passive or active mixing techniques or sources be incorporated onto the chip. Once the droplets of two different compositions are fused, the reagents or solutions must then be mixed at sufficiently rapid speeds. Mixing processes on stagnant or continuous flow systems rely on molecular diffusion; however, diffusive mixing across laminar streams is slow. The diffusion mixing time can be approximated by $t_{diff} = \frac{s_0^2}{2D}$, where s_0 [m] is the initial striation length and D [m^2 s^{-1}] is the diffusion coefficient. As a result, convective flow and chaotic advection have been used in passive systems to reduce the mixing time by essentially reducing the striation length. For a droplet traversing through a straight channel, there exists a critical velocity, $V_c = \pi^2 \left(\frac{L}{d}\right)\left(\frac{D}{d}\right)$, where L is the length of the droplet, D is the diffusivity of a solute, and d is the depth of the microchannel, at which convection-based mixing dominates at velocities above this value, and below the critical value, diffusion-based mixing dominates.[80] For convective mixing, the fluid re-circulates within itself; however, there is an invisible plane longitudinal to the droplet in which the fluid flow patterns do not overlap. In order for sufficient mixing to occur in this regime, the initial solutions must be precisely distributed at the front and the back of the droplet.[81] Another technique to accelerate mixing is chaotic advection, in which unsteady fluid flow is formed as the droplets move through winding channels. This results in an exponential decrease in the striation

length[82,83] and the mixing time, $t_{mix,ca}$, is proportional to the time scale for transport by convection; in particular, $t_{mix,ca} \sim \left(\frac{aw}{U}\right) \log (Pe)$, where a is the dimensionless length of the plug relative to the width, w, U is the flow velocity [m s^{-1}].[83] Chaotic advection has been reported to reduce mixing time significantly as the winding channels cause droplets to undergo the "baker's transformation," in which the droplets are stretched, folded, and reoriented.[83,84]

Active mixing methods, predominantly activated through electrical controls, show benefits over passive techniques in that mixing occurs in more confined regions and can be individually controlled. Manipulating droplets using electrodes allows mixing to occur through oscillations, consecutive splitting and merging methods, or array mixing techniques.[85,86] Rapid oscillation-based mixing is achieved through controlling the charging of neighboring electrodes, causing the substrate surface to sequentially wet and de-wet.[87] Splitting and merging techniques often utilize a three electrode system; droplets are split when current is applied to neighboring electrodes and merged by re-activating the central electrode.[86] In addition, a linear and planar array method can be used to introduce bidirectional fluid motion in the droplet.[85,86] Furthermore, with active techniques, the abovementioned methods can all be coupled and repeated to intensify the mixing process.

Chemical Assays: Post-processing

After the solutions are properly mixed and reactions have taken place, purification of the product or splitting a larger droplet into smaller droplets for further assaying or analysis may be needed. In other cases, the initial droplet may be split into smaller droplets for parallel assay applications or for controlling content concentrations.[88] Passive

techniques for droplet fission include the use of T-junctions, branching channels, or channel obstructions. Passive fission techniques in T-junctions are governed by the *Ca* number, the viscosity ratio η_1/η_2, and the flow rate ratio Q_1/Q_2, where η is the viscosity and Q is the flow rate.[89] The relative size of the daughter droplets is precisely controlled by addressing at least one of these variables. Droplets fission in microchannels was first demonstrated by constricting the channel dimensions at the branching point (T-junction), causing the droplet to elongate into both the daughter channels; this system closely mimicked essentially a laminar flow system.[82] For other T-junction based systems, the relative daughter droplet sizes can be controlled by modulating the relative resistances of the side channels and the flow rate of both the dispersed and continuous phase. In this case, the formation of identical sized daughter droplets at the T-junction is governed by the critical capillary number, $Ca_{cr} = \alpha\varepsilon_0 \left(\frac{1}{\varepsilon^{2/3}} - 1\right)^2$, in which α is a dimensionless constant that is a function of the viscosity contrast of the two fluidics and the geometry of the channel, and ε_0 is the ratio of the initial droplet length over the initial droplet circumference.[90] In addition, droplet splitting and the resulting sizes of the daughter droplets can also be controlled through the strategic placement of channel obstructions.[64]

As with all operations, droplet fission can be controlled actively, with electrical, magnetic, or thermal control. The concept of droplet fission is essentially identical to that of droplet formation since both processes involve separating a liquid entity from another. For instance, in EWOD, electrodes on opposite ends of the droplet are activated in order to reduce the liquid-surface interfacial energy so that the droplet wets across the surface; upon removal of the field in the central electrode, the central region is rendered hydrophobic, separating the droplets.[91] Magnetic based mechanisms have also been used,

as magnetic particles within a droplet are actuated to move apart from the bulk fluid.[78] Droplets can be split by thermal actuation, in which heat is applied to neighboring sides of the droplet, reducing the viscosity and lowering the interfacial tension of the outer edges of the droplets. As a result, the droplets naturally veer towards regions of higher temperatures. By strategically heating certain regions in the microfluidic channels, such as in one of the daughter channel of a T-junction system, uneven sized droplets can result from the fission process. Droplets that enter the channel will be attracted towards the temperature gradient and the resultant size of the daughter droplets is dependent on the temperature of the heater.[89]

Droplet sorting is highly advantageous to control droplet volume for fission or fusion processes or for selectively enriching specific droplet subpopulations. Passive sorting is most commonly achieved with size-based sorting techniques by controlling the flow rate and flow geometry.[88,92] For instance, size-based sorting can be used to remove residual or satellite droplets that were formed during the droplet formation process, thereby increasing the monodispersity of the subpopulation.[88] However, sorting based primarily on size does not find many applications in biochemical assays where content-based sorting is desired. Passively sorting droplet content has been demonstrated when the droplet content is directly correlated with the droplet size; for instance, the incorporation of a large substrate, such as a whole cell, into a droplet will render the droplet slightly larger than an empty droplet. A system that uses a triggered Rayleigh-Plateau instability in jet flow, with shear-induced drift, and excluded volume driven dispersion of individual droplets, has been developed which hydrodynamically separates empty and cell-occupied droplets.[92]

Content-based sorting has traditionally been achieved with active mechanisms, such as through actuators and valves. Recently, non-mechanical active sorting mechanisms have been developed that separate target droplets with electric fields[90] or localized heating.[93] DEP-based sorting techniques have been based on using electric fields to electrostatically charge the droplets and guide the droplets into their designated downstream channels, through steering or deflection mechanisms.[90] The degree of control is determined by the field gradient generated, which is based on the location and shape of the electrodes.[64] Using DEP, droplets can be sorted according to their fluorescent content; droplets are determined by their fluorescent intensity and target droplets are separated from the main channel as a pulse of high-voltage alternating current is emitted across electrodes adjacent to the sorting channel, thereby isolating the target droplets.[94] Although not as common as DEP-based sorting, EWOD sorting mechanisms are achieved by selectively changing the interfacial energy between the droplet and the surface to split the droplet. Most importantly, its driving mechanism for droplet splitting can be applied for electrophoresis; as a result, the particles contents can be sorted and split sequentially.[91] Localized heating is another technique for sorting, as localized heat regions generate thermocapillary flow, such that the heating increases the surface tension, providing a blocking force to halt or diverge droplet flow.[93]

1.3.5 Applications

The high control and integrative ability available for operating and manipulating droplets make droplet microfluidic technology ideal for chemical and biochemical assays applications. The aim of microfluidic system is to develop a lab-on-chip device that includes sequential sample preparation, reaction, assay, detection, and analysis on a

single device; the commercialization and wide-spread development and use of these fully integrated and automated systems are still distant in the future. Integrating components into a single system results in a significant increase in the level of difficulty in system design and operation, compared to the single component system. Nevertheless, in recent years, there is increasing research towards automation and integration of microfluidic droplet systems.

In 1998, Burns et al. developed one of the first highly integrative droplet microfluidic analysis systems, which consist of fluidic channels, heaters, temperature sensors, and fluorescent detectors.[95] The device required no external equipment, such as heaters or pumps, and aqueous reagents could be sequentially measured and dispensed, solutions mixed, DNA amplified or digested, and products separated and detected. This system allowed for smaller samples and reagents to be detected at increased speeds compared to conventional systems.

Polymerase chain reaction (PCR) microfluidic devices are still being extensively studied because of their clinical importance in diagnostics and genetic analysis.[96] The conventional PCR systems are limited both spatially and temporally, the large number of preparation steps often result in sample loss and contamination, and heterogeneous samples are treated as a homogenous population.[67] Significant advancement for a complete lab-on-chip PCR technology has been done, with the integration of on-chip thermal cyclers, electrophoresis, and detection.[95] However, these highly integrative systems lack the ability to run multiple reactions in parallel. Recently, a droplet-based microfluidic device has been developed that integrated sample preparation and PCR analysis in addition to processing multiple samples in parallel in a semi-automated

fashion.[96] PCR-droplet technology has a high potential in significantly advancing biomedical technology. Current research in this field focuses on the optimization of a fully integrative PCR device, the development of an automated control system, and the ability to conduct high-throughput, high-sensitivity single-cell analysis PCR studies.[67]

Droplet microfluidic technology has also been applied towards enzyme assay or chemical reaction analysis, as large-scale isolated reactions can be conducted concurrently. Recently, there has been interest in the development of multiplexed reaction kinetic systems to study chemically diverse samples; in this case, a large number of droplets containing a different ratio or type of reagent or solution can be chemically analyzed in parallel. With an automated technique to fuse samples with reagents at multiple mixing ratios, large-scale screening assays for enzymatic, drug-discovery, or crystallization studies would be made possible.[97] Screening times can be further reduced if detection methods that monitor the reaction kinetics in array systems or in constant flow conditions is incorporated and automated.[98,99]

Recovering droplets with the desired reaction kinetics can be achieved with content-based sorting mechanisms that allow for selectively enriching a specific droplet subpopulation. In some content-sorting techniques, the relative size of the droplet is directly related to the droplet content; for instance, the incorporation of a large substrate, such as a whole cell, into a droplet causes cell-containing droplets to be slightly larger than empty droplets. A system was developed that uses a triggered Rayleigh-Plateau instability in jet flow, that, when complemented with shear-induced drift, hydrodynamically separates empty and cell-occupied droplets.[92] Recently, an integrated on-chip fluorescence-activated droplet sorting system was developed which is based on

DEP-sorting; target droplets that possess a fluorescent intensity above a set threshold are sorted from other droplets as a pulse of high-voltage alternating current is emitted across electrodes adjacent to the sorting channels.[100] This field electrostatically charges, deflects, and guides the droplet into their designated downstream channels.[90] Here we demonstrate various droplet operations and a select few applications that droplet microfluidics enables.

Microfluidic systems have the capability of replacing many conventional "macro" systems because of their low consumption of reagents and samples, ability to manipulate small volumes at ease, and high speed reactions and separations due to high surface to volume ratios; furthermore, processes are conducted at scales more relevant to biological conditions and large numbers of samples can be processed in parallel.[101] In recent years, there has been significant advancement in the development and implementation of high-density microfluidic chips and commercially available chips for a diverse set of biochemical applications in biological and chemical analysis, such as single cell analysis, and biomedicine, such as in diagnostics, treatment, or quantitative analysis.[102] There continues a general trend towards a micro-total analytical system, in which the system performs automatic sampling, sample transport, chemical reactions, and detection in a single, miniaturized platform. Specifically, there has been escalating interest in using microfluidics for biosensing applications, for single molecule or single cell detection and analysis, and for the development of inexpensive, portable diagnostics that can be implemented in third world countries and for personal care.[102]

Recently, there has been a greater pursuit for even smaller dimensions than the typical micron-scale used in microfluidics; this resulted in the rapid emergence of

nanofluidics, the study of fluidic transport at the nanometer scale. At the nanoscale, it is possible to study individual macromolecules; moreover, new fluidic functionalities arise as new fluidic phenomena appear on the nano-scale.[103] This steady decrease in dimensions to the nanoscale approaches a point at which the continuum approximation no longer holds and the Navier-Stokes equations break down. However, for water, under normal conditions, the continuum hydrodynamic limit remains robust down to dimensions of 1-2 nanometers; the Navier-Stokes equation remains accurate for approximating the fluid hydrodynamics. As a result, nanofluidics is limited to the study of surface effects that are not apparent at the micron-scale. The ability to study effects at the molecular scale at which the continuum approximation breaks down is limited to advancements in microfabrication technology to generate feature sizes in the sub-nanoliter range.

Despite significant advances in the young field of microfluidics, microfluidics have not yet been extensively commercialized for various reasons, such as cost of fabrication and the small sampling sizes. Even though PDMS lithography has extensively reduced the cost of microfluidic devices, fabrication of devices remains costly due to the equipment and processes required during manufacturing. In addition, the lack of wide-spread use of commercial microfluidic systems render these devices relatively foreign to the general consumer who may prefer the continued use of conventional technology. Furthermore, microfluidic devices have also not yet reached the stage at which the system can be easily operated and the analysis can be easily read and interpreted by an everyday consumer. World-wide research efforts to develop a fully automated and integrative system for bioanalysis application are extensive; microfluidics indeed possess enormous

potential, as significant advancments in recent years have transformed microfluidics to cost-effective, user-friendly, and high-throughput systems.

1.4 Outline of Dissertation

The chapters in this dissertation have either been published in some form or have been submitted. All published materials have received Publisher's permission for reprint. The full references for each publication are listed, following a brief summary.

Chapter 1 - Introduction: The introduction (microfluidics portion) was partially modified from the following: **Livak-Dahl E,* Sinn I,* and Burns MA. Microfluidic Chemical Analysis Systems.** ***Annu. Rev. Chem. Biomol. Eng.*** **2, 325-353 (2011) –** *[Reprinted with permission by Annual Reviews, Inc.]*. *Authors contributed equally and were listed in alphabetical order.

Chapter 2 – Magnetically Uniform Janus Particles: Currently, the AMBR sensor is limited to relative measurements due to the high variability in magnetic response of commercial magnetic particles. Furthermore, these spherical particles are more difficult to follow because we relied on particle asymmetry to provide a unique detectable signal. We present a fabrication method to create magnetically uniform and tunable magnetic particles, which not only creates an optical asymmetry that can be easily detectable, but also potentially enabling more sensitive and absolute measurements to be made. **[Sinn I, Kinnunen P, Pei S, Clarke R, McNaughton BH, and Kopelman R. Magnetically uniform and tunable Janus particles.** ***Appl. Phys. Lett.*** **98, 024101 (2011)]** *[Reprinted with permission by American Institute of Physics.]*

Chapter 3 – Single Bacterium Growth: Traditional measurements for bacterial growth are based on microscopy-based techniques; however, these methods are inherently diffraction limited (i.e. 250 nm). We evaluate the sensitivity of the AMBR sensor by measuring a single *E. coli* elongation event, and a 75 nm change in bacterial length can be detected. Furthermore, with the high sensitivity of this system, we demonstrate the ability to detect bacterial division events and subsequent growth from daughter bacteria. This potentially enables single cell homogeneity studies. **[Kinnunen P,* Sinn I,* McNaughton BH, Newton DW, Burns MA, and Kopelman R. Monitoring the growth and drug susceptibility of individual bacteria using asynchronous magnetic bead rotation sensors. *Biosensors and Bioelectronics* 26, 2751-2755 (2011)]** *[Reprinted with permission by Elsevier.]*

*Authors contributed equally and was listed in alphabetical order.

Chapter 4 – Small Bacteria Population Growth: The AMBR sensor has largely been limited to short-duration experiments because of possible particle-to-surface stiction effects and bead translation. To address these issues, we enclose individual AMBR sensors in microfluidic droplets. Droplet encapsulation not only enables long-duration measurements, but also enables potentially high-throughput experiments and limits the effects of diffusion and translation that may result from bulk-scale experiments. With this platform, we demonstrate the ability to monitor bacterial growth (at the single cell and small population scale level) and apply our AMBR microfluidic droplet platform towards measuring the antimicrobial susceptibility of *E. coli* to gentamicin. [**Sinn I, Kinnunen P, Albertson T, McNaughton BH, Newton DW, Burns MA, and Kopelman R. Asynchronous**

magnetic bead rotation (AMBR) biosensor in microfluidic droplets for rapid bacterial growth and susceptibility measurements. *Lab Chip* 11, 2604 (2011)]

[Reprinted with permission by RSC.]

Chapter 5 – Label-free, Viscosity Approach: A universal, non-targeted approach towards detecting bacterial growth is to monitor environmental changes upon bacterial proliferation. Depending on metabolism, motility, and concentration, bacterial species are known to have an effect on the suspension viscosity. We encapsulate individual AMBR sensors in microfluidic nanoliter bacterial suspensions and monitor how the viscosity in the bacterial suspension changes upon growth and division. Using this universal, non-targeted approach, as antibodies are unnecessary, we demonstrated the ability to detect bacterial growth and determine antimicrobial susceptibility of *E. coli* to gentamicin. [**Sinn I, Albertson T, Kinnunen P, Breslauer DN, McNaughton BH, Burns MA, and Kopelman R. Asynchronous magnetic bead rotation (AMBR) micro-viscometer for rapid, sensitive, and label-free studies of bacterial growth and drug sensitivity. *submitted to Nature Biotechnology* (2011)**].

Chapter 6 - Conclusion: We have successfully demonstrated proof-of-concept studies indicating the feasibility of the AMBR microfluidic platform towards bacterial growth studies, such as antimicrobial susceptibility tests (AST). There is a considerable optimization potential for this platform, such as improving system sensitivity, increasing throughput, and improving system platform. In addition, in order to transform this early-stage product into a potentially marketable product

(e.g. AST), platform characterizations on different bacterial species and antibiotics are needed.

1.5 References

1. Gijs, M.A.M., Lacharme, F. & Lehmann, U. Microfluidic Applications of Magnetic Particles for Biological Analysis and Catalysis. *Chemical Reviews* **110**, 1518-1563 (2010).

2. Gijs, M.A.M. Magnetic bead handling on-chip: new opportunities for analytical applications. *Microfluidics and Nanofluidics* **1**, 22-40 (2004).

3. McNaughton, B.H., Kehbein, K.A., Anker, J.N. & Kopelman, R. Sudden Breakdown in Linear Response of a Rotationally Driven Magnetic Microparticle and Application to Physical and Chemical Microsensing. *The Journal of Physical Chemistry B* **110**, 18958-18964 (2006).

4. McNaughton, B.H., Agayan, R.R., Wang, J.X. & Kopelman, R. Physiochemical microparticle sensors based on nonlinear magnetic oscillations. *Sensors and Actuators B: Chemical* **121**, 330-340 (2007).

5. Sinn I, Kinnunen P, Albertson T, McNaughton BH, Newton DW, Burns MA, and Kopelman R. Asynchronous magnetic bead rotation (AMBR) biosensor in microfluidic droplets for rapid bacterial growth and susceptibility measurements. *Lab Chip* 11, 2604 (2011).

6. Centers for Disease Control and Prevention. Get Smart: Know When Antibiotics Work. at <http://www.cdc.gov/getsmart/antibiotic-use/anitbiotic-resistance-faqs.html>

7. Centers for Disease Control and Prevention. Campaign to Prevent Antimicrobial Resistance in Healthcare Settings: Why a Campaign? at <http://www.cdc.gov/drugresistance/healthcare/problem.htm>

8. Kang, C.-I. *et al.* Bloodstream Infections Caused by Antibiotic-Resistant Gram-Negative Bacilli: Risk Factors for Mortality and Impact of Inappropriate Initial Antimicrobial Therapy on Outcome. *Antimicrob. Agents Chemother.* **49**, 760-766 (2005).

9. Cosgrove, S.E. The Relationship between Antimicrobial Resistance and Patient Outcomes: Mortality, Length of Hospital Stay, and Health Care Costs. *CLIN INFECT DIS* **42**, S82-S89 (2006).

10. Centers for Disease Control and Prevention. Diagnoses of HIV infection and AIDS in the United States and Dependent Areas, 2008. at <http://www.cdc.gov/hiv/surveillance/resources/reports/2008report/>

11. Klevens, R.M. *et al.* Invasive Methicillin-Resistant Staphylococcus aureus Infections in the United States. *JAMA: The Journal of the American Medical Association* **298**, 1763 -1771 (2007).

12. Kerremans, J.J. *et al.* Rapid identification and antimicrobial susceptibility testing reduce antibiotic use and accelerate pathogen-directed antibiotic use. *Journal of Antimicrobial Chemotherapy* **61**, 428 -435 (2008).

13. Harbarth, S. Inappropriate initial antimicrobial therapy and its effect on survival in a clinical trial of immunomodulating therapy for severe sepsis. *The American Journal of Medicine* **115**, 529-535 (2003).

14. Chen, C.H. *et al.* Antimicrobial Susceptibility Testing Using High Surface-to-Volume Ratio Microchannels. *Analytical Chemistry* **82**, 1012-1019 (2010).

15. Gould, I.M. Antibiotic resistance: the perfect storm. *Int. J. Antimicrob. Agents* **34 Suppl 3**, S2-5 (2009).

16. Kumar, A. *et al.* Duration of hypotension before initiation of effective antimicrobial therapy is the critical determinant of survival in human septic shock*. *Critical Care Medicine* **34**, 1589-1596 (2006).

17. Tortoli, E., Benedetti, M., Fontanelli, A. & Simonetti, M.T. Evaluation of Automated BACTEC MGIT 960 System for Testing Susceptibility of Mycobacterium tuberculosis to Four Major Antituberculous Drugs: Comparison with the Radiometric BACTEC 460TB Method and the Agar Plate Method of Proportion. *J. Clin. Microbiol.* **40**, 607-610 (2002).

18. Scarparo, C., Ricordi, P., Ruggiero, G. & Piccoli, P. Evaluation of the Fully Automated BACTEC MGIT 960 System for Testing Susceptibility of Mycobacterium tuberculosis to Pyrazinamide, Streptomycin, Isoniazid, Rifampin, and Ethambutol and Comparison with the Radiometric BACTEC 460TB Method. *J. Clin. Microbiol.* **42**, 1109-1114 (2004).

19. Huang, T.-S., Tu, H.-Z., Lee, S.S.-J., Huang, W.-K. & Liu, Y.-C. Antimicrobial Susceptibility Testing of Mycobacterium tuberculosis to First-Line Drugs: Comparisons of the MGIT 960 and BACTEC 460 Systems. *Ann Clin Lab Sci* **32**, 142-147 (2002).

20. Proulx, N., Fréchette, D., Toye, B., Chan, J. & Kravcik, S. Delays in the administration of antibiotics are associated with mortality from adult acute bacterial meningitis. *QJM* **98**, 291 -298 (2005).

21. Peters, N.K., Dixon, D.M., Holland, S.M. & Fauci, A.S. The Research Agenda of the National Institute of Allergy and Infectious Diseases for Antimicrobial Resistance. *Journal of Infectious Diseases* **197**, 1087 -1093 (2008).

22. Jorgensen, J.H. & Ferraro, M.J. Medical Microbiology: Antimicrobial Susceptibility Testing: A Review of General Principles and Contemporary Practices. *Clinical Infectious Diseases* **49**, 1749-1755 (2009).

23. Reller, L.B., Weinstein, M., Jorgensen, J.H. & Ferraro, M.J. Antimicrobial Susceptibility Testing: A Review of General Principles and Contemporary Practices. *Clinical Infectious Diseases* **49**, 1749 -1755 (2009).

24. Kinnunen P, Sinn I, McNaughton BH, Newton DW, Burns MA, and Kopelman R. Monitoring the growth and drug susceptibility of individual bacteria using asynchronous magnetic bead rotation sensors. *Biosensors and Bioelectronics* 26, 2751-2755 (2011).

25. Ginsberg, A.M. & Spigelman, M. Challenges in tuberculosis drug research and development. *Nat Med* **13**, 290-294 (2007).

26. McNaughton, B.H., Agayan, R.R., Clarke, R., Smith, R.G. & Kopelman, R. Single bacterial cell detection with nonlinear rotational frequency shifts of driven magnetic microspheres. *Appl. Phys. Lett.* **91**, 224105 (2007).

27. McNaughton, B.H. *et al.* Compact sensor for measuring nonlinear rotational dynamics of driven magnetic microspheres with biomedical applications. *Journal of Magnetism and Magnetic Materials* **321**, 1648–1652 (2009).

28. Janssen, X.J.A., Schellekens, A.J., van Ommering, K., van IJzendoorn, L.J. & Prins, M.W.J. Controlled torque on superparamagnetic beads for functional biosensors. *Biosensors and Bioelectronics* **24**, 1937-1941 (2009).

29. Sinn I, Albertson T, Kinnunen P, Breslauer DN, McNaughton BH, Burns MA, and Kopelman R. Asynchronous magnetic bead rotation (AMBR) micro-viscometer for rapid, sensitive, and label-free studies of bacterial growth and drug sensitivity, *submitted to Nature Biotechnology (2011)*.

30. Kinnunen, P. *Asynchronous Magnetic Bead Rotation (AMBR) for Biosensors*. (University of Michigan, Ph.D. Thesis: 2011).

31. Magnetic Properties of Nanoparticle Assemblies Part 1 (Nanotechnology). at <http://what-when-how.com/nanoscience-and-nanotechnology/magnetic-properties-of-nanoparticle-assemblies-part-1-nanotechnology/>

32. Biswal, S.L. & Gast, A.P. Mechanics of semiflexible chains formed by poly(ethylene glycol)-linked paramagnetic particles. *Phys. Rev. E* **68**, 021402 (2003).

33. Cēbers, A. & Ozols, M. Dynamics of an active magnetic particle in a rotating magnetic field. *Phys. Rev. E* **73**, 021505 (2006).

34. Hecht, A., Kinnunen, P., McNaughton, B.H. & Kopelman, R. Label-acquired magnetorotation for biosensing: An asynchronous rotation assay. *Journal of Magnetism and Magnetic Materials* **323**, 272-278 (2011).

35. Hecht, A., Kumar, A.A. & Kopelman, R. Label-Acquired Magnetorotation As a Signal Transduction Method for Protein Detection: Aptamer-Based Detection of Thrombin. *Anal. Chem.* **83**, 7123-7128 (2011).

36. Elbez, R., McNaughton, B., Patel, L., Pienta, K. & Kopelman, R. Nanoparticle induced Cell Magneto-Rotation: Monitoring Morphology, Stress and Drug Sensitivity of a Suspended Single Cancer Cell. *unpublished*

37. Rafaï, S., Jibuti, L. & Peyla, P. Effective Viscosity of Microswimmer Suspensions. *Phys. Rev. Lett.* **104**, 098102 (2010).

38. Sokolov, A. & Aranson, I.S. Reduction of Viscosity in Suspension of Swimming Bacteria. *Phys. Rev. Lett.* **103**, 148101 (2009).

39. Ong, K.G., Wang, J., Singh, R.S., Bachas, L.G. & Grimes, C.A. Monitoring of bacteria growth using a wireless, remote query resonant-circuit sensor: application to environmental sensing. *Biosensors and Bioelectronics* **16**, 305-312 (2001).

40. Suresh Kumar, A., Mody, K. & Jha, B. Bacterial exopolysaccharides – a perception. *Journal of Basic Microbiology* **47**, 103-117 (2007).

41. Sutherland, I.W. Biofilm exopolysaccharides: a strong and sticky framework. *Microbiology* **147**, 3 -9 (2001).

42. Kinnunen, P., Sinn, I., McNaughton, B.H. & Kopelman, R. High Frequency Asynchronous Magnetic Bead Rotation for Improved Biosensors. *Applied Physics Letters* **97**, 223701 (2010).

43. Whitesides, G.M. The origins and the future of microfluidics. *Nature* **442**, 368-373 (2006).

44. Stone, H.A. & Kim, S. Microfluidics: Basic Issues, Applications, and Challenges.

45. Tabeling, P. *Introduction to microfluidics*. (Oxford University Press: 2005).

46. Reyes, D.R., Iossifidis, D., Auroux, P.-A. & Manz, A. Micro Total Analysis Systems. 1. Introduction, Theory, and Technology. *Analytical Chemistry* **74**, 2623-2636 (2002).

47. Sundberg, S.A. High-throughput and ultra-high-throughput screening: solution- and cell-based approaches. *Current Opinion in Biotechnology* **11**, 47-53 (2000).

48. Nguyen, N.-T. & Wereley, S.T. *Fundamentals and applications of microfluidics*. (Artech House: 2002).

49. Bruus, H. *Theoretical microfluidics*. (Oxford University Press US: 2008).

50. Squires, T.M. & Quake, S.R. Microfluidics: Fluid physics at the nanoliter scale. *Rev. Mod. Phys.* **77**, 977 (2005).

51. Purcell, E.M. Life at low Reynolds number. *Am. J. Phys* **45**, 11 (1977).

52. deMello, A.J. Control and detection of chemical reactions in microfluidic systems. *Nature* **442**, 394-402 (2006).

53. Beebe, D.J., Mensing, G.A. & Walker, G.M. Physics and Applications of Microfluidics in Biology. *Annu. Rev. Biomed. Eng.* **4**, 261-286 (2002).

54. Stewart, K.K. Flow-injection analysis: A review of its early history. *Talanta* **28**, 789-797 (1981).

55. Patton, C.J. & Crouch, S.R. Experimental comparison of flow-injection analysis and air-segmented continuous flow analysis. *Analytica Chimica Acta* **179**, 189-201 (1986).

56. Ruzicka, J. & Hansen, E.H. Flow injection analysis. principles, applications and trends. *Analytica Chimica Acta* **114**, 19-44 (1980).

57. Luque de Castro, M. & Valcarcel, M. *"Flow injection analysis" in Automation in the Laboratory*. (VCH Publishers: New York, 1995).

58. Christopher, G.F. & Anna, S.L. Microfluidic methods for generating continuous droplet streams. *J. Phys. D: Appl. Phys.* **40**, R319-R336 (2007).

59. Lee, J., Moon, H., Fowler, J., Schoellhammer, T. & Kim, C.-J. Electrowetting and electrowetting-on-dielectric for microscale liquid handling. *Sensors and Actuators A: Physical* **95**, 259-268 (2002).

60. Zeng, J. & Korsmeyer, T. Principles of droplet electrohydrodynamics for lab-on-a-chip. *Lab Chip* **4**, 265-277 (2004).

61. Pollack, M.G., Shenderov, A.D. & Fair, R.B. Electrowetting-based actuation of droplets for integrated microfluidics. *Lab Chip* **2**, 96-101 (2002).

62. Beyssen, D., Le Brizoual, L., Elmazria, O. & Alnot, P. Microfluidic device based on surface acoustic wave. *Sensors and Actuators B: Chemical* **118**, 380-385 (2006).

63. Thorsen, T., Roberts, R.W., Arnold, F.H. & Quake, S.R. Dynamic Pattern Formation in a Vesicle-Generating Microfluidic Device. *Phys. Rev. Lett.* **86**, 4163 (2001).

64. Teh, S.-Y., Lin, R., Hung, L.-H. & Lee, A.P. Droplet microfluidics. *Lab Chip* **8**, 198-220 (2008).

65. Stone, H.A. Dynamics of Drop Deformation and Breakup in Viscous Fluids. *Annu. Rev. Fluid. Mech.* **26**, 65-102 (1994).

66. Garstecki, P., Fuerstman, M.J., Stone, H.A. & Whitesides, G.M. Formation of droplets and bubbles in a microfluidic T-junction-scaling and mechanism of break-up. *Lab Chip* **6**, 437-446 (2006).

67. Markey, A.L., Mohr, S. & Day, P.J.. High-throughput droplet PCR. *Methods* (2010).

68. Clausell-Tormos, J. *et al.* Droplet-Based Microfluidic Platforms for the Encapsulation and Screening of Mammalian Cells and Multicellular Organisms. *Chemistry & Biology* **15**, 427-437 (2008).

69. Song, H., Chen, D.L. & Ismagilov, R.F. Reactions in Droplets in Microfluidic Channels. *Angewandte Chemie International Edition* **45**, 7336-7356 (2006).

70. Clausell-Tormos, J., Griffiths, A.D. & Merten, C.A. An automated two-phase microfluidic system for kinetic analyses and the screening of compound libraries. *Lab Chip* **10**, 1302-1307 (2010).

71. Jones, T.B., Gunji, M., Washizu, M. & Feldman, M.J. Dielectrophoretic liquid actuation and nanodroplet formation. *J. Appl. Phys.* **89**, 1441 (2001).

72. Hung, P.J., Lee, P.J., Sabounchi, P., Lin, R. & Lee, L.P. Continuous perfusion microfluidic cell culture array for high-throughput cell-based assays. *Biotechnology and bioengineering* **89**, 1–8 (2005).

73. Cristini, V. & Tan, Y.C. Theory and numerical simulation of droplet dynamics in complex flows—a review. *Lab on a Chip* **4**, 257–264 (2004).

74. Hung, L.-H. *et al.* Alternating droplet generation and controlled dynamic droplet fusion in microfluidic device for CdS nanoparticle synthesis. *Lab Chip* **6**, 174-178 (2006).

75. Hudson, S.D., Jamieson, A.M. & Burkhart, B.E. The effect of surfactant on the efficiency of shear-induced drop coalescence. *Journal of Colloid and Interface Science* **265**, 409-421 (2003).

76. Zheng, B., Tice, J.D. & Ismagilov, R.F. Formation of Droplets of Alternating Composition in Microfluidic Channels and Applications to Indexing of Concentrations in Droplet-Based Assays. *Analytical Chemistry* **76**, 4977-4982 (2004).

77. Schwartz, J.A., Vykoukal, J.V. & Gascoyne, P.R.C. Droplet-based chemistry on a programmable micro-chip. *Lab Chip* **4**, 11-17 (2004).

78. Lehmann, U., Vandevyver, C., Parashar, V.K. & Gijs, M.A.M. Droplet-Based DNA Purification in a Magnetic Lab-on-a-Chip. *Angew. Chem. Int. Ed.* **45**, 3062-3067 (2006).

79. Lorenz, R.M., Edgar, J.S., Jeffries, G.D.M. & Chiu, D.T. Microfluidic and Optical Systems for the On-Demand Generation and Manipulation of Single Femtoliter-Volume Aqueous Droplets. *Analytical Chemistry* **78**, 6433-6439 (2006).

80. Handique, K. & Burns, M.A. Mathematical modeling of drop mixing in a slit-type microchannel. *Journal of Micromechanics and Microengineering* **11**, 548 (2001).

81. Tice, J.D., Song, H., Lyon, A.D. & Ismagilov, R.F. Formation of Droplets and Mixing in Multiphase Microfluidics at Low Values of the Reynolds and the Capillary Numbers. *Langmuir* **19**, 9127-9133 (2003).

82. Song, H., Tice, J.D. & Ismagilov, R.F. A Microfluidic System for Controlling Reaction Networks in Time. *Angewandte Chemie International Edition* **42**, 768-772 (2003).

83. Song, H., Bringer, M.R., Tice, J.D., Gerdts, C.J. & Ismagilov, R.F. Experimental test of scaling of mixing by chaotic advection in droplets moving through microfluidic channels. *Appl. Phys. Lett.* **83**, 4664 (2003).

84. Stroock, A.D. *et al.* Chaotic Mixer for Microchannels. *Science* **295**, 647-651 (2002).

85. Paik, P., Pamula, V.K., Pollack, M.G. & Fair, R.B. Electrowetting-based droplet mixers for microfluidic systems. *Lab Chip* **3**, 28–33 (2003).

86. Paik, P., Pamula, V.K. & Fair, R.B. Rapid droplet mixers for digital microfluidic systems. *Lab Chip* **3**, 253-259 (2003).

87. Cooney, C., Chen, C.-Y., Emerling, M., Nadim, A. & Sterling, J. Electrowetting droplet microfluidics on a single planar surface. *Microfluidics and Nanofluidics* **2**, 435-446 (2006).

88. Tan, Y.-C., Fisher, J.S., Lee, A.I., Cristini, V. & Lee, A.P. Design of microfluidic channel geometries for the control of droplet volume, chemical concentration, and sorting. *Lab Chip* **4**, 292-298 (2004).

89. Ting, T.H. *et al.* Thermally mediated breakup of drops in microchannels. *APPLIED PHYSICS LETTERS* **89**, 234101 (2006).

90. Link, D.R. *et al.* Electric Control of Droplets in Microfluidic Devices13. *Angewandte Chemie* **118**, 2618-2622 (2006).

91. Cho, S.K., Zhao, Y. & Kim, C.J.C.. Concentration and binary separation of micro particles for droplet-based digital microfluidics. *Lab on a Chip* **7**, 490–498 (2007).

92. Chabert, M. & Viovy, J.-L. Microfluidic high-throughput encapsulation and hydrodynamic self-sorting of single cells. *Proceedings of the National Academy of Sciences* **105**, 3191 -3196 (2008).

93. Baroud, C.N., Delville, J.-P., Gallaire, F. & Wunenburger, R. Thermocapillary valve for droplet production and sorting. *Phys. Rev. E* **75**, 046302 (2007).

94. Baret, J.-C. *et al.* Fluorescence-activated droplet sorting (FADS): efficient microfluidic cell sorting based on enzymatic activity. *Lab Chip* **9**, 1850-1858 (2009).

95. Burns, M.A. *et al.* An Integrated Nanoliter DNA Analysis Device. *Science* **282**, 484-487 (1998).

96. Zhang, Y., Park, S., Yang, S. & Wang, T.-H. An all-in-one microfluidic device for parallel DNA extraction and gene analysis. *Biomedical Microdevices* doi:10.1007/s10544-010-9458-6

97. Li, L., Du, W. & Ismagilov, R. User-loaded SlipChip for equipment-free multiplexed nanoliter-scale experiments. *J. Am. Chem. Soc* **132**, 106-111 (2010).

98. Granieri, L., Baret, J.C., Griffiths, A.D. & Merten, C.A. High-Throughput Screening of Enzymes by Retroviral Display Using Droplet-Based Microfluidics. *Chemistry & biology* **17**, 229–235 (2010).

99. Han, Z., Li, W., Huang, Y. & Zheng, B. Measuring Rapid Enzymatic Kinetics by Electrochemical Method in Droplet-Based Microfluidic Devices with Pneumatic Valves. *Analytical Chemistry* **81**, 5840-5845 (2009).

100. Ehrnström, R. *Profile: Miniaturization and integration: challenges and breakthroughs in microfluidics*. **2**, (Royal Society of Chemistry: 2002).

101. Oita, I. *et al.* Microfluidics in macro-biomolecules analysis: macro inside in a nano world. *Analytical and Bioanalytical Chemistry* doi:10.1007/s00216-010-3857-7

102. Manz, A., Graber, N. & Widmer, H.M. Miniaturized total chemical analysis systems: A novel concept for chemical sensing. *Sensors and Actuators B: Chemical* **1**, 244-248 (1990).

103. Bocquet, L. & Charlaix, E. Nanofluidics, from bulk to interfaces. *Chem. Soc. Rev.* **39**, 1073-1095 (2010).

CHAPTER 2:

Monitoring the growth and drug susceptibility of individual bacteria using asynchronous magnetic bead rotation sensors

2.1 Abstract

Continuous growth of individual bacteria has been previously studied by direct observation using optical imaging. However, optical microscopy studies are inherently diffraction limited and limited in the number of individual cells that can be continuously monitored. In this chapter, we report on the use of the asynchronous magnetic bead rotation (AMBR) sensor, which is not diffraction limited. The AMBR sensor allows for the measurement of nanoscale growth dynamics of individual bacterial cells, over multiple generations. This torque-based magnetic bead sensor monitors variations in drag caused by the attachment and growth of a single bacterial cell. In this manner, we observed the growth and division of individual Escherichia coli, with 80-nm sensitivity to the cell length. Over the life cycle of a cell, we observed up to a 300% increase in the rotational period of the biosensor due to increased cell volume. In addition, we observed single bacterial cell growth response to antibiotics. We demonstrate the non-microscopy limited AMBR biosensor for monitoring individual cell growth dynamics, including cell elongation, generation time, lag time, and division, as well as their sensitivity to antibiotics.

2.2 Introduction

Optical microscopy is currently the most widely used tool for studying single cell behavior, as it offers the ability to measure the elongation of individual bacteria over multiple generations.[1-3] However, the spatial resolution of far-field optical microscopy techniques is limited by the diffraction of light. High sensitivity tools that have proven useful for single cell analysis include scanning probe techniques[4] and cantilevers,[5,6] but studies spanning multiple generations of individual cells have not yet been demonstrated with these techniques. We note that high-resolution techniques, such as electron microscopy and cantilevers are optimal in vacuum or air, rather than in water. Here we present a high-resolution sensing method that works optimally in aqueous environments.[7]

In this manuscript, we implement asynchronous magnetic bead rotation (AMBR) to measure the nanogrowth of individual bacterial cells. AMBR biosensors, developed by our lab, have previously been used for a variety of applications.[7-12] The rotational dynamics of magnetic objects rotating asynchronously with the driving magnetic field have also been used for a other applications and studies. One of the first investigations was done on a system consisting of a ferrofluid and a pair of nonmagnetic rotating spheres called "magnetic holes".[13,14] Similar magnetic rotational studies have been used for the characterization of magnetic carbon nanotubes,[15] magnetotactic bacteria,[16] traveling wave magnetophoresis,[17,18] micro mixing,[19,20] and artificial microscopic swimmers and microdrills.[21,22] Additionally, nonmagnetic systems that undergo asynchronous rotation have been used for the rotation of glass nanorods in fluid.[23] The presented AMBR biosensor enables the growth of a single bacterium to be measured throughout its life cycle and over sequential generations. Indeed, we show that the

elongation of individual Escherichia coli bacterial cells can be observed with 80 nm sensitivity in cell length. This high-sensitivity, prolonged monitoring, single cell analysis technique could be useful in population heterogeneity studies, and could radically shorten the test time for identification (ID) and antimicrobial susceptibility testing (AST) of microorganisms.

As mentioned, these single cell studies employ the AMBR biosensor, which is based on the torque exerted on a magnetic bead in the presence of a rotating magnetic field. At sufficiently high rotating field frequencies, the magnetic bead rotates asynchronously with the magnetic field,[8,16,24-26] and in the case of a superparamagnetic bead the rotational period, T, is proportional to the effective volume of the rotating body, $T \propto V_{eff}$. For the derivation, see **Section 3.3.1**. Therefore, by monitoring the rotational period of the magnetic bead, it is possible to detect single bacterium binding events[9] and, as demonstrated in this manuscript, measure single bacterial cell growth on the nanometer scale. When a single cell attaches to a magnetic bead, or grows, the effective volume of the bead complex increases; this process can be monitored by measuring changes in the bead's rotational period. The *E. coli* are assumed to grow only in length,[3] with a constant diameter; thus changes in the rotational period of the bead correspond to bacterial elongation. A schematic of this is shown in **Figure 2-1**(a–c). Within this manuscript, the sensitivity is defined as the smallest detectable change in the sensor or its environment.

2.3 Materials and Methods

2.3.1 Theoretical derivation

The torque exerted on a magnetic bead in a magnetic field can be expressed by

$$\tau_{mag} = m \times B = \left(m_{perm} + m_{ind}\right) \times B \quad [3\text{-}1]$$

where τ_{mag} is the total magnetic torque due to the induced magnetic moment m_{ind} and permanent magnetic moment m_{perm}, in a magnetic field B. In a time varying magnetic field, the induced magnetic moment is not necessarily parallel to the magnetic field, and therefore can contribute to the torque. By using the previously described equations for asynchronous rotation, arising from magnetic torque,[8,16,26] the total magnetic torque in a rotating magnetic field can be expressed by

$$\tau_{mag} = \left[m_{perm} + (\chi' + i\chi'')V_m B\right] \times B = m_{perm} B \sin(\Omega t - \theta)\hat{e} + \chi'' V_m \frac{B^2}{\mu_0}\hat{e} \quad [3\text{-}2]$$

where χ' is the real part and χ'' is the imaginary part of the magnetic susceptibility, Ω is the driving frequency, V_m is the magnetic content volume, μ_0 the permeability of free space, and $\hat{e}$ is the unit vector of the rotating field. The real part of the susceptibility, χ', does not contribute to the cross product in **Equation 3-2**, as it remains parallel with the magnetic field. The first term on the right hand side of **Equation 3-2** corresponds to the permanent magnetic moment, and the second term corresponds to the induced (superparamagnetic) moment. In the experiments, we implement a 500 Hz driving field while the critical frequency of the system, Ω_c, is on the order of 1 Hz. As a result, the superparamagnetic torque dominates and the first term in **Equation 3-2** can be neglected $\left(\Omega >> \Omega_c\right)$. This allows for **Equation 3-1** to be simplified to

$$\tau_{mag} = m_{ind} \times B \quad [3\text{-}3]$$

leading to

$$\tau_{mag} = \chi'' V_m \frac{B^2}{\mu_0}\hat{e}. \quad [3\text{-}4]$$

Neglecting both inertial forces (where drag forces dominate) and Brownian rotation

forces (where magnetic torque dominates) the torque of a rotating body in a viscous fluid can be expressed by

$$\tau_{drag} = -\tau_{mag} = -\kappa\eta V\dot{\theta}\hat{e} \quad [3\text{-}5]$$

where κ is the Einstein shape factor (6 for a sphere), η is the dynamic viscosity of the surrounding fluid, V is the total volume of the rotating body, and $\dot{\theta}$ is the angular orientation ($\dot{\theta}$ is the rotational rate of the object, in radians/s). The rotational rate of the object can be solved by combining **Equation 3-4** and **Equation 3-5**, which yields

$$\dot{\theta} = \frac{\chi'' V_m B}{\kappa\eta V \mu_0}. \quad [3\text{-}6]$$

At a constant temperature and a constant rotating magnetic field, the imaginary susceptibility χ'', magnetic content volume V_m, magnetic field strength B, and the dynamic viscosity η, remain constant. Under these conditions, the rotation rate of the particle is primarily a function of the effective volume

$$\dot{\theta} \propto \frac{1}{V_{eff}}. \quad [3\text{-}7]$$

The rotational period of the particle, T, can be written in terms of the rotational rate, $\dot{\theta}$, as $T = 2\pi/\dot{\theta}$, which yields the basis of the superparamagnetic AMBR sensor, namely **Equation 3-8**:

$$T \propto V_{eff} \quad [3\text{-}8]$$

Notably, a similar equation has been reported for the measurement of the Brownian relaxation peak of magnetic particles as measured with AC susceptometry.[27-29] However, the AMBR method implements constant magnitude rotating magnetic fields and does not use varying magnitude non-rotating fields as is done with AC susceptometers. Thus, **Equation 3-8** does not describe the location of the Brownian relaxation peak. Instead,

Equation 3-8 describes how the real- time rotational period of a magnetic particle relates to the effective volume of the particle, when driven at a single frequency.

2.3.2 Cell culture and attachment methods

Uropathogenic *E. coli* bacteria (obtained from the Clinical Microbiology Laboratory, University of Michigan Hospital) were grown on Mueller-Hinton agar plates (BBL) at 37 ˚C for 12–18 h. The bacteria were then suspended in 2.2% Mueller Hinton II (MH) broth (Teknova, Hollister CA) to the approximate concentration of 1.5×10^8 CFU/mL (e.g. a 0.5 McFarland Standard value). Anti-*E. coli* (ab20640-1; Abcam, Cambridge MA) functionalized magnetic particles (M-280; Invitrogen, Carlsbad CA) were introduced to the bacteria solution (to yield 106 beads/mL concentration). The sample was incubated, with 175 rpm shaking at 37 ˚C, for another 1.5 h. Before rotational data were obtained, the beads with attached bacteria were isolated using a magnetic separator (PickPen 1-M; Sunrise Science, San Diego CA) and re-suspended into a solution containing MH broth with 1% Pluronic $F\text{-}68^{30}$ (MP Biochemicals, Solon MH) and 0.1% BSA (Thermo Scientific, Waltham MA). All experiments were conducted at room temperature. The ampicillin minimum inhibitory concentration (MIC) of the *E. coli* was 8 μg/mL, as determined by conventional broth microdilution methods.

2.3.3 Experimental setup and measurement conditions

Isolated bead-bacteria complexes were placed in a rotating magnetic field on an inverted optical microscope (Olympus IX71, 100×/1.3 oil) and 1 min videos were taken at 5 min intervals at 16fps using a digital camera (piA640-210gm; Basler, Exton PA), see **Figure 2-1**. Videos were analyzed using ImageJ software by plotting the “z-axis profile” of an area of interest next to the rotating particle; this yields an intensity profile that

reflects the rotational frequency of the bead-bacterium complex.[8] The intensity plot was analyzed by applying a Fast Fourier Transform (FFT) in MATLAB, and the frequency of the highest amplitude FFT peak indicate the rotational rate of the particle [**Figure 2-1**].

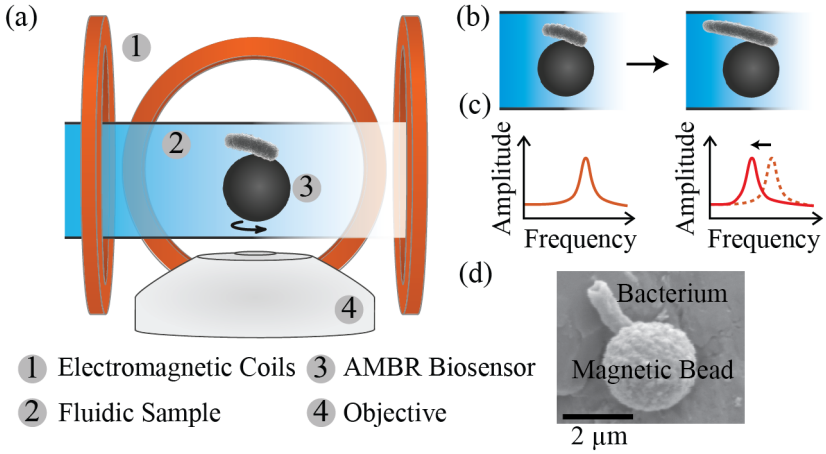

Figure 2-1. The concept of measuring single cell elongation using the asynchronous magnetic bead rotation (AMBR) method. (a) A schematic representation of the AMBR sensor on a microscope. (b) Cell elongation (schematic). (c) Schematic illustrating how the rotational period change is observed as a peak shift in the FFT spectrum (i.e. the elongation of the attached bacterium can be measured by observing the change in the rotational period of the sensor-bacterium complex, which is caused by the increase in the system's effective volume). (d) Scanning electron microscopy image of a single *E. coli* cell attached to a 2.8 μm magnetic bead.

Occasionally, the highest amplitude FFT peak did not correspond to the observed rotational frequency of the particle, and instead was twice the observed rotational rate. The peaks were fit- ted with a Gaussian function in order to determine the peak position and width. The rotating magnetic field was generated with a custom LabView (National Instruments, Austin TX) program and Data Acquisition Board (NI PCI-6221; National Instruments, Austin TX) in conjunction with an amplifier and a custom made pair of air core Helmholtz coils. The magnetic field frequency used to rotate the magnetic beads was 500 Hz with a 0.9 mT magnitude, which was measured with a 3-axis magnetic field probe (C-H3A-2m; Senis Gmbh, Switzerland).

2.3.4 Experimental errors

The error in determining the rotational period was designated as the FFT peak width (full width at half maximum) of the amplitude signal. Fixed cells (*E. coli* suspended in 1% glutaraldehyde for 30 min) were measured over 120 min, yielding a 6.0% CV in the rotational response of the sensor. Fluctuations in the rotational response of a single AMBR probe, with no bacteria present, were under 10% after 20 h, showing long-term stability in the rotational period. Bacterial length measurements were performed with a bright field microscope and a 100X oil immersion objective. The theoretical diffraction limit is estimated to be $\lambda/2N.A. \approx 700nm/2.6 \approx 270nm$, which we assumed to be our error in the bacterium length measurements on the micro- scope. To determine the bacterial cell length, intensity profiles were taken across the length of the bacterium, with ImageJ software.

2.4 Results and discussion

We demonstrated the sensitivity of the AMBR biosensor by measuring the growth and division of a single *E. coli* cell throughout its life cycle and over multiple generations [**Figure 2-2**]. Bacterial cells were attached to 2.8 μm diameter magnetic beads coated with specific antibodies. Individual cell growth and response to antibiotics were observed by using the AMBR method. Measurements were performed on an inverted bright-field microscope, which allowed for visualization of bacterial elongation and division, **Figure 2-2**(b), and quantification of the resulting changes in the rotational period of the sensor, **Figure 2-2**(c) (normalized data).

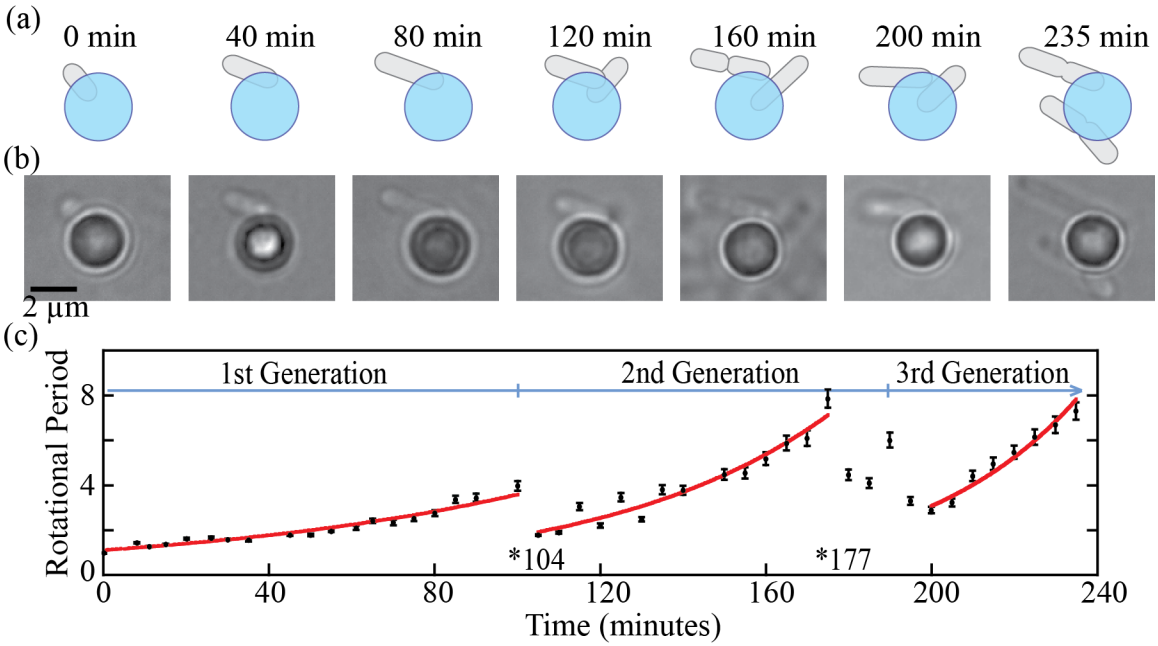

Figure 2-2. Growth and division of a single *E. coli* bacterium, measured with the AMBR biosensor and observed with an optical microscope. (a) Schematic and (b) 100× oil immersion optical microscopy images of the AMBR sensor with initially a single bacterium attached and subsequent cell divisions. (c) Cell growth and division as observed with the AMBR sensor. After a period of growth, the first cell division is observed at 104 min and again at 177 and 199 min. The error bars correspond to the measurement error in the rotational period and the exponential fits are a guide to the eye. Data is normalized to 1 at time zero.

Over the first cell division cycle, the rotational period of the AMBR sensor changed from (0.8 ± 0.03) to (3.2 ± 0.2) s, which corresponds to a 300% increase in the rotational period. Similarly, over the second and third cell divisions, the periods changed from (1.0 ± 0.1) to (6.2 ± 0.4) s (520%) and from (2.3 ± 0.2) to (5.8 ± 0.3) s (150%), respectively. These dramatic changes in the rotational period are governed by the volumetric changes of the attached bacteria. The significant abrupt reduction in rotational period at time 104 min (e.g. a factor of 2.1 ± 0.3) is exactly, time wise, correlated to cell division as observed on the optical microscope. Furthermore, the rotation of the bead did not lead to the detachment of any bacteria from the bead, thus enabling studies spanning

multiple generations. Detachment was only observed as a result of cell division. Upon division, the daughter cell either re-bound to the sensor or detached itself from the sensor and remained free-floating in the medium. For example, a division event that did not result in detachment can be seen in **Figure 2-2**(c) at 104 min; and a division with detachment occurred at 177 min. In the case where the daughter cell remained bound to the sensor, an abrupt decrease in the rotational period was observed as the bacteria reoriented itself on the bead and lowered the effective volume by reducing the shape factor [**Figure 2-3**].

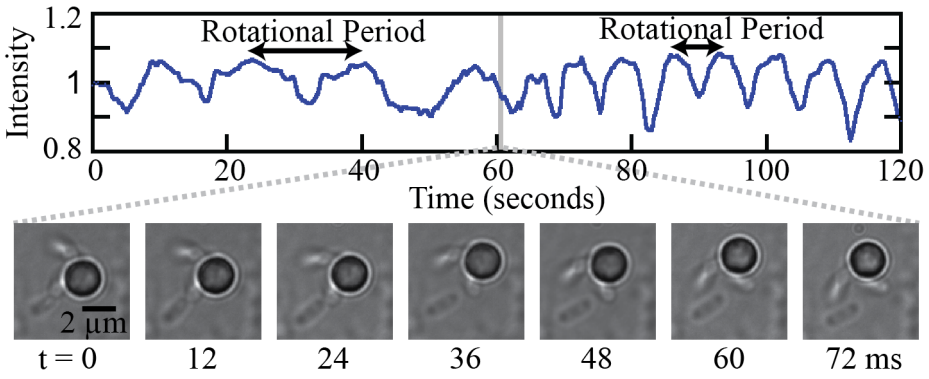

Figure 2-3. (a) Rotational data of the AMBR sensor after 177 minute incubation [see Figure 3.2(c)], showing the second cell division. Intensity data is acquired from a region of interest in the microscopy video. The data is normalized to 1, at time zero. (b) Optical microscopy images of the cell division.

Changes in the rotational period of the AMBR sensor are indeed due to bacterial growth, as there were no significant rotational period changes observed when bacteria were not present or when fixated *E. coli* cells were attached [**Figure 2-4**(a)]. A comparison shows that the rotational period of the AMBR sensor and the optical microscopy measurements of the cell elongation were in good agreement [**Figure 2-4**(b)] and consistent with the derived linear relationship. To estimate the sensitivity of the

AMBR sensor in response to cell elongation, the rotational period of the sensor was compared to the cell length as measured by optical microscopy. The sensitivity depends on the orientation of the bacterium, and is therefore case dependent. An example of the relationship between the rotational period of the AMBR sensor and the attached bacterium is shown in **Figure 2-3**(b), where the error in measuring the AMBR rotational period was estimated to correspond to (80 ± 38) nm change in bacterium length. The fit in **Figure 2-3**(b) was used as the relationship between the rotational period and the bacterium length.

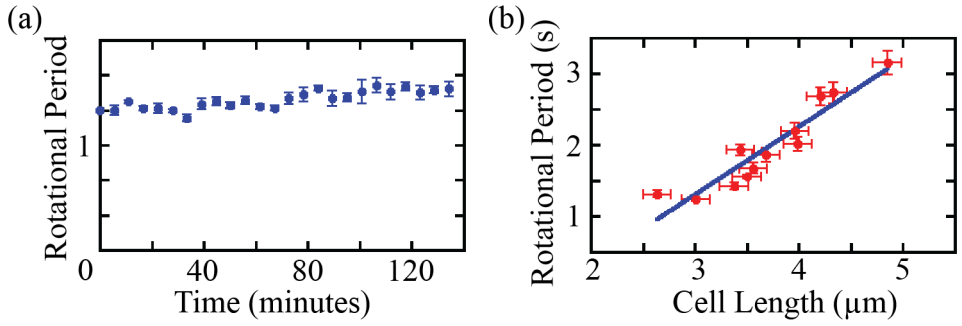

Figure 2-4. AMBR sensor measurements of elongation, compared with microscope observations, and the effect of ampicillin on cell elongation. (a) Fixed *E. coli* bacterium control data; normalized rotational period of an AMBR sensor with a fixed *E. coli* attached. (b) The rotational period of the AMBR sensor vs. the bacterium length measured from microscopy images, using image analysis. The error bars in the microscope measurement data are 270 nm. The error in the rotational period of the AMBR sensor is explained in Section 3.3.4.

The error in optical cell length measurements was approximately 270 nm with our microscope setup; see Section 3.3.4 for the calculation. We measured the rotational period from a series of images, obtained with an optical microscope; however, with the AMBR method, rotation can also be observed without a microscope, by using a combination of a low power laser and a photodiode.[10] The authors note that the AMBR method is based on the rotational period of the magnetic particle and as a result is

unaffected by the optical resolution.

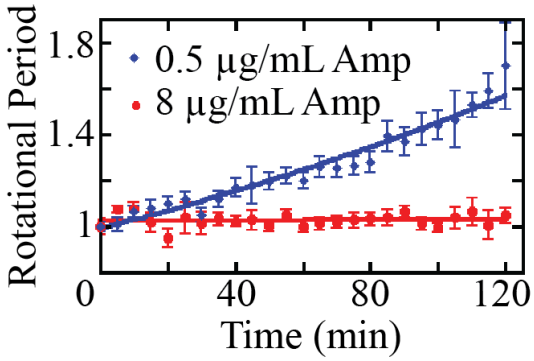

Figure 2-5. The response of two individual *E. coli* bacteria from the same culture (data normalized to 1 at time zero) in the presence of 0.5 and 8 µg/mL ampicillin, i.e. well below the MIC (growth) and at MIC (no growth), respectively, measured with the AMBR sensor.

To demonstrate the use of an AMBR sensor for observing single cell response to different environmental conditions, the response of individual *E. coli* cells to two concentrations of antibiotics was measured. The *E. coli* growth, in the presence of a low concentration of antibiotics (0.5 µg/mL ampicillin), and growth inhibition, in the presence of a high antibiotic concentration (8 µg/mL ampicillin), were observed using the AMBR sensor [**Figure 2-5**]. The observed response of the individual cells to the specified concentration of ampicillin should not be generalized to the whole population, since different cells within the same population may respond differently at the same concentration of antibiotics, due to the heterogeneity within the bacterial population. Nevertheless, a drastic difference is seen between the normal growth pattern below the antibiotics MIC (minimum inhibitory concentration) value and the "no growth" pattern at the MIC. The ultimate sensitivity of this method depends on the orientation of the attached bacterium and the axis of rotation of the bacterium-sensor complex. However, irrespective of this sensitivity limitation, the method can be used to clearly distinguish

between growth and no growth of individual bacteria, as shown in **Figure 2-3**(c), where growth was arrested by a sufficient concentration of ampicillin. This validates the AMBR sensor as a useful tool for sensitively observing the response of individual *E. coli* cells to environmental effects, in particular to antibiotics, within only minutes.

In addition to using the AMRB sensor to study single cell response to environmental conditions, it is envisioned that this method could ultimately also be used for drug discovery research and for rapid antimicrobial susceptibility testing (AST) in clinical settings. The current clinical standard in AST is based on turbidity measurements of bacteria populations, leading to an approximately 24-h instrument time when performed on pure cultures.[31] Since the AMBR sensor measures the response of individual bacterial cells instead of changes in the entire population, multiplexing this technique could dramatically reduce AST times. Furthermore, integration with a high-throughput microfluidic technology should enable studies on growth dynamics of individual bacteria, and on their susceptibility to environmental factors such as nutrients, temperature, pH and salt levels, as well as to the introduction of antimicrobial agents.

2.5 Conclusions

The growth of individual *E. coli* bacteria over multiple generations and the effect of antibiotics were measured, at the nanometer scale, using the AMBR biosensor. The AMBR biosensor was observed to respond to changes of as little as 80 nm in length of single *E. coli* cells. The sensor was also demonstrated to monitor growth over the entire life cycle of the cells. Furthermore, measurement of the response of individual *E. coli* cells to 0.5 and 8 μg/mL concentrations of the antibiotic ampicillin demonstrate a drastic difference between growth and inhibition. Finally, while the demonstrated AMBR sensor

has been optimized for bacteria, preliminary work has extended the method to studies on other individual cells, such as yeast and cancer cells.

2.6 References

1. Brehm-Stecher, B.F. & Johnson, E.A. Single-Cell Microbiology: Tools, Technologies, and Applications. *Microbiol. Mol. Biol. Rev.* **68**, 538-559 (2004).

2. Elfwing, A., LeMarc, Y., Baranyi, J. & Ballagi, A. Observing Growth and Division of Large Numbers of Individual Bacteria by Image Analysis. *Appl. Environ. Microbiol.* **70**, 675-678 (2004).

3. Inoue, I., Wakamoto, Y., Moriguchi, H., Okano, K. & Yasuda, K. On-chip culture system for observation of isolated individual cells. *Lab Chip* **1**, 50 (2001).

4. Touhami, A., Jericho, M.H. & Beveridge, T.J. Atomic Force Microscopy of Cell Growth and Division in Staphylococcus aureus. *J. Bacteriol.* **186**, 3286-3295 (2004).

5. Gfeller, K.Y., Nugaeva, N. & Hegner, M. Micromechanical oscillators as rapid biosensor for the detection of active growth of Escherichia coli. *Biosensors and Bioelectronics* **21**, 528-533 (2005).

6. Bryan, A.K., Goranov, A., Amon, A. & Manalis, S.R. Measurement of mass, density, and volume during the cell cycle of yeast. *Proceedings of the National Academy of Sciences* **107**, 999 -1004 (2010).

7. McNaughton, B.H., Agayan, R.R., Wang, J.X. & Kopelman, R. Physiochemical microparticle sensors based on nonlinear magnetic oscillations. *Sensors and Actuators B: Chemical* **121**, 330-340 (2007).

8. McNaughton, B.H., Kehbein, K.A., Anker, J.N. & Kopelman, R. Sudden Breakdown in Linear Response of a Rotationally Driven Magnetic Microparticle and Application to Physical and Chemical Microsensing. *The Journal of Physical Chemistry B* **110**, 18958-18964 (2006).

9. McNaughton, B.H., Agayan, R.R., Clarke, R., Smith, R.G. & Kopelman, R. Single bacterial cell detection with nonlinear rotational frequency shifts of driven magnetic microspheres. *Appl. Phys. Lett.* **91**, 224105 (2007).

10. McNaughton, B.H. et al. Compact sensor for measuring nonlinear rotational dynamics of driven magnetic microspheres with biomedical applications. *Journal of Magnetism and Magnetic Materials* **321**, 1648-1652 (2009).

11. Hecht, A., Kinnunen, P., McNaughton, B.H. & Kopelman, R. Label-acquired magnetorotation for biosensing: An asynchronous rotation assay. *Journal of Magnetism and Magnetic Materials* **323**, 272-278 (2011).

12. Kinnunen, P., Sinn, I., McNaughton, B.H. & Kopelman, R. High Frequency Asynchronous Magnetic Bead Rotation for Improved Biosensors. *Applied Physics Letters* **97**, 223701 (2010).

13. Helgesen, G., Pieranski, P. & Skjeltorp, A.T. Nonlinear phenomena in systems of magnetic holes. *Phys. Rev. Lett.* **64**, 1425 (1990).

14. Helgesen, G., Pieranski, P. & Skjeltorp, A.T. Dynamic behavior of simple magnetic hole systems. *Phys. Rev. A* **42**, 7271 (1990).

15. Korneva, G. et al. Carbon Nanotubes Loaded with Magnetic Particles. *Nano Letters* **5**, 879-884 (2005).

16. Cēbers, A. & Ozols, M. Dynamics of an active magnetic particle in a rotating magnetic field. *Phys. Rev. E* **73**, 021505 (2006).

17. Yellen, B.B. et al. Traveling wave magnetophoresis for high resolution chip based separations. *Lab Chip* **7**, 1681 (2007).

18. Yellen, B.B. & Virgin, L.N. Nonlinear dynamics of superparamagnetic beads in a traveling magnetic-field wave. *Phys. Rev. E* **80**, 011402 (2009).

19. Biswal, S.L. & Gast, A.P. Mechanics of semiflexible chains formed by poly(ethylene glycol)-linked paramagnetic particles. *Phys. Rev. E* **68**, 021402 (2003).

20. Tierno, P., Johansen, T.H. & Fischer, T.M. Magnetically Driven Colloidal Microstirrer. *The Journal of Physical Chemistry B* **111**, 3077-3080 (2007).

21. Honda, T., Arai, K.I. & Ishiyama, K. Micro swimming mechanisms propelled by external magnetic fields. *Magnetics, IEEE Transactions on* **32**, 5085-5087 (1996).

22. Dreyfus, R. et al. Microscopic artificial swimmers. *Nature* **437**, 862-865 (2005).

23. Shelton, W.A., Bonin, K.D. & Walker, T.G. Nonlinear motion of optically torqued nanorods. *Phys. Rev. E* **71**, 036204 (2005).

24. Caroli, C. & Pincus, P. Response of an isolated magnetic grain suspended in a liquid to a rotating field. *Phys kondens Materie* **9**, 311-319 (1969).

25. Rosensweig, R.E. *Ferrohydrodynamics*. (Courier Dover Publications: 1997).

26. Janssen, X.J.A., Schellekens, A.J., van Ommering, K., van IJzendoorn, L.J. & Prins, M.W.J. Controlled torque on superparamagnetic beads for functional biosensors. *Biosensors and Bioelectronics* **24**, 1937-1941 (2009).

27. Astalan, A.P., Ahrentorp, F., Johansson, C., Larsson, K. & Krozer, A. Biomolecular reactions studied using changes in Brownian rotation dynamics of magnetic particles. *Biosensors and Bioelectronics* **19**, 945-951 (2004).

28. Chung, S.-H. et al. Magneto-optic measurement of Brownian relaxation of magnetic nanoparticles. *Journal of Magnetism and Magnetic Materials* **320**, 91-95 (2008).

29. Connollya, J., Pierre, T.G.S. & Dobsonb, J. Experimental evaluation of the magnetic properties of commercially available magnetic microspheres. *Bio-Medical Materials and Engineering* **15**, 421–431 (2005).

30. King, A.T., Davey, M.R., Mulligan, B.J. & Lowe, K.C. Effects of Pluronic F-68 on plant cells in suspension culture. *Biotechnol Lett* **12**, 29-32 (1990).

31. Jorgensen, J.H. & Ferraro, M.J. Medical Microbiology: Antimicrobial Susceptibility Testing: A Review of General Principles and Contemporary Practices. *Clinical Infectious Diseases* **49**, 1749-1755 (2009).

CHAPTER 3:

Asynchronous Magnetic Bead Rotation (AMBR) biosensor in microfluidic droplets for rapid bacterial growth and susceptibility measurements

3.1 Abstract

Inappropriate antibiotic use is a major factor contributing to the emergence and spread of antimicrobial resistance. The long turnaround time (over 24 hours) required for clinical antimicrobial susceptibility testing (AST) often results in patients being prescribed empiric therapies, which may be inadequate, inappropriate, or overly broad-spectrum. A reduction in the AST time may enable more appropriate therapies to be prescribed earlier. Here we report a new diagnostic asynchronous magnetic bead rotation (AMBR) biosensor droplet microfluidic platform that enables single cell and small cell population growth measurements for applications aimed at rapid AST. We demonstrate the ability to rapidly measure bacterial growth, susceptibility, and the minimum inhibitory concentration (MIC) of a small uropathogenic *Escherichia coli* population that was confined in microfluidic droplets and exposed to concentrations above and below the MIC of gentamicin. Growth was observed below the MIC, and no growth was observed above the MIC. A 52 % change in the sensor signal (i.e. rotational period) was observed

within 15 minutes, thus allowing AST measurements to be performed potentially within minutes.

3.2 Introduction

The emergence and spread of antibiotic resistance is a global health concern, as pathogenic species increasingly adapt to antimicrobial agents and classes.[1] Standard antimicrobial susceptibility testing (AST) protocols typically take over 24 hours for a full analysis; as a result, patients are often prescribed empiric therapies prior to diagnosis.[2] Incorrect empiric therapies, such as the inadequate, inappropriate, or overly broad-spectrum use of antimicrobial agents[3] result in poor patient response and contribute to the increase in multi-drug resistant pathogens. Decreasing the use of unnecessary antibiotics and treating patients with narrow-spectrum agents will help confront this global problem.[3] One approach towards this goal is through the development of rapid AST for earlier diagnosis. Earlier diagnosis will enable more appropriate therapies to be prescribed,[4,5] reduce antibiotic use,[4] and may lead to more effective treatments.[6,7] Subsequently, early diagnosis will reduce health care costs, length of hospital stays, and the spread of antimicrobial resistance.[5]

Traditional methods of microbial identification and differentiation of the infectious organisms rely on phenotypic characteristics, such as morphology and growth. However, molecular diagnostic techniques are increasingly used as adjuncts in clinical AST.[8] These diagnostic techniques, in particular the polymerase chain reaction (PCR), enable rapid detection of pathogen-derived nucleic acids in clinical specimens, thereby reducing identification and diagnosis to a few hours.[9] However, molecular methods are typically more expensive than phenotype-based assays; genetically identical bacteria may

exhibit phenotypic heterogeneity potentially leading to inappropriate treatments,[10] and only a few resistance genes have been firmly associated with phenotypic resistance.[11] Ultimately, phenotype-based methods, specifically those that determine the minimum inhibitory concentration (MIC) of the infectious organism, remain the 'gold standard' for clinical AST.[12] Currently, rapid clinical AST measurement tools utilize the growth-based microdilution technique (incorporated by the various commercially available AST systems) to determine the MIC, which is defined as the lowest antibiotic concentration that inhibits visible growth after overnight incubation. Nevertheless, the complete AST protocol, from pathogen isolation to MIC determination, takes well over 24 hours due to the combination of the long culture time (18-24 hours) and the AST measurement time (requiring 6-24 hours). Towards the goal of achieving faster AST measurements, there is a need for the improvement of optical detection methods and/or the development of new approaches to detect microbial proliferation.[11,13]

Microfluidic technologies have been used to reduce the turnaround time for AST, specifically in determining the MIC for infectious bacterial populations. By confining single or small cell populations of bacteria in nanoliter volume droplets, the effective concentration of cells in a system increases.[14] Furthermore, droplet systems are not subjected to dilution effects that are apparent in bulk systems; as a result, cellular biochemical signals or reaction products accumulate in the droplet more rapidly.[14] Using a microfluidic droplet system, the MIC values for *Staphylococcus aureus* cells that were exposed to antibiotics were obtained within 7 hours by measuring the accumulation of a fluorescence viability indicator.[14] Another microfluidic approach confines cells in gas-permeable microchannels with high surface-to-volume ratios, which increases oxygen

diffusion into the system.[2] Increased levels of oxygen available to the cells resulted in faster replication rates, and bacterial cells accumulated in the channels more rapidly.[2] *Escherichia coli* bacteria exposed to antibiotics were cultivated in these high surface-to-volume microfluidic channels, allowing AST measurements based on the turbidity of the sample to be obtained within 2 hours from the start of cultivation.[2]

Asynchronous magnetic bead rotation (AMBR) is a recently-developed technique that has found many applications as biosensors, specifically in bacterial cell and analyte detection.[15,16] These AMBR biosensors are based on the concept that a magnetic bead that is placed within an external rotating magnetic field has a unique rotational frequency; changes in this magnetic bead's physical properties (i.e. shape and volume), or changes in its environment (i.e. viscosity), result in detectable changes in the bead's rotational rate.[17] For instance, a bare magnetic bead within a rotating magnetic field has a unique rotational rate; when bacteria bind to the bead, the increased volume of the bead complex results in a decrease in the rotation of the bead.[15] Similarly, a modified form of the described method, known as label-acquired-magnetorotation (LAM), was used to measure the analyte concentration in solution by measuring the bead's rotational rate.[16] However, as experiments were conducted under bulk experimental conditions, the AMBR biosensors were subjected to bead translation and magnetic particle-to-particle interactions; as a result, the sensors were actively monitored and tracked, and solutions were highly diluted. Furthermore, the AMBR biosensors were limited to relatively short-term studies because the AMBR biosensor was sensitive to time-dependent effects that were caused by particle-surface adhesion and stiction effects,[17] both of which may reduce the efficiency or accuracy of the sensing system.

Here we report on a new diagnostic sensor platform in which individual AMBR biosensors are confined within nanoliter-sized water-in-oil (w/o) droplets for rapid antimicrobial susceptibility testing. Individual AMBR sensors in microfluidic droplets are suspended within a defined space, which allows for easy handling and more efficient measurements, and enables long-duration experiments, such as growth studies, as the beads are separated from the channel walls by a thin oil layer. In addition, enclosing AMBR biosensors in microfluidic droplets allows for the future extension of this platform towards a large-scale, parallel analysis system. For instance, a large array of AMBR sensors that are compartmentalized in droplets of unique chemical, biological, or physical conditions can be monitored continuously over long time-scales.

We apply the AMBR biosensor droplet microfluidic platform for monitoring the growth of bacterial cells at the single cell and small cell-population level and measure bacterial susceptibility to antibiotics. *E. coli* cells that are attached to magnetic beads were encapsulated in microfluidic droplets, and their rotations were monitored through time; as the viable cells grew, the bead's rotation consequently decreased. At the single cell level, heterogeneity studies or single cell kinetics studies become possible due to the high sensitivity of the system.[18] Moreover, for clinical AST testing, the collective cellular behavior is of interest, since cells act in a cooperative manner to provide protection, improve survival against competitors[19] and initiate quorum sensing.[20] We extend and apply this AMBR biosensor droplet microfluidic platform towards rapid AST, demonstrate its ability to measure bacterial growth response to antibiotics and determine the MIC value. Towards this end, the AMBR droplet microfluidic platform described here, when used at the small cell-population level, enables rapid measurement of changes

in bacterial cell growth in response to external factors. In particular, this system enables the growth response to gentamicin, an aminoglycoside antibiotic, for uropathogenic *E. coli* cells to be detectable within 15 minutes, as shown below.

3.3 Methods

3.3.1 Materials and Reagents

The following materials and reagents were used. PCR grade mineral Oil, Span® 80, and Bovine Serum Albumin (BSA) were purchased from Sigma-Aldrich Corp (St. Louis MO). Dulbecco-PBS was purchased from Invitrogen (Carlsbad CA). Mueller Hinton II (MH Broth) was purchased from Teknova (Hollister CA). Dispense tips, syringe barrels, and a barrel adapter kit were purchased from Nordson, EFD (East Providence RI). Pluronic F-68 was purchased from MP Biochemicals (Santa Ana CA). The Tygon Silicon Tubing (02-587-1D) was purchased from Saint-Gobain Performance Plastics (Aurora OH). Inlet/Outlet adapters were purchased from Small Parts Inc. (St. Logansport IN). The 8.8 μm streptavidin-coated superparamagnetic beads (8.8 ± 0.8 μm) were purchased from Spherotech, Inc. (Lake Forest IL), and Dynabead ® M-280 Streptavidin-coated superparamagnetic beads (2.8 ± 0.2 μm) were purchased from Invitrogen (Carlsbad CA).

The continuous phase consisted of mineral oil with 1 % Span® 80 (v/v). For bead characterization experiments, the aqueous phase consisted of PBS solution: PBS with 1% Pluronic F-68 and 0.1% BSA. For biological experiments, the aqueous phase consisted of MH broth solution: MH with 1% Pluronic F-68 and 0.1% BSA, which will be referred to as MH-PB.

3.3.2 Device Fabrication

Channel geometries were designed with LEdit. The procedure for the fabrication process, including the photolithography and wet chemical etching steps, on a glass wafer is detailed elsewhere.[21] Briefly, 50 nm Cr and 250 nm gold Au was deposited onto a 4" borosilicate glass wafer (Precision Glass & Optics, Santa Ana CA). The wafer was patterned and the glass channels were etched in CMOS grade hydrofluoric acid (49%) (J. T. Baker, Philipsburg NJ) to a depth between 45 μm and 50 μm, as measured with a surface profilometer. The photoresist and metal layers were removed, the glass wafer diced to obtain individual devices, and inlet and outlet holes were electrochemically drilling. The devices were cleaned in Piranha solution (2:1 solution of sulfuric acid and hydrogen peroxide, respectively) and subsequently coated with a 2 μm layer of Parylene-C (PDS 1020 Labcoater, Specialty Coating Systems, Indianapolis IN). The devices were UV-glued to a standard No. 0 cover glass slide (Goldseal cover glass Thickness #0 260320; Tedpella, Redding CA), and inlet and outlet ports were UV-glued to the device. A simplified schematic of the fabrication process is outlined in **Figure 3-1**(a), and the assembled glass microfluidic droplet device is shown in **Figure 3-1**(b).

3.3.3 Set-up and Operation

Experiments were conducted on an Olympus IX71 inverted microscope. The microfluidic device was placed inside custom-built electromagnet coils that were integrated on the microscope stage [**Figure 3-1**(c)]. The rotating magnetic field was generated with a custom LabView (National Instruments, Austin TX) program and data acquisition board (NI PCI-6221; National Instruments, Austin TX). The magnetic field driving frequency range was 0.1 Hz to 1 kHz, and the magnetic field strength at the

region of interest, e.g. microchannel, was 0.9 mT, as measured with a 3-axis magnetic field probe (C-H3A-2m; Senis GmbH, Switzerland).

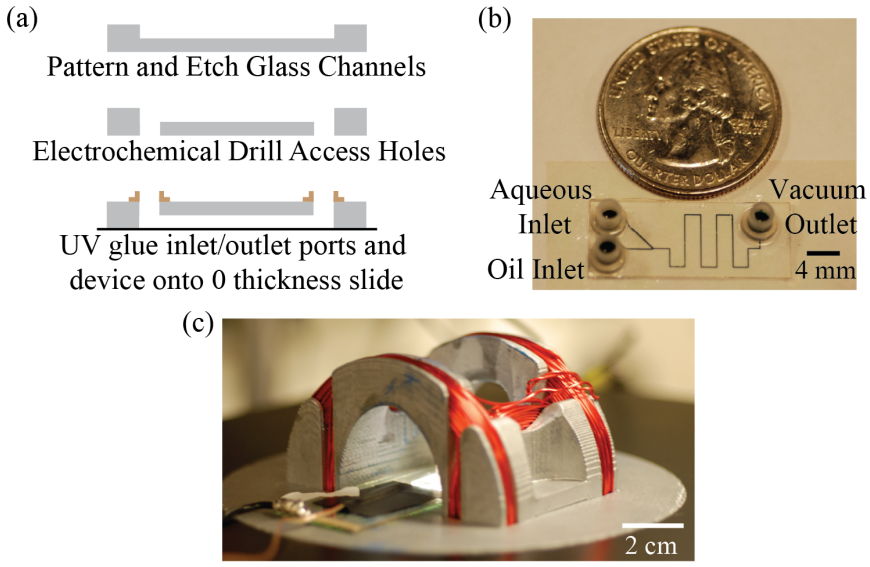

Figure 3-1. (a) Microfluidic glass channels were patterned and etched using standard glass lithography. (b) Image of the microfluidic droplet device. (c) A picture of the microfluidic device inside the electromagnet coils, which generate a rotating magnetic field at its core.

Bead characterization experiments and the preliminary experiments for the single cell growth measurements were conducted at room temperature (21 $\pm$ 2 °C), with a 100X oil immersion objective. The magnetic field driving frequency was set at 500 Hz for control and growth experiments. One-minute videos at 15 frames per second (fps) were taken in 5-minute intervals with a digital camera. Small cell-population experiments were conducted at near physiological temperatures, 35 $\pm$ 0.2 °C, with a 40X objective. The microfluidic device was placed on an ITO slide (SPI Supplies, West Chester PA) that was heated from room temperature and maintained at a set temperature, 35 $\pm$ 0.2 °C. This temperature was monitored by a thermocouple that was coupled to the surface of the slide with a thermally conducting silver paste, Arctic Silver 5 (Arctic Silver Incorporated,

Visalia CA). The magnetic field driving frequency for small cell-population control and growth experiments was set at 50 Hz, and continuous 2 fps videos were taken for a minimum of 5 hours. For small cell-population control and antibiotic response experiments, 1-minute videos were taken at 20 fps in either 5-minute or 20-minute intervals.

3.3.4 Data Acquisition and Analysis

Movies were captured with a digital camera (piA640-210gm; Basler Inc, Exton PA). The videos were analyzed using ImageJ – see **Figure 3-2**(a). The rotational frequency of the bead complex was determined by monitoring the fluctuations in intensity profile at the target area of interest using ImageJ's 'plot z-axis profile' functionality. This intensity plot was analyzed by applying a Fast Fourier Transform (FFT) to the raw ImageJ data in MATLAB. The experimental error in determining the rotational period was designated as the FFT peak's full width at half max (FWHM) of the amplitude signal.[22]

3.3.5 Droplet Formation

To further increase channel hydrophobicity, the channels were treated with Rain-X® Original Glass Treatment (SOPUS Products, Houston TX) prior to experiments; 10 μL of Rain-X was pipetted into the outlet reservoir, and the channel's inherent hydrophobicity resulted in the solution rapidly filling the channels. The Rain-X solution was allowed to stay in the devices for 10 minutes, after which vacuum was applied at the outlet by a vacuum pump (Rocker 300; Lab Depot Inc, Dawsonville GA) until the channels were replaced by air. Then, the continuous phase (mineral oil) and 10 μL of aqueous phase were introduced at their respective inlet reservoirs; the continuous phase

wetted the channel walls and fully entered the channels. The hydrostatic pressure applied at the inlet of the continuous phase was controlled by adjusting the pressure at the inlet, i.e. the height of the oil reservoir. To create droplets of approximately 0.5 – 1 nL in volume – see **Figure 3-2**(b), the vacuum strength was set between 70 kPa to 90 kPa and the hydrostatic pressure of the continuous phase was set between 1.2 kPa and 1.9 kPa.

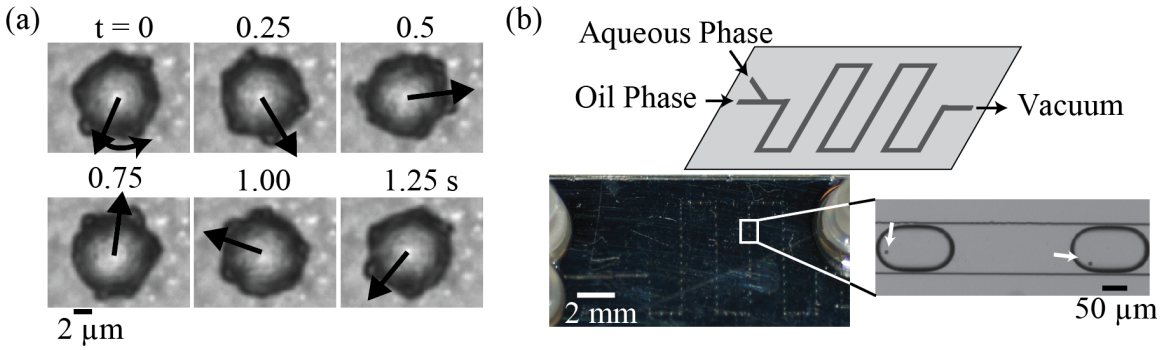

Figure 3-2. (a) Optical microscopy image of an 8.8 μm magnetic bead rotating asynchronously with an external rotating magnetic field at a 50 Hz driving frequency, bead rotational rate being much lower (0.8 Hz). Visual aid is provided to observe the bead rotation. (b) Droplets of 0.5 nL to 1 nL in volume were formed by applying a vacuum at the outlet and applying hydrostatic pressure at the oil inlet. A microfluidic device of this design holds between 50 and 75 droplets.

3.3.6 Bacterial Growth in Droplets

The streptavidin coated M-280s and 8.8 μm magnetic beads were incubated with biotinylated anti-*E. coli* (ab20640-1; Abcam Cambridge UK) at 37 °C for 2 hours on a shaking platform at 175rpm. A uropathogenic clinical *E. coli* isolate was grown on Muller-Hinton agar plates (BD Diagnostic Systems, Franklin Lakes NJ) at 37 °C for 16 to 18 hours. A 2 mL vial of MH broth was inoculated with bacteria to a 0.5 McFarland standard (approximately 1.5 x 10^8 CFU/mL). Anti *E. coli* functionalized magnetic beads, M-280 beads for single-cell growth experiments and 8.8 μm magnetic beads for small cell-population growth experiments were introduced to the bacteria solution, and the

sample was incubated at 37 °C for 1.5 hours in a 1.5 mL microcentrifuge tube on a shaking platform at 175 rpm. This allowed the bacteria to bind to the beads and enter the exponential phase. The bacteria-bound beads were isolated with a magnetic separator (PickPen 1-M; Sunrise Science Products, San Diego CA), washed in MH broth twice and re-suspended into MH-PB.

For experiments in which bacteria were fixed with glutaraldehyde, an MH broth solution with 0.5 % glutaraldehyde was used. Bacteria-bound beads were isolated with a magnetic separator, washed twice and re-suspended into MH-PB with 0.5 % glutaraldehyde solution (Sigma-Aldrich, St. Louis MO).

3.3.7 Bacterial Antibiotic Response

Gentamicin solution (Sigma-Aldrich, St. Louis MO) serial dilutions were prepared in MH-PB broth at concentrations of 4, 16, and 32 µg/mL, and aliquots were stored refrigerated at 4 °C. Before each experiment, the antibiotic solution was diluted to their final concentrations of 0.5, 2, and 4 µg/mL, respectively, by adding 350 µL MH broth experimental solution to the 50 µg/mL of the initial gentamicin aliquot solutions. The bacteria-bound beads were isolated with a magnetic separator, washed twice, and re-suspended into the antibiotic solution. Experiments started within 20 minutes of antibiotic exposure.

3.3.8 Clinical Vitek2® Testing

Reference MIC values were measured for the uropathogenic *E. coli* isolate using the VITEK 2 XL (bioMérieux, Inc., Durham NC) automated antimicrobial susceptibility testing platform in a clinical setting.

3.4 Results and Discussion

3.4.1 Device Characterization

Compartmentalizing single magnetic beads in water droplets suspended in oil reduced bead-to-bead magnetic interaction effects, bead-to-surface interaction effects, and prevented the bead from translating out of the field-of-view. The applied vacuum pressure at the outlet and the applied pressure at the inlets determined the resultant droplet size. For the following experiments, the droplets ranged from 0.5 to 1 nL in volume. The current device design accommodated between 50 and 70 droplets [**Figure 3-2**(b)]. For single magnetic bead experiments, we maximized the number of droplets containing a single magnetic bead; the encapsulation process follows Poisson statistics, which can be expressed by $(\lambda, n) = \frac{\lambda^n e^{-\lambda}}{n!}$, where $f(\lambda, n)$ is the frequency of observing a droplet containing *n* beads at a given λ value, and λ is the expected average number of beads per droplet (e.g. $\lambda = 1$, if 1 mL droplets were formed from an aqueous solution at a concentration 1 bead/mL). Droplets were formed from aqueous solution of 8.8 μm bead at the following concentrations: 1 x 10^5, 5 x 10^5, 1 x 10^6, and 5 x 10^6 beads/mL, and the number of beads observed in each droplet was counted. The data was fitted with the Poisson distribution, and the corresponding Lambda values were found to be 0.043, 0.43, 0.75, and 3.2 [**Figure 3-3**]. Using an initial concentration of 1 x 10^6 beads/mL ($\lambda = 0.75$), we obtained single beads in 35 % of the droplets formed.

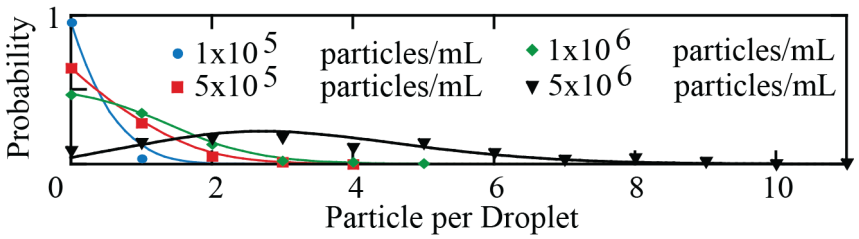

Figure 3-3. (a) The frequency of the number of beads per droplet with various particle concentrations. The data is fitted to the Poisson model.

The frequency-dependent rotational responses of the 8.8 µm and M-280 magnetic beads isolated in individual droplets were characterized with AMBR at driving frequencies between 0.1 Hz and 1 kHz. The rotational behavior of the 8.8 µm beads was dominated by its permanent dipole for frequencies up to 1 kHz, whereas the rotational behavior of the M-280 beads was dominated by its permanent dipole at frequencies below 10 Hz and by its induced dipole above 10 Hz [**Figure 3-4**(a)]. The rotational responses of fifty plain 8.8 µm magnetic beads were observed at 50 Hz driving frequency [**Figure 3-4**(b)], and the average rotational period was determined to be 2.12 ± 0.62 s, resulting in a magnetic responsiveness variability of 30 %. Similar variability in magnetic responsiveness has been reported previously.[23]

Under controlled environmental conditions, the rotational rate of a magnetic bead is expected to be time-independent. The rotational periods for single 8.8 µm beads and single M-280 beads were monitored for 2 hours. The rotational response varied by 5 % for the 8.8 µm beads and by 3 % for the M-280 beads, as shown in **Figure 3-4**(c). The sensitivity of the system was taken to be the minimum effective volumetric change needed to observe a change in the bead's rotational response (greater than the 5 % experimental error observed for the 8.8 µm beads and the 3 % experimental error observed for the M-280 beads, see above), corresponding to 0.09 µm sensitivity for

8.8 µm beads, and 0.03 µm sensitivity for the M-280 beads. Since the bead sensitivity was largely dependent on the initial bead diameter, the size choice of the magnetic bead is application dependent.[22]

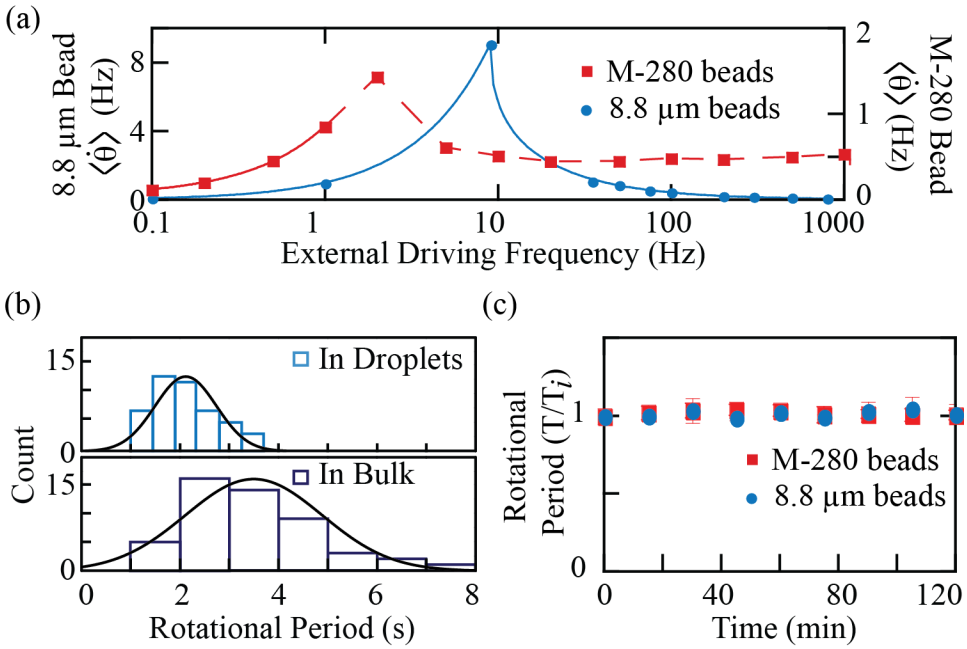

Figure 3-4. (a) Frequency-dependent rotational response curves at driving frequencies between 0.1 Hz and 1000 Hz. The solid line represents the rotational response dominated by a permanent dipole; the dotted lines connect the data to aid in visualization. (b) Rotational response of fifty 8.8 µm beads in 50 Hz driving field in droplets (top) and on glass surface (bottom) with 10^6 beads/mL concentration. The rotational period for beads in droplets was calculated to be 2.11 $\pm$ 0.62 s, providing a coefficient of variation of 30%. The beads on glass surface are subject to magnetic and surface interactions; as a result, the average rotational period was 3.5 $\pm$ 1.4 s, (40 % CV). The data is fitted to the normal distribution. (c) Normalized rotational response of 8.8 µm magnetic beads at a driving frequency of 50 Hz for 120 minutes under constant environmental conditions.

3.4.2 Theory of Magnetic Bead Rotation

The rotational response of a magnetic bead, when placed within an external rotational magnetic field, is frequency dependent and is governed by its permanent or induced magnetic dipole. A magnetic bead with a permanent magnetic dipole, in a rotating magnetic field with a frequency of Ω will have an average rotational frequency

of $\langle\dot{\theta}\rangle = \Omega$, $\langle\dot{\theta}\rangle = \Omega$when $\Omega < \Omega_c$, and $\langle\dot{\theta}\rangle = \sqrt{\Omega^2 - \Omega_c^2}$, when $\Omega > \Omega_c$, where the critical frequency $\Omega_c = mB/\kappa\eta V_H$ $\Omega_c = mB/\kappa\eta V_H$,[17,24] where m is the bead's magnetic moment, B is the magnetic field amplitude, κ is the shape factor (6 for a sphere), η is the dynamic viscosity, and V_H is the hydrodynamic volume of the rotating body.[17,24,25] When $\Omega > \Omega_c$, information about the magnetic bead complex or the external environment can be calculated by observing its rotational rate.[26] For experimental conditions in which m, B, and η are constant, Ω_c is inversely proportional to κ and V_H, which we define as the effective volume, $V_{eff} = \kappa V_H$ as shown by

$$\langle\dot{\theta}\rangle = \sqrt{\Omega^2 - \left(A/V_{eff}\right)^2} \qquad [3\text{-}1]$$

where $A = mB/\eta$ $A = mB/\eta$ is a constant.

For magnetic beads with an induced dipole, the bead's rotational frequency is $\dot{\theta} = (\chi'' B^2 V_m)/(\mu_0 \eta \kappa V_H)$, where χ'' is the imaginary susceptibility of the bead, V_m is the volume of the magnetic content of the bead, and μ_0 is the permeability of free space.[18,27] For experimental conditions in which η, B, χ'', μ_0, and V_m are constant, the rotational rate of the bead is expressed by

$$\dot{\theta} \propto {}^{1}/_{\kappa V_H} \propto {}^{1}/_{V_{eff}}. \qquad [3\text{-}2]$$

In summary, the changes in the effective volume for beads can be observed by measuring changes in the rotational rate for particles with either a permanent or induced magnetic dipole.

3.4.3 Single Bacterium Growth

Monitoring single cell growth with high sensitivity without the influence from neighboring cells is of interest in scientific and clinical applications such as cell

heterogeneity,[10,28] bacterial persistence[10] and cellular kinetics. M-280 magnetic beads were used to monitor single bacterium growth and division events, as smaller beads are more sensitive to monitoring smaller cell volumetric changes. The average size of an *E. coli* bacterium is 2 μm in length and 0.5 μm in diameter, which is comparable in size with a M-280 magnetic bead. In this system, nanometer growth was detectable by measuring changes in the bead's rotational response.[22]

The schematic of the growth and division process for a single bacterium at room temperature (21 $\pm$ 2 °C) is presented in **Figure 3-5**(a). The corresponding changes observed with light microscopy and rotational response measurements are shown in **Figure 3-5**(b,c), and are in good agreement. Since the effective volume is dependent on the shape factor and the volume of the rotating body (AMBR biosensor), the time at which a substantial change can be observed depends largely on the orientation of the bacteria on the bead. For the case in which the bacterium was bound at one end and grew perpendicularly to the magnetic bead [**Figure 3-5**(a,b)], a 17 $\pm$ 1 % change in the rotational period was observed within 5 minutes [**Figure 3-5**(c)], which is above the experimental error of 3 %. From the time at which the rotational rate was first monitored until the time at which the bacterium divided (103 min), the rotational period increased by 400 %.

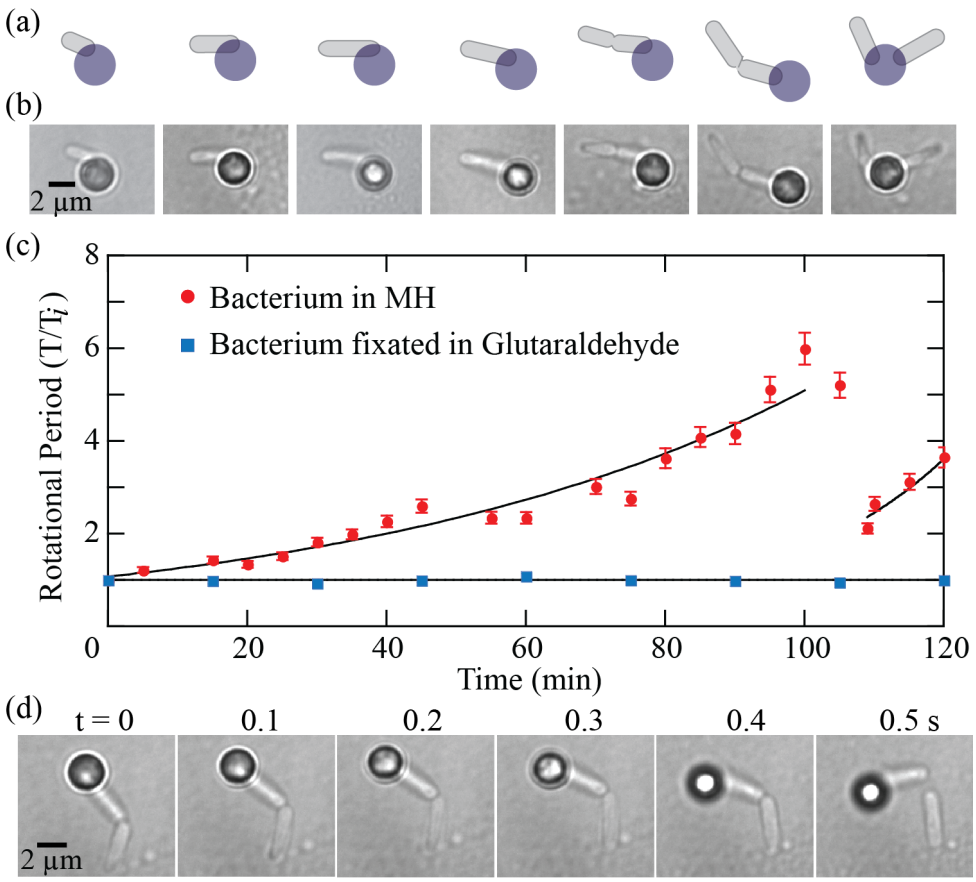

Figure 3-5. Single cell growth measurements using the AMBR sensor. (a) A schematic representation of bacterial growth and division at select time points, which corresponds to (b) light microscopy images of bacterial growth and division. (c) The rotational period of the bead and bacteria complex (AMBR biosensor) shown in (b). At the point of division, at 103 minutes, the rotational period decreases, as the effective volume of the biosensor is substantially reduced. The data, of each bacteria generation, is fitted by an exponential curve. The error bars represent the measurement error. (d) Optical microscopy image sequence of the bacteria division process at time 103 minutes.

The substantial drop in rotational period (reduction in the sensors effective volume) that was observed at 103 minutes corresponded with bacterial division. As a control, a single bacterium that was attached to a magnetic bead was fixed with glutaraldehyde and the rotational response was measured. No substantial change in the bead's rotational period was observed in 2 hours, which indicated a lack of growth [**Figure 3-5**(c)]. As a result, we concluded that the observed changes in the rotational

period of the AMBR sensor were indeed due to the growth, or elongation, of a single bacterial cell. These findings correspond well with a previous study on single cell growth with AMBR biosensors.[22]

3.4.4 Small Cell Population Growth

To monitor small cell-population growth, 8.8 μm magnetic beads were used since the larger surface area provided greater binding capacity. Experiments were conducted at near physiological conditions, 35 ± 2 °C, and therefore, bacteria replication time was substantially reduced as compared to the single cell growth experiments. The growth of a small population of bacterial cells attached to a bead was measured with AMBR, as shown in **Figure 3-6**(a). As the bacteria grew and divided, some daughter cells re-attached to the magnetic bead and some remained detached, free-floating in the solution [**Figure 3-6**(a)]. Daughter cells that re-attached to the bead increased the bead's effective volume, which was observed by an increase in the rotational period [**Figure 3-6**(b)]. An 8 ± 0.3% average increase in the rotational period was detected after 5 minutes, which is above the 5 % experimental error [**Figure 3-6**(a,b)]. As a result, the concentration of bacteria in the liquid environment exponentially increased. To ensure that the initial increase in rotational period was indeed a result of growth, the rotational period was monitored for bacteria-bound beads that were fixed with glutaraldehyde. A 3% variation in rotational period was observed for fixed bacteria, which was consistent with the control experiments for beads without bacteria. Therefore, the measured changes in the rotational period are attributed to bacterial growth.

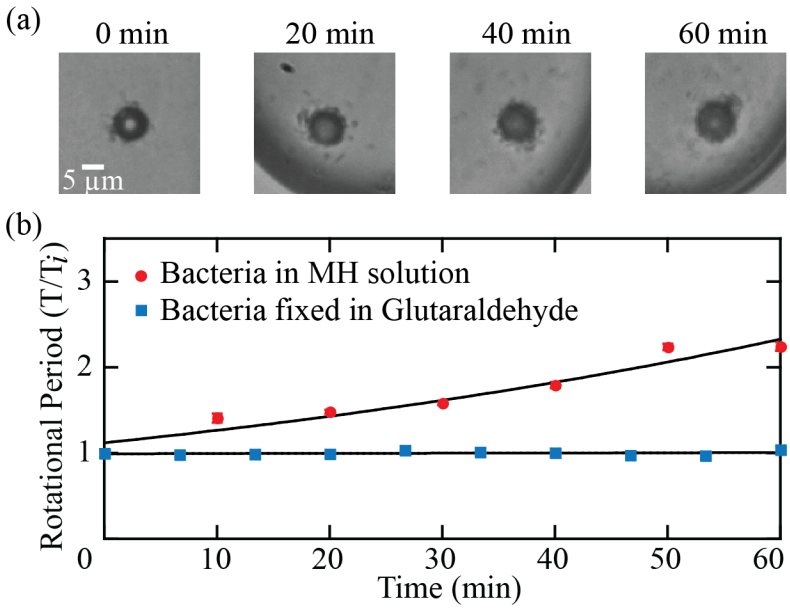

Figure 3-6. Small cell-population growth and susceptibility measurements using the AMBR sensor. (a) Optical microscopy images of small cell-population growth on an 8.8 µm magnetic bead in MH-PB solution. (b) The rotational period of the 8.8 µm bead corresponding to the figures above (red circles), and bacteria that have been fixed in glutaraldehyde (blue squares). The data is fitted with an exponential curve.

3.4.5 Small Cell-Population Growth Response to Gentamicin

The AMBR droplet microfluidic platform was tested with respect to AST applications by measuring the growth response of a small population of uropathogenic *E. coli* towards gentamicin, a bactericidal antibiotic that interrupts protein synthesis. The effects of the antibiotics on the growth of the bacteria could be discerned within an hour. Bacteria bound to 8.8 µm beads were grown in 0, 0.5, 2, and 4 µg/mL concentrations of gentamicin, and the rotational periods of the beads were monitored for a minimum of one hour. Data for the first 60 minutes are presented in **Figure 3-7**. An increase in rotational period was observed for the bacteria cultured in 0 and 0.5 µg/mL gentamicin, which indicates bacterial growth. No substantial change in the rotational period was observed for the bacteria cultured in 2 and 4 µg/mL gentamicin, which suggests a lack of growth.

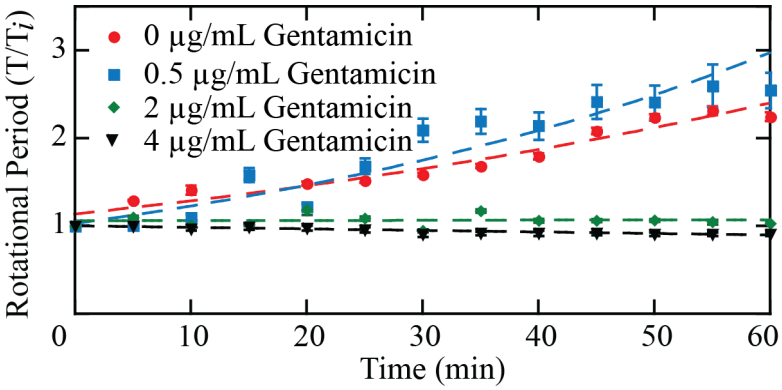

Figure 3-7. Averaged rotational responses from 3 separate experiments, each of 0 µg/mL and 0.5 µg/mL and 2 separate experiments, each of 2 µg/mL and 4 µg/mL gentamicin. The MIC, as determined by the Vitek2, is 1 µg/mL. Bacteria treated with gentamicin concentrations below the MIC continued to grow, whereas bacteria treated with concentrations above the MIC did not show noticeable growth. The difference is evident within 15 min. Data sets are fitted to an exponential curve. The error bars represent the measurement error.

The estimated MIC as determined with AMBR is consistent with the MIC value of 1 µg/mL, as determined with the Vitek 2 system. A 100% difference in the rotational period between bacteria that were treated with gentamicin above and below the MIC was measured within 30 minutes. After only 15 minutes a 52% difference in the rotational period was observed. The rotational trend observed for bacteria treated with gentamicin above the MIC was indeed similar to the results for bacteria fixed with glutaraldehyde. With the presented AMBR microfluidic droplet platform, the effects of an antibiotic on bacterial growth can be discerned within 30 minutes (15 minutes for sample preparation and 15 minutes for AST measurements). The high sensitivity of this method and the highly parallel nature of microfluidics suggest a promising future potential of this AMBR microfluidic droplet platform sensor towards rapid MIC measurements.

3.5 Conclusion

In this paper we demonstrated an AMBR biosensor microfluidic droplet platform that could have significant clinical importance in rapid AST, especially with the incorporation of high-throughput capabilities and portability. Large-scale analysis on single cells and small populations of cells is possible through the use of surfactants that allow droplets to be closely packed[29] or through structures that enable parallel experiments.[20] This will enable the study of cell heterogeneity and behavior at the single cell level and MIC tests to be conducted on the small cell population level. Microfluidic device technologies to study single cells[30,31] or small cell populations exist;[32,33] nevertheless, most phenotype-based systems are limited to direct microscope examination and analysis.[20] Cantilevers provide a non-microscopy, highly sensitive technique to measure growth,[34,35] but these systems require labor-intensive fabrication procedures, in addition to expensive and precisely controlled equipment.

In contrast, the AMBR biosensor platform is a potentially inexpensive, large-scale analysis system. For instance, the AMBR signal can be measured with a low-power laser and a photodiode combination; the light scattered by a rotating magnetic bead can be captured by a photodiode and subsequently analyzed.[36] AMBR biosensors can also be monitored using an inexpensive CMOS pixel array that is placed directly under the microfluidic platform.[37] The CMOS pixel array approach offers a highly parallel method for measuring the signal of multiple AMBR sensors concurrently, provided the magnetic bead is larger in size than a single pixel. Furthermore, optical detection methods may also be replaced with magnetic detection methods, such as magneto-resistive sensors, Hall sensors, or field coils.[18] Although in the present manuscript, the AMBR sensors used to

measure bacterial growth were monitored with optical microscopy, continuing development in large-scale AMBR detection methods would eliminate the need for microscope observations in future developments.

In summary, the presented AMBR microfluidic droplet platform enables single cell and small cell-population growth to be rapidly monitored; we demonstrated that this platform could be extended towards application for AST, in measuring MIC values. The droplets provide magnetic and hydrodynamic isolation between AMBR sensors and allow a single sensor to be monitored continuously for hours. Single cell growth and division events and small cell-population growth, in the absence and presence of antibiotics, was detected by measuring changes in the magnetic bead's rotational response; the results were verified with optical microscopy. We functionally characterized a uropathogenic clinical *E. coli* isolate's response to a gentamicin dose within 15 minutes and, based on such measurements on 4 doses, estimated the MIC to be between 0.5 to 2 μg/mL, a value that is consistent with clinical results. Further development of this platform, such as parallelizing the channels to conduct concurrent measurements on multiple antibiotic concentrations; close-packing the droplets to monitor multiple droplets;[31] and heating the system to physiological temperature, will enable a full AST analysis to be conducted in a single run. This would subsequently reduce the current standard phenotypic AST measurement time (6-24 hours) to within 15-30 minutes.

3.6 References

1. Martinez, J.L. et al. A global view of antibiotic resistance. *FEMS Microbiology Reviews* **33**, 44-65 (2009).

2. Chen, C.H. et al. Antimicrobial Susceptibility Testing Using High Surface-to-Volume Ratio Microchannels. *Analytical Chemistry* **82**, 1012-1019 (2010).

3. Schwartz, B. Preventing the spread of antimicrobial resistance among bacterial respiratory pathogens in industrialized countries: the case for judicious antimicrobial use. *Clinical Infectious Diseases* **28**, 211–213 (1999).

4. Kerremans, J.J. et al. Rapid identification and antimicrobial susceptibility testing reduce antibiotic use and accelerate pathogen-directed antibiotic use. *Journal of Antimicrobial Chemotherapy* **61**, 428 -435 (2008).

5. Barenfanger, J., Drake, C. & Kacich, G. Clinical and Financial Benefits of Rapid Bacterial Identification and Antimicrobial Susceptibility Testing. *J. Clin. Microbiol.* **37**, 1415-1418 (1999).

6. Gupta, K., Scholes, D. & Stamm, W.E. Increasing Prevalence of Antimicrobial Resistance Among Uropathogens Causing Acute Uncomplicated Cystitis in Women. *JAMA* **281**, 736-738 (1999).

7. Doern, G.V., Vautour, R., Gaudet, M. & Levy, B. Clinical impact of rapid in vitro susceptibility testing and bacterial identification. *J. Clin. Microbiol.* **32**, 1757-1762 (1994).

8. Goldman, E. & Green, L.H. *Practical Handbook of Microbiology*. (CRC Press: 2008).

9. Weile, J. & Knabbe, C. Current applications and future trends of molecular diagnostics in clinical bacteriology. *Anal Bioanal Chem* **394**, 731-742 (2009).

10. Balaban, N.Q., Merrin, J., Chait, R., Kowalik, L. & Leibler, S. Bacterial Persistence as a Phenotypic Switch. *Science* **305**, 1622-1625 (2004).

11. Jorgensen, J.H. & Ferraro, M.J. Medical Microbiology: Antimicrobial Susceptibility Testing: A Review of General Principles and Contemporary Practices. *Clinical Infectious Diseases* **49**, 1749-1755 (2009).

12. Andrews, J.M. Determination of minimum inhibitory concentrations. *Journal of Antimicrobial Chemotherapy* **48**, 5 (2001).

13. Jorgensen, J.H. & Ferraro, M.J. Antimicrobial Susceptibility Testing: General Principles and Contemporary Practices. *Clinical Infectious Diseases* **26**, 973-980 (1998).

14. Boedicker, J.Q., Li, L., Kline, T.R. & Ismagilov, R.F. Detecting bacteria and determining their susceptibility to antibiotics by stochastic confinement in nanoliter droplets using plug-based microfluidics. *Lab Chip* **8**, 1265 (2008).

15. McNaughton, B.H., Agayan, R.R., Clarke, R., Smith, R.G. & Kopelman, R. Single bacterial cell detection with nonlinear rotational frequency shifts of driven magnetic microspheres. *Appl. Phys. Lett.* **91**, 224105 (2007).

16. Hecht, A., Kinnunen, P., McNaughton, B.H. & Kopelman, R. Label-acquired magnetorotation for biosensing: An asynchronous rotation assay. *Journal of Magnetism and Magnetic Materials* **323**, 272-278 (2011).

17. McNaughton, B.H., Kehbein, K.A., Anker, J.N. & Kopelman, R. Sudden Breakdown in Linear Response of a Rotationally Driven Magnetic Microparticle and Application to Physical and Chemical Microsensing. *The Journal of Physical Chemistry B* **110**, 18958-18964 (2006).

18. Kinnunen, P. et al. Monitoring the growth and drug susceptibility of individual bacteria using asynchronous magnetic bead rotation sensors. *Biosensors and Bioelectronics* **26**, 2751-2755 (2011).

19. Shapiro, J.A. Thinking about bacterial populations as multicellular organisms. *Annu. Rev. Microbiol.* **52**, 81-104 (1998).

20. Weibel, D.B., DiLuzio, W.R. & Whitesides, G.M. Microfabrication meets microbiology. *Nat Rev Micro* **5**, 209-218 (2007).

21. Pal, R. et al. An integrated microfluidic device for influenza and other genetic analyses. *Lab Chip* **5**, 1024-1032 (2005).

22. Kinnunen, P., Sinn, I., McNaughton, B.H. & Kopelman, R. High Frequency Asynchronous Magnetic Bead Rotation for Improved Biosensors. *Applied Physics Letters* **97**, 223701 (2010).

23. Häfeli, U.O., Lobedann, M.A., Steingroewer, J., Moore, L.R. & Riffle, J. Optical method for measurement of magnetophoretic mobility of individual magnetic microspheres in defined magnetic field. *Journal of Magnetism and Magnetic Materials* **293**, 224-239 (2005).

24. Cēbers, A. & Ozols, M. Dynamics of an active magnetic particle in a rotating magnetic field. *Phys. Rev. E* **73**, 021505 (2006).

25. Korneva, G. et al. Carbon Nanotubes Loaded with Magnetic Particles. *Nano Letters* **5**, 879-884 (2005).

26. McNaughton, B.H., Agayan, R.R., Wang, J.X. & Kopelman, R. Physiochemical microparticle sensors based on nonlinear magnetic oscillations. *Sensors and Actuators B: Chemical* **121**, 330-340 (2007).

27. Janssen, X.J.A., Schellekens, A.J., van Ommering, K., van IJzendoorn, L.J. & Prins, M.W.J. Controlled torque on superparamagnetic beads for functional biosensors. *Biosensors and Bioelectronics* **24**, 1937-1941 (2009).

28. Dhar, N. & McKinney, J.D. Microbial phenotypic heterogeneity and antibiotic tolerance. *Current Opinion in Microbiology* **10**, 30-38 (2007).

29. Brouzes, E. et al. Droplet microfluidic technology for single-cell high-throughput screening. *Proceedings of the National Academy of Sciences* **106**, 14195-14200 (2009).

30. Wheeler, A.R. et al. Microfluidic Device for Single-Cell Analysis. *Analytical Chemistry* **75**, 3581-3586 (2003).

31. Di Carlo, D., Wu, L.Y. & Lee, L.P. Dynamic single cell culture array. *Lab on a Chip* **6**, 1445–1449 (2006).

32. Hung, P.J. et al. A novel high aspect ratio microfluidic design to provide a stable and uniform microenvironment for cell growth in a high throughput mammalian cell culture array. *Lab on a Chip* **5**, 44–48 (2005).

33. Gómez-Sjöberg, R., Leyrat, A.A., Pirone, D.M., Chen, C.S. & Quake, S.R. Versatile, Fully Automated, Microfluidic Cell Culture System. *Analytical Chemistry* **79**, 8557-8563 (2007).

34. Gfeller, K.Y., Nugaeva, N. & Hegner, M. Micromechanical oscillators as rapid biosensor for the detection of active growth of Escherichia coli. *Biosensors and Bioelectronics* **21**, 528-533 (2005).

35. Godin, M. et al. Using buoyant mass to measure the growth of single cells. *Nat Meth* **7**, 387-390 (2010).

36. McNaughton, B.H. et al. Compact sensor for measuring nonlinear rotational dynamics of driven magnetic microspheres with biomedical applications. *Journal of Magnetism and Magnetic Materials* **321**, 1648-1652 (2009).

37. Kinnunen, P. Asynchronous magnetic bead rotation (AMBR) for biosensors. *Ph.D. Thesis* (2011).

CHAPTER 4:

Asynchronous magnetic bead rotation (AMBR) micro-viscometer for rapid, sensitive and label-free studies of bacterial growth and drug sensitivity

4.1 Abstract

The long turnaround time in antimicrobial susceptibility testing (AST) endangers patients and encourages the administration of wide spectrum antibiotics, thus resulting in alarming increases of multi-drug resistant pathogens. A method for faster detection of bacterial proliferation presents one avenue towards addressing this global concern. We report on a label-free asynchronous magnetic bead rotation (AMBR) based viscometry method that rapidly detects bacterial growth and determines drug sensitivity by measuring changes in the suspension's viscosity. With this platform, we observed the growth of a uropathogenic *Escherichia coli* isolate, with an initial concentration of 50 cells per drop, within 20 minutes; in addition, we determined the gentamicin minimum inhibitory concentration (MIC) of the *E. coli* isolate within 100 minutes. We thus demonstrated a label-free, micro-viscometer platform that can measure bacterial growth and drug susceptibility more rapidly, with lower initial bacterial counts than existing commercial systems, and potentially with any microbial strains.

4.2 Introduction

Early diagnosis of microbial infections helps patients and helps address the global problem of the emergence and spread of antimicrobial resistance.[1–3] The current 'gold standard' for clinical antimicrobial susceptibility testing (AST) is a growth-based broth microdilution technique used to determine the minimum inhibitory concentration (MIC). The broth microdilution MIC is defined as the lowest antibiotic concentration that inhibits visible microbial growth after overnight incubation. In contrast to the traditional methods that require overnight incubation, modern and automated techniques can provide results in 6-24 hours, after the initial incubation and enrichment process. These long testing times lead to patients being prescribed empiric, wide spectrum therapies, which can result in poor patient response and, moreover, contribute to increases in multi-drug resistant pathogens.[4] As a result, there is a need for an AST method that can provide results within hours rather than days, enabling patients to be treated more rapidly and with more appropriate therapies,[5] while minimizing increases in drug resistant populations.[4,6–8] The ongoing goal of the authors is to develop an ultra-rapid technology that expedites and refines the use of antibiotics for patients with life-threatening bacterial infections, including outbreaks due to newly emerged antibiotic resistant strains. Nucleic acid tests (NAT), which detect resistant genes, are increasingly used as adjuncts for AST;[9] however, NAT lacks the ability to determine antibiotic MIC, differentiate mutant strains, or identify resistance of species, where resistance is expressed through many mechanisms (e.g. gram-negative bacteria).[7,8] As a result, phenotypic growth-based assays remain the gold standard for AST.[10,11]

Commercial automated phenotypic AST systems commonly use the *colorimetric turbidity-based broth microdilution technique* to measure bacterial proliferation. These AST systems require an initial bacteria count of at least 10^5 bacteria per antibiotic sample, i.e. test well, and take 6-24 hours to determine the MIC value; this still does not take into account the initial bacterial enrichment and isolation stage, which typically takes over 24 hours. There have been recent advancements towards reducing the detection time, by measuring bacterial metabolism,[12] by elongation and division of a single or small population of bacteria,[13,14] and by increasing the effective bacterial concentrations through confinement into smaller volumes.[2,12,14,15] Although these techniques can detect proliferation and determine susceptibility within hours, they often rely on microscopy (e.g. fluorescence microscopy) or specific-antibody based techniques.

Measuring environmental (e.g. change in viscosity) changes due to bacterial proliferation offers a versatile technique for measuring microbial growth without relying on antibodies or complex detection systems.[16–19] Bacteria in a planktonic state exhibit unique hydrodynamic and rheological properties that depend on bacterial species, concentration, and health.[20] For instance, directional motility of planktonic bacteria affects solution viscosity; specifically, contractile bacteria increase solution viscosity and extensile bacteria reduces solution viscosity.[17,19–22] The bacterial concentration and availability of oxygen and nutrients also affect solution viscosity through their effect on bacterial motility and polysaccharides secretion.[23–25] For example, a high concentration of bacteria in a suspension, such as biofilm-forming of quorum-sensing bacteria, secrete polysaccharides that are typically higher in molecular weight and more viscous;[26] these polysaccharides change the solution's rheology from Newtonian to viscoelastic and non-

Newtonian.[23] It has also been reported that the viscosity of a broth solution decreases upon proliferation, as bacteria ingest the large, viscous macromolecules within the broth.[16,18,27] Despite the variety of mechanisms that cause viscosity changes, our experiments, as described below, illustrate that bacterial proliferation alters the hydrodynamic and rheological properties of a suspension.

Here we report on an asynchronous magnetic bead rotation (AMBR) droplet microfluidic micro-viscometer that detects bacterial proliferation by measuring changes in the suspension's rheological properties. The AMBR sensor is a recently reported device that is based on monitoring the time-dependent *asynchronous* rotation of a magnetic bead that is within an external rotating magnetic field.[13,14,28–34] This sensor monitors the magnetic and physical properties of the magnetic bead and the environmental viscosity in which the bead resides.[13,14,29–35] Notably, only in the asynchronous regime can such parameters, including viscosity, be measured continuously by the magnetorotation frequency.[13,14,28–34] We apply this sensitive AMBR micro-viscometer towards rapid AST applications. The approach reported herein is a significant advancement over our previously reported antibody-based AST system as the AMBR micro-viscometry is a novel, label-free approach for measuring microbial growth and AST.[14] As a result, the AMBR micro-viscometer is a versatile platform that can be used with any bacterial strain. Furthermore, individual AMBR viscometers are encapsulated in microfluidic water-in-oil (w/o) nanoliter droplets,[14] which allows for AST to be performed with an initial bacterial count of 50, or fewer, cells per droplet. With the AMBR micro-viscometry, we successfully determined the gentamicin MIC of a uropathogenic *Escherichia coli* isolate within 100 minutes. Therefore, we have

demonstrated a label-free, AMBR micro-viscometer platform that can be used to perform rapid AST applications on any microbial strain. Furthermore, to perform AST, this platform requires 1000-fold fewer bacteria than commercial systems; this may further reduce the overall AST time, i.e. reduce the sample prep and enrichment time. This new system, as a tool that significantly reduces AST time, has the potential to help patients get prompt and focused drug treatment, as well as to combat the global threat of antimicrobial resistance.

4.3 Methods

4.3.1 Device Fabrication

The fabrication process on a glass wafer is detailed elsewhere.[14,36] Briefly, 50 nm Cr and 250 nm Au were evaporated onto the wafer. After patterning, the microfluidic channels were etched with hydrofluoric acid to a depth of 40 – 45 μm, as measured with a surface profilometer. The metal layers were removed, devices diced, and inlets/outlet electrochemically drilled. The devices were cleaned in Piranha solution and subsequently coated with a 2 μm parylene layer. The devices were UV-glued to a standard cover glass slide, thickness No. 2 (Electron Microscopy Sciences), and the inlet and outlet ports (Small Parts, Inc.) were UV-glued to the device. The schematic and assembled microfluidic droplet device is shown in **Figure 4-1**(a). All used devices were recovered and re-used. Device recovery entails separating the glass device from the cover glass and inlet/outlet ports with methanol and heating devices to 410 °C for 2 hours. Used devices were cleaned in Piranha solution and the process above was repeated.

4.3.2 Magnetic Janus Particle Fabrication

The fabrication procedure for Janus particles is detailed elsewhere.[37,38] Briefly, 500 μL of 16 μm carboxyl magnetic particles (1% w/v) (Spherotech) were spin-coated onto a 4" glass wafer. A 50 nm layer of Al was evaporated onto the surface. The particles were recovered and suspended in PBS. The resultant Janus particles, which will be referred to as magnetic Janus particles, enabled better visualization of the particle's rotation (following the "MagMOON" principle)[28,37,39] at lowered magnification, enabling multiple AMBR sensors to be monitored concurrently. Non-specific binding was not observed, and the Al coating was not observed to affect bacterial cell growth.

Magnetically uniform Janus particles were fabricated using the process detailed above, with modifications. Rather, 300 nm of Ni was evaporated onto the 10 μm NIST polystyrene particles (Polysciences), the wafer was magnetized in a 60 mT permanent magnetic field for 3 days and the particles were recovered. The resultant Janus particles will be referred to as magnetically uniform Janus particles.

4.3.3 Particle Characterizations on non-specific binding.

10 μL of each of the 8.8 μm carboxyl-, amino-, and streptavidin-functionalized magnetic particles (Spherotech) were added to 1 mL of a 1 x 10^7 CFU/mL solution. The particles and bacteria were incubated at 37 °C on a shaking platform for 2 hours. After incubation, 10 μL of the solution was visualized with light microscopy to determine the degree of non-specific binding.

4.3.4 Experimental Procedure

The microfluidic device was flushed with Rain-X® Original Glass Treatment (SOPUS Products) for 5 minutes to increase surface hydrophobicity.[14] The continuous

phase and 15 μL of aqueous phase were introduced to their respective inlet reservoir. 1 nL w/o droplets were formed by adjusting the vacuum strength and hydrostatic pressure of the outlet and oil phase, respectively.

For characterization experiments, the aqueous phase consisted of MH-PB and the magnetically uniform Janus particles. For growth experiments, an MH-PB solution was inoculated with a clinical uropathogenic *E. coli* isolate to a 0.5 McFarland standard (~ 1.5 x 10^8 CFU/mL), and subsequently diluted to achieve approximately 50 bacteria per droplet. Magnetic Janus particles were added to the aqueous solution at a concentration to capture 1 particle per droplet. Antibiotic response experiments were conducted serially for the present system; the bacteria inoculated into a gentamicin solution, with final gentamicin concentrations of 0, 0.25, 0.5, 1, and 2 μg/mL. Experiments started within 30 minutes of antibiotic exposure.

The description of the experimental set-up is detailed elsewhere.[14] Briefly, the temperature was maintained at 37 $\pm$ 0.2 °C using a temperature-controlled ITO slide. This system was placed inside custom-built electromagnet coils, and the rotating magnetic field was generated with a custom LabView program. The magnetic field strength at the region of interest, e.g. droplet chamber, was measured to be 0.71 $\pm$ 0.03 mT, and the driving frequency was set at 200 Hz for experiments using magnetically uniform Janus particles. For growth experiments, the magnetic field strength at the region of interest was set at 2.4 $\pm$ 0.4 mT, with a driving frequency of 10 Hz.

For the growth experiments, continuous videos at 10 frames per second (fps) were taken over at least 3 hours. Videos were analyzed with ImageJ and MATLAB. Experiments were run in triplicates. The illustrated experimental error in the rotational

period is the full width half max (FWHM) of the Fourier transform of the raw rotational signal, and equal to the standard deviation of measurement where appropriate, of a representative run.[28]

4.4 Results and Discussion

4.4.1 AMBR Microfluidic Viscometer

Bacterial growth and AST were performed on a microfluidic device platform [**Figure 4-1**(a,b)], in which individual AMBR biosensors were encapsulated into nanoliter volume droplets [**Figure 4-1**(c)]. As bacteria in their planktonic state grow and divide in the surrounding solution [**Figure 4-1**(d)], the viscosity of the AMBR complex changes, which is detected by a measurable shift in the bead's rotational frequency [**Figure 4-1**(e)].

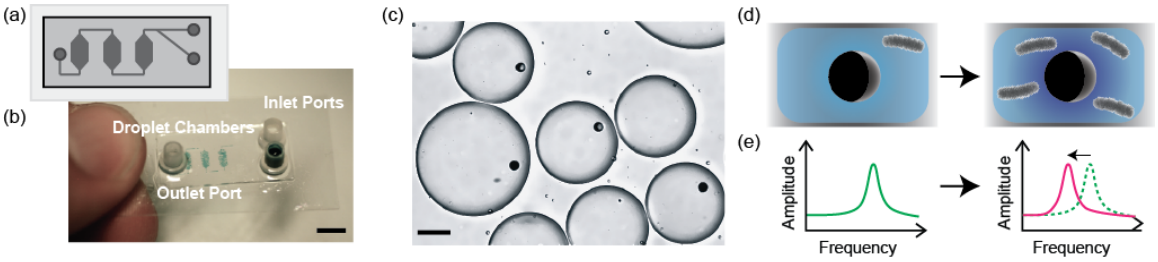

Figure 4-1. AMBR micro-viscometer platform for cell proliferation studies. (a) Schematic and (b) assembled microfluidic droplet device. The chambers are filled with droplets dyed with blue food coloring. Scale bar: 5 mm (c) Light microscopy image of individual AMBR viscometers compartmentalized in nanoliter w/o microfluidic droplets. Scale bar: 50 µm. (d-e) Schematic of AMBR viscometer. (d) Bacterial growth in the surrounding solution changes the solution viscosity, which (e) shifts the particle's rotational frequency.

4.4.2 Concept of the Asynchronous Magnetic Bead Rotation (AMBR) Viscometer

The theory behind the AMBR biosensor is detailed elsewhere.[13,31] In general, AMBR is meant to describe a rotating magnetic bead system that rotates in an asynchronous fashion and can be used to monitor analyte. For the ferromagnetic system

described here, the underlying behavior is as follows. When a magnetic particle is placed within an external rotating magnetic field, the average rotational frequency of the particle, $\langle\dot{\theta}\rangle$, is dependent on the driving field frequency, Ω. For magnetic particles with a permanent magnetic dipole, the external-field dependent rotational response of the bead is

$$\langle\dot{\theta}\rangle = {}^{1}/_{T} = \begin{cases} \Omega - \sqrt{\Omega^2 - \Omega_c^2}; & \Omega < \Omega_c \\ \Omega; & \Omega > \Omega_c \end{cases}; \quad \Omega_c = mB/\eta V_{eff}. \qquad [4\text{-}1]$$

Here Ω_c is the rotational critical frequency, m is the particle's magnetic moment, B is the magnetic field amplitude, η is the solution viscosity, and V_{eff} is the effective volume of the rotating body (which depends on both its volume and shape; for a spherical shape, it is 6 times the volume).[31] In order for the AMBR sensor to behave as a viscometer, the magnetic bead must be torqued at driving frequencies that are higher than the critical frequency; also, m, B, and V_{eff} must be held constant, such that the particle's rotational rate is solely dependent on the viscosity of the solution.[30,31] We also note that while the particle's rotation in this asynchronous regime is not in a steady-state, its *average* rotation frequency $\langle\dot{\theta}\rangle$ is well defined by **Equation 4-1**. The authors note that in principle, the described method will work with other types of magnetic beads, such as paramagnetic beads. For paramagnetic AMBR systems, the rotational period depends inversely on viscosity, namely $\langle\dot{\theta}\rangle \propto 1/\eta$.

4.4.3 AMBR viscometer characterization

The AMBR viscometer accurately measures temperature-dependent changes in the viscosity. To demonstrate this with the current system, a solution of PBS was heated from 34 – 46 °C, at 2 °C increments; increasing the solution temperature decreases

suspension viscosity, which consequently decrease the bead's rotational period – see **Equation 4-1** [**Figure 4-2**(a)].

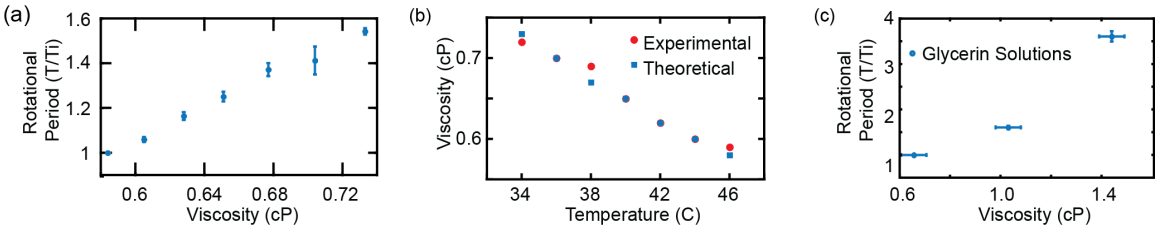

Figure 4-2. AMBR micro-viscometer characterization. (a) Viscosity-dependent rotational response characterization of the AMBR viscometer sensor in the PBS buffer solution at different temperature values (34 to 46 °C). (b) The corresponding experimental and theoretical temperature-dependent viscosity values, as calculated with **Equation 4-2**, at temperature values ranging from 34 to 46 °C in PBS solution. (c) Rotational response of the AMBR viscometer in glycerin solutions at different viscosities at 37 °C. Magnetically uniform Janus particles were used for all characterization experiments.

To validate these measurements, we calculated the viscosity of the PBS solutions at different temperature conditions using **Equation 4-1**, given that the $m \sim 5.6 \times 10^{-16}$ Am^2, B = 0.7 mT, $V_{eff} = 3.14 \times 10^{-15}$ m^3 and from the bead's rotational rate. The viscosity of the solution can be determined from $\eta = v_w(T)/\rho(T)$, where

$$\ln(v_w(T)) = 0.55908 - 0.03051T + 0.00015T^2,^{40} \qquad [4\text{-}2]$$

where $v_w(T)$ is the temperature-dependent viscosity and $\rho(T)$ is the temperature-dependent density of PBS. As shown in [**Figure 4-2**(b)], the viscosity measurements from AMBR agree with expected values that were calculated with **Equation 4-2**. In addition, the AMBR sensor accurately measured the viscosity of various aqueous PBS-Glycerin solutions, at different glycerin concentrations, at a constant temperature [**Figure 4-2**(c)]. This agrees with what was reported in Ref 24. As a result, the AMBR viscometer was demonstrated to function accurately as a viscometer within the viscosity range

between 0.58 – 1.5 cP, which is sufficient to measure microbial growth within the experimental ranges described in this paper.

For use with bacteria, the AMBR particles must be passivated to eliminate the potential for bacterial binding to the particle. Particles functionalized with either carboxyl, amino, or streptavidin groups were incubated with the uropathogenic *E. coli* to determine the extent of non-specific binding. The magnetic particles that were functionalized with carboxyl-groups appeared to have little to no non-specific binding. In contrast, the amino- and streptavidin-functionalized magnetic particles had a large degree of non-specific binding to the particle surface [**Figure 4-3**]. Nevertheless, non-specific binding may in fact improve platform sensitivity, as bacterial proliferation may result in both a viscosity and effective volume change of the particle, and thereby enhance the effect of bacterial growth on the particle's rotation.[13,14] However, to validate the AMBR as a bacterial viscometer, the carboxyl-functionalized magnetic particles were used.

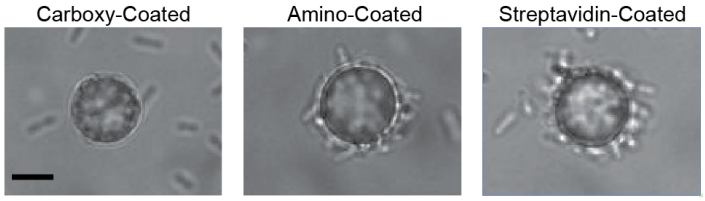

Figure 4-3. Light microscopy image of functionalized magnetic particle after 2 hours incubation with 1×10^7 CFU/mL *E. coli* at 37 °C. As compared to the amino- and streptavidin-functionalized magnetic particles, the carboxyl-magnetic particles visually had reduced non-specific binding. Scale bar: 5 μm.

4.4.4 Bacterial Growth

Individual AMBR viscometers that were suspended in an MH-PB bacteria solution were confined in nanoliter w/o (water/oil) droplets and the sensors were monitored with light microscopy. Within 20 minutes, there was a 20% increase in the

AMBR sensor's rotational period for proliferating bacteria, i.e. growth and division, as compared to the non-proliferating bacteria [**Figure 4-4**(a,b)]. Bacterial growth resulted in an increase in the measured rotational period, which contrasted the steady rotational period value for bacteria treated with a lethal dose of sodium azide (NaN_3) [**Figure 4-4**(b)]. As the driving magnetic field and particle properties (magnetic moment, volume and shape) remained constant, we were able to isolate changes in rotational period to changes in the solution viscosity as bacteria proliferated [**Equation 4-1**].

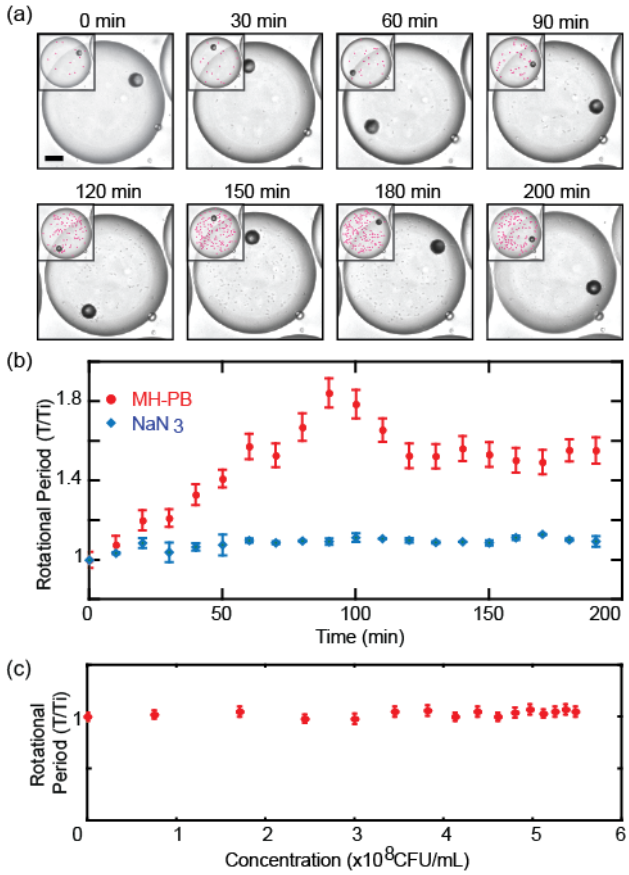

Figure 4-4. Measuring growth-dependent viscosity changes using the AMBR micro-viscometer. (a) Light microscopy image of the AMBR viscometer system during bacterial growth in MH-PB growth medium. Scale-bar is 20 um. Inset: bacteria are highlighted in red to aid visualization. (b) Corresponding AMBR response curve for bacteria grown in MH-PB vs. a lethal dose of 0.5% Sodium Azide (NaN_3) in MH-PB. Bacterial growth is observed as an increase in the rotational period. There is no observed bacterial growth upon treatment with NaN_3, as indicated by "no change" in the rotational period. (c)

Rotational response of the AMBR viscometer at different bacterial concentrations upon initial conditions (i.e. at time: 0 minutes). The steady rotational response suggests that the absolute number of bacteria in a given suspension does not affect the bead's rotation, within the shown concentration range.

While planktonic growth was the primary mechanism acting to affect the rotational rate, other mechanisms may also affect the viscosity, including changes in the interfacial friction, increases in the absolute bacterial cell number, and protein secretion and accumulation during bacterial proliferation. Towards understanding and optimizing the AMBR viscometer, it was important to isolate the predominant factor affecting the bead's rotation. As the AMBR biosensor rests at the bottom of the droplet, near the aqueous/oil/glass interface, the magnetic particle experiences a frictional as well as a viscous resistive torque. The viscous torque of a sphere, T_s, is expressed by $T_s = \left(\frac{4\pi}{3}\right)\beta R^3 \eta \Omega_s$, where β is a coefficient that is on the order of unity, R is the radius of the sphere, and Ω_s is the sphere's angular velocity.[41] The frictional torque, T_f, is expressed by $T_f = \left(\frac{8\pi}{9}\right)\alpha\mu\Delta\rho g R^4$, where μ is the friction coefficient, $\Delta\rho$ is the difference between the densities of the sphere and the sample liquid, g is the gravity acceleration, and αR is the contact area between the sphere and the bottom of the cell.[41] Therefore, the total resistive torque on the AMBR system is,

$$T = T_s + T_f = \left(\frac{4\pi}{3}\right)\beta R^3 \eta \Omega_s + \left(\frac{8\pi}{9}\right)\alpha\mu\Delta\rho g R^4. \quad [4\text{-}3]$$

Considering that R is sufficiently small in our system, $R \sim 4 \times 10^{-6}$ to 9×10^{-6} μm, the viscous force dominates the frictional torque, $T_s > T_f$. Furthermore, the viscous torque near the particle's equator dominates, as shown by

$$T(\theta)d\theta = 6\pi\eta R^3 \sin^3\theta \, d\theta; 0 < \theta < \pi, \quad [4\text{-}4]$$

where $T(\theta)$ is the viscous torque at given regions of the particle, and $\theta = 0$ and $\theta = \pi$ at the bottom and top of the particle surface, respectively.[42] We thus demonstrate that both the frictional torque and the viscous torque near the outer regions of the hemispheres are negligible [**Equation 4-2** and **Equation 4-3**] and that edge effects are not a major contributing factor to the changes in the bead's rotation. We examined this experimentally by repeating the experiment under different interfacial conditions, including using a different growth media, eliminating the oil phase, and removing the surfactant from the aqueous phase. Identical particle behavior was observed under all of these conditions [**Figure 4-5**]. We can, therefore, conclude that the change in the rotational response is caused by a change in the viscosity within the droplet.

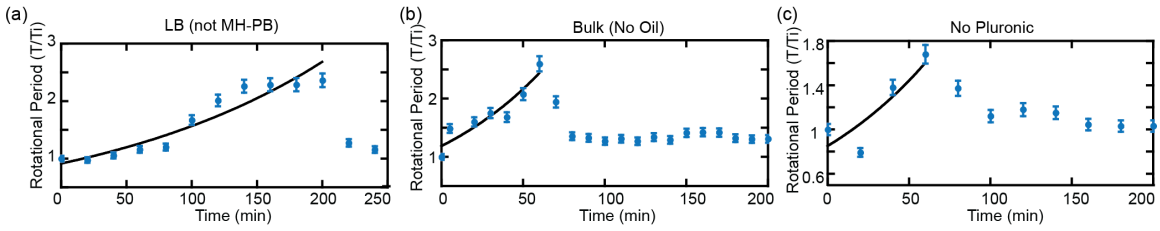

Figure 4-5. AMBR characterization of bacterial growth in different external environments. The rotational response trends upon bacterial growth is consistent upon (a) changing the growth media from MH-PB to LB broth, (b) bulk analysis (no encapsulation into w/o droplets) and (c) without the use of Pluronic F-68 in the aqueous phase.

The increase in the suspension viscosity upon bacterial proliferation may be a result from the accumulation of bacterial polysaccharides in the matrix, not from the absolute cell number [**Figure 4-4**(c)]. Bacteria are known to secrete bacterial polysaccharides, resulting in the broth developing viscoelastic, non-Newtonian characteristics,[24] which would lend itself to a slower rotational rate, as compared to Newtonian fluids.[43] The amount and type of bacterial polysaccharides secreted varies depending on the bacterial concentration and environmental conditions. As a result, the

accumulation of polysaccharides and the transition to a viscoelastic suspension naturally increase the viscosity,[24] which subsequently translate to the increase in the particle's rotational period. While the accumulation of polysaccharides when cells proliferate may be one factor affecting the solution viscosity, the aim of this manuscript was to demonstrate the ability of the AMBR micro-viscometer to measure the viscosity of a bacterial system and to run AST and determine the MIC. As a result, confirmation of the presence of polysaccharides was not studied in this manuscript.

Even though bacterial growth resulted in viscosity increases, it was observed that at a unique time point, the AMBR viscometer's rotational period decreased, which would suggest an apparent decrease in the solution viscosity [**Figure 4-4**(b)]. The sudden drop in the rotational period may be explained by either biology or fluid dynamics. Possible explanations are that when bacteria grow to a significantly large population, bacteria motility changes, bacteria may excrete enzymes that break down the surrounding polysaccharide matrix, or the bacteria may incorporate polysaccharides from its surroundings.[17,24] Another possibility is that the rotating sensor may have generated a sufficient stress on the fluid, at which the viscoelastic behavior 'breaks down'. Nevertheless, this decrease in rotational period is consistent across various experimental conditions [**Figure 4-5**].

4.4.5 Bacterial Response to Gentamicin

The AMBR viscometer was applied towards determining the gentamicin MIC of a uropathogenic strain of *E. coli*. The bacteria were cultured in 0, 0.25, 0.5, 1, and 2 µg/mL gentamicin concentrations and the rotational response and the corresponding viscosity changes of the suspension were monitored. The effects of gentamicin on bacterial

proliferation could be discerned within 100 min [**Figure 4-6**]. The rotational period for bacteria cultured in 0, 0.25, and 0.5 µg/mL gentamicin increased as the suspension's viscosity increased, thereby indicating bacterial growth. There was no observed change in the rotational period for bacteria cultured in solutions of 1 and 2 µg/mL gentamicin, which suggests that these are sufficiently high antibiotic concentrations for inhibition of bacterial growth. As demonstrated here, the AMBR viscometer, in its current state, is a tool that can measure the presence or lack of bacterial proliferation. Towards this end, we were unable to use the slope of the growth curve to indicate any quantitative information about the environmental condition or bacterial health.

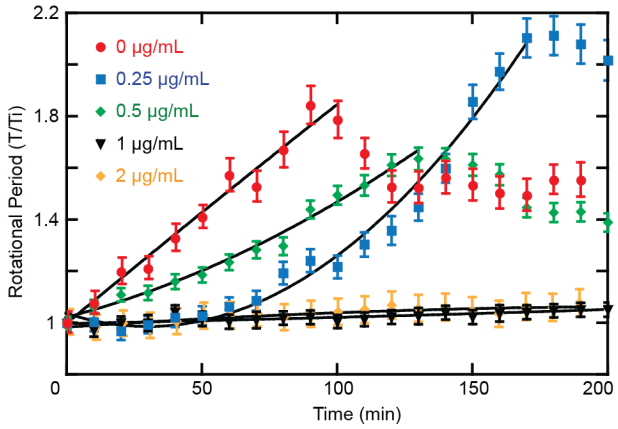

Figure 4-6. Performing AST with the AMBR micro-viscometer. AMBR viscometer response to the proliferation of *E. coli* exposed to 0, 0.25, 0.5, 1, and 2 µg/mL gentamicin. An increase in the rotational period suggests bacterial growth/proliferation whereas a constant rotational period suggests growth inhibition. The data indicates an MIC of 1 µg/mL for gentamicin. The curve fits are provided to guide the eye.

We presume that the different slopes of the growth curves may result from slightly varying initial environmental and bacterial conditions that may affect the growth rate [**Figure 4-5** and **Figure 4-6**]; however, further sensor and platform optimization and characterization need to be conducted to test this assumption. From the AMBR results

shown in **Figure 4-6**, the gentamicin MIC was 1 μg/mL, which corresponds very well with the 1 μg/mL gentamicin MIC value of this strain, determined with the standard VITEK2 system.[14] When comparing MIC values of two methods, typically a two-fold dilution difference is acceptable.[10] A significant difference between the rotational responses of bacteria treated with the antibiotic above MIC conditions, versus below it, could be observed clearly, within 100 minutes. The authors suggest that this could be further reduced by measuring AMBR in a real-time manner and by applying more sophisticated algorithms, such as inflection point analysis.

4.5 Conclusions

We have demonstrated a label-free AMBR micro-viscometer that can measure the growth and drug susceptibility of a bacterial isolate more rapidly and using 1000-fold fewer initial bacteria counts than commercial phenotypic systems. We present proof-of-concept studies of the AMBR micro-viscometer towards measuring the gentamicin MIC of *E. coli* by measuring changes in the rheological properties of the bacterial suspension, comprised of an initial count of 50 bacteria. As bacteria proliferate, the viscosity of the solution increases, which translates to an increase in the magnetic bead's rotational period. This contrasts the constant rotational period that results from bacteria that are not proliferating, and hence do not change the solution viscosity. This label-free AST technique is extremely versatile, and therefore, can be easily extended for use on any planktonic bacteria strain without the need to develop specific antibodies.

Further developments of the system includes (1) increasing the throughput by monitoring a larger array of AMBR micro-viscometers consecutively and in real time, (2) using droplet sorting techniques to isolate droplets that contain AMBR micro-

viscometers, and (3) integrating the system with an off-microscope sensor.[28,32] We anticipate that through parallelizing the platform and incorporating real-time data capture and analysis, the time to results for AST can be further reduced. In addition to microbial AST applications, we anticipate that the AMBR viscometer may be beneficial for measuring growth of any cell population, including prokaryotic and eukaryotic suspension cells, and for applications that require viscosity measurements of small samples, such as for biopolymer characterizations.[44]

4.6 References

1. Barenfanger, J., Drake, C. & Kacich, G. Clinical and Financial Benefits of Rapid Bacterial Identification and Antimicrobial Susceptibility Testing. *J. Clin. Microbiol.* **37**, 1415-1418 (1999).

2. Chen, C.H. *et al.* Antimicrobial Susceptibility Testing Using High Surface-to-Volume Ratio Microchannels. *Analytical Chemistry* **82**, 1012-1019 (2010).

3. Martinez, J.L. *et al.* A global view of antibiotic resistance. *FEMS Microbiology Reviews* **33**, 44-65 (2009).

4. Costelloe, C., Metcalfe, C., Lovering, A., Mant, D. & Hay, A.D. Effect of antibiotic prescribing in primary care on antimicrobial resistance in individual patients: systematic review and meta-analysis. *BMJ* **340**, c2096-c2096 (2010).

5. Alvarez-Lerma, F. *et al.* Empiric broad-spectrum antibiotic therapy of nosocomial pneumonia in the intensive care unit: a prospective observational study. *Crit Care* **10**, R78 (2006).

6. Mach, K.E. *et al.* A Biosensor Platform for Rapid Antimicrobial Susceptibility Testing Directly From Clinical Samples. *The Journal of Urology* **185**, 148-153 (2011).

7. Jorgensen, J.H. & Ferraro, M.J. Antimicrobial Susceptibility Testing: General Principles and Contemporary Practices. *Clinical Infectious Diseases* **26**, 973-980 (1998).

8. Jorgensen, J.H. & Ferraro, M.J. Medical Microbiology: Antimicrobial Susceptibility Testing: A Review of General Principles and Contemporary Practices. *Clinical Infectious Diseases* **49**, 1749-1755 (2009).

9. Goldman, E. & Green, L.H. *Practical Handbook of Microbiology*. (CRC Press: 2008).

10. Health, C. for D. and R. Guidance Documents (Medical Devices and Radiation-Emitting Products) - Class II Special Controls Guidance Document: Antimicrobial Susceptibility Test (AST) Systems. at <http://www.fda.gov/MedicalDevices/DeviceRegulationandGuidance/GuidanceDocuments/ucm080564.htm>

11. Andrews, J.M. Determination of minimum inhibitory concentrations. *Journal of Antimicrobial Chemotherapy* **48**, 5 (2001).

12. Boedicker, J.Q., Li, L., Kline, T.R. & Ismagilov, R.F. Detecting bacteria and determining their susceptibility to antibiotics by stochastic confinement in nanoliter droplets using plug-based microfluidics. *Lab Chip* **8**, 1265 (2008).

13. Kinnunen, P. *et al.* Monitoring the growth and drug susceptibility of individual bacteria using asynchronous magnetic bead rotation sensors. *Biosensors and Bioelectronics* **26**, 2751-2755 (2011).

14. Sinn, I. *et al.* Asynchronous magnetic bead rotation (AMBR) biosensor in microfluidic droplets for rapid bacterial growth and susceptibility measurements. *Lab Chip* **11**, 2604 (2011).

15. Boedicker, J.Q., Vincent, M.E. & Ismagilov, R.F. Microfluidic Confinement of Single Cells of Bacteria in Small Volumes Initiates High-Density Behavior of Quorum Sensing and Growth and Reveals Its Variability13. *Angewandte Chemie* **121**, 6022-6025 (2009).

16. Ong, K.G., Wang, J., Singh, R.S., Bachas, L.G. & Grimes, C.A. Monitoring of bacteria growth using a wireless, remote query resonant-circuit sensor: application to environmental sensing. *Biosensors and Bioelectronics* **16**, 305-312 (2001).

17. Rafaï, S., Jibuti, L. & Peyla, P. Effective Viscosity of Microswimmer Suspensions. *Phys. Rev. Lett.* **104**, 098102 (2010).

18. Stoyanov, P.G. & Grimes, C.A. A remote query magnetostrictive viscosity sensor. *Sensors and Actuators A: Physical* **80**, 8-14 (2000).

19. Sokolov, A. & Aranson, I.S. Reduction of Viscosity in Suspension of Swimming Bacteria. *Phys. Rev. Lett.* **103**, 148101 (2009).

20. Cui, Z. Weakly sheared active suspensions: hydrodynamics, stability, and rheology. *Phys Rev E Stat Nonlin Soft Matter Phys* **83**, 031911 (2011).

21. Hatwalne, Y., Ramaswamy, S., Rao, M. & Simha, R.A. Rheology of Active-Particle Suspensions. *Phys. Rev. Lett.* **92**, 118101 (2004).

22. Saintillan, D. & Shelley, M.J. Instabilities and pattern formation in active particle suspensions: kinetic theory and continuum simulations. *Phys. Rev. Lett.* **100**, 178103 (2008).

23. Toda, K., Furuse, H., Amari, T. & Wei, X. Cell concentration dependence of dynamic viscoelasticity of Escherichia coli culture suspensions. *Journal of Fermentation and Bioengineering* **85**, 410-415 (1998).

24. Suresh Kumar, A., Mody, K. & Jha, B. Bacterial exopolysaccharides – a perception. *Journal of Basic Microbiology* **47**, 103-117 (2007).

25. Furuse, H., Amari, T., Miyawaki, O., Asakura, T. & Toda, K. Characteristic behavior of viscosity and viscoelasticity of Aureobasidium pullulans culture fluid. *Journal of Bioscience and Bioengineering* **93**, 411-415 (2002).

26. Sutherland, I.W. Biofilm exopolysaccharides: a strong and sticky framework. *Microbiology* **147**, 3 -9 (2001).

27. Pang, P., Cai, Q., Yao, S. & Grimes, C.A. The detection of Mycobacterium tuberculosis in sputum sample based on a wireless magnetoelastic-sensing device. *Talanta* **76**, 360-364 (2008).

28. Kinnunen, P., Sinn, I., McNaughton, B.H. & Kopelman, R. High frequency asynchronous magnetic bead rotation for improved biosensors. *Appl. Phys. Lett.* **97**, 223701 (2010).

29. McNaughton, B.H., Agayan, R.R., Clarke, R., Smith, R.G. & Kopelman, R. Single bacterial cell detection with nonlinear rotational frequency shifts of driven magnetic microspheres. *Appl. Phys. Lett.* **91**, 224105 (2007).

30. McNaughton, B.H., Agayan, R.R., Wang, J.X. & Kopelman, R. Physiochemical microparticle sensors based on nonlinear magnetic oscillations. *Sensors and Actuators B: Chemical* **121**, 330-340 (2007).

31. McNaughton, B.H., Kehbein, K.A., Anker, J.N. & Kopelman, R. Sudden Breakdown in Linear Response of a Rotationally Driven Magnetic Microparticle and Application to Physical and Chemical Microsensing. *The Journal of Physical Chemistry B* **110**, 18958-18964 (2006).

32. McNaughton, B.H. *et al.* Compact sensor for measuring nonlinear rotational dynamics of driven magnetic microspheres with biomedical applications. *Journal of Magnetism and Magnetic Materials* **321**, 1648-1652 (2009).

33. Hecht, A., Kinnunen, P., McNaughton, B. & Kopelman, R. Label-acquired magnetorotation for biosensing: An asynchronous rotation assay. *Journal of Magnetism and Magnetic Materials* **323**, 272-278 (2011).

34. Hecht, A., Kumar, A.A. & Kopelman, R. Label-Acquired Magnetorotation As a Signal Transduction Method for Protein Detection: Aptamer-Based Detection of Thrombin. *Anal. Chem.* **83**, 7123-7128 (2011).

35. Behrend, Anker, J., McNaughton, B. & Kopelman, R. Microrheology with modulated optical nanoprobes (MOONs). *Journal of Magnetism and Magnetic Materials* **293**, 663-670 (2005).

36. Pal, R. *et al.* An integrated microfluidic device for influenza and other genetic analyses. *Lab Chip* **5**, 1024-1032 (2005).

37. Sinn, I. *et al.* Magnetically uniform and tunable Janus particles. *Appl. Phys. Lett.* **98**, 024101 (2011).

38. McNaughton, B.H. *et al.* Fabrication of Nanoparticles and Microspheres with Uniform Magnetic Half-Shells. *MRS Proceedings, 899E* **988**, (2006).

39. Anker, J.N. & Kopelman, R. Magnetically modulated optical nanoprobes. *Appl. Phys. Lett.* **82**, 1102 (2003).

40. Shankar, P.N. & Kumar, M. Experimental Determination of the Kinematic Viscosity of Glycerol-Water Mixtures. *Proceedings of the Royal Society of London. Series A: Mathematical and Physical Sciences* **444**, 573-581 (1994).

41. Sakai, K., Hirano, T. & Hosoda, M. Electromagnetically Spinning Sphere Viscometer. *Applied Physics Express* **3**, 016602 (2010).

42. Hosoda, M., Hirano, T. & Sakai, K. Extension of Measurement Viscosity Range of EMS System. *Proceedings of Symposium on Ultrasonic Electronics* **31**, 293-294 (2010).

43. D'Avino, G., Cicale, G., Hulsen, M.A., Greco, F. & Maffettone, P.L. Effects of confinement on the motion of a single sphere in a sheared viscoelastic liquid. *Journal of Non-Newtonian Fluid Mechanics* **157**, 101-107 (2009).

44. Teyssandier, F. & Love, B.J. MMA bulk polymerization and its influence on in situ resin viscosity comparing several chemorheological models. *Journal of Applied Polymer Science* **120**, 1367-1371 (2011).

CHAPTER 5:

Magnetically uniform and tunable Janus particles

5.1 Abstract

Magnetic particles serve as an important tool for a variety of biomedical applications but often lack uniformity in their magnetic responsiveness. For quantitative analysis studies, magnetic particles should ideally be monodisperse and possess uniform magnetic properties. Here we fabricate magnetically uniform Janus particles with tunable magnetic properties using a spin-coating and thermal evaporation method. The resulting 2 μm ferromagnetic particles exhibited a 4% magnetic response variability, and the 10 μm ferromagnetic particles exhibited a 1% size variability and an 8% magnetic response variability. Furthermore, by reducing the film thickness, the particle behavior was tuned from ferromagnetic to superparamagnetic.

5.2 Introduction

Magnetic particles are used extensively in biomedicine and biophysical research. The ability to manipulate functionalized magnetic particles with external magnetic fields is advantageous for applications such as whole cell and biomolecular separation,[1] magnetic resonance imaging contrast agents,[2] targeted drug delivery,[3] and immunoassays.[1] Methods used to fabricate magnetic particles or scaffolds include loading magnetic material within a nonmagnetic matrix,[4,5] depositing magnetic material

onto nonmagnetic particles,[6-8] and polymerizing magnetic bead hydrogels using microfluidic droplet technology.[9,10] While magnetic particles serve as a ubiquitous and important tool, they often lack uniformity in magnetic responsiveness. Indeed, numerous magnetic particles have been reported to have a 30 to 80% variation in magnetophoretic mobility.[11] Morphological and magnetic content uniformity are important parameters for quantitative analysis methods, such as magnetoresistive sensors[12,13] and asynchronous magnetic bead rotation (AMBR) biosensors.[14-20] To improve the quality and reproducibility of quantitative studies, particles should ideally be monodisperse[12] and possess uniform magnetic properties.[21]

We fabricated and characterized magnetically uniform Janus particles with tunable magnetic properties using a combined method of spin coating and thermal evaporation of nickel (Ni). The fabricated magnetic Janus particles, which are characterized by the AMBR method[5,14-16] and with a DC superconducting quantum interference device (SQUID), possess greater particle- to-particle magnetic uniformity than previously reported particles.[11] In addition, the particles' magnetic behavior may be tuned by adjusting the magnetic coating thickness to be above or below the reported 8 nm superparamagnetic (SPM) limit for Ni.[22] The 2 μm diameter polystyrene particles coated with 60 nm Ni and the 10 μm diameter particles coated with 300 nm Ni, thickness values well above the SPM limit, behaved largely ferromagnetic, with a small SPM component. The same 2 μm and 10 μm diameter polystyrene particles that were coated with a Ni layer below the SPM limit, 5 nm Ni layer and a 20 nm Au layer, exhibited SPM behavior.

5.3 Materials and Methods

5.3.1 Magnetic Particle Fabrication

The magnetic Janus particles were fabricated by spin- coating a disordered monolayer of National Institute of Standards and Technology (NIST) approved size standard (Polysciences, Inc., Warrington PA) polystyrene particles onto a wafer and by thermally evaporating Ni onto the wafer **[Figure 5-1]**. The evaporation technique has been previously demonstrated in the fabrication of magnetic and nonmagnetic Janus particles.[6-8,23]

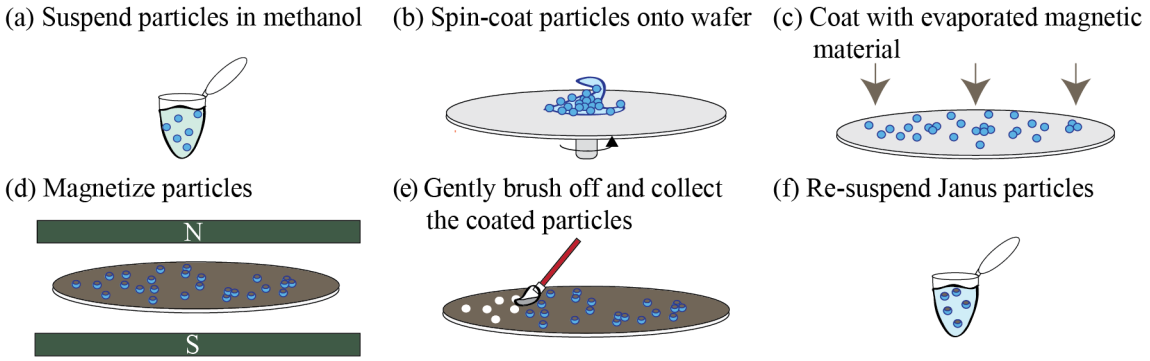

Figure 5-1. Fabrication schematic for magnetic Janus particles. Polystyrene particles are spin-coated onto a glass wafer and magnetic material (Ni) is evaporated onto the wafer surface. The particles are identically and directionally magnetized and subsequently re-suspended in the desired medium.

Solutions of 1 μm, 2 μm, 10 μm and 100 μm diameter particles, of National Institute of Standards and Technology (NIST) approved size standards (Polysciences, Inc., Warrington PA), were suspended in methanol at 1 % weight to volume concentration. A 500 μL aliquot of the solution was spin-coated onto a 4" glass wafer (Precision Glass & Optics, Santa Ana CA). The ferromagnetic particles were fabricated by evaporating 30 nm Ni on 1 μm particles, 60 nm Ni on 2 μm particles, 300 nm Ni on 10 μm particles, and 300 nm Ni on 100 μm particles. The maximum thickness is limited

by the need to keep the particles from being linked together by the deposited layer; as a result, the evaporated layer thickness was limited to 3 % of the particle diameter. The SPM particles were fabricated by sequentially evaporating 5 nm Ni and 20 nm Au onto both the 2 μm and 10 μm diameter particles, resulting in a multi-layered particle. The Au coating was to aid in the visualization of the particles (and for potential biochemical functionalization). The wafers were magnetized in a 60 mT uniform magnetic field for over 24 hours. The particles were recovered by brushing off the coated particles with a damp acrylic paintbrush and suspending them in DI water with 0.1 % Bovine Serum Albumin (BSA). Particles were stored at 4 °C and remained magnetically responsive for over 12 months. To fabricate SPM particles, 5 nm of Ni and 20 nm of Au were evaporated sequentially onto both 2 μm and 10 μm polystyrene particles at 1 Å/s and 1.8 $\times 10^{-6}$ Torr. Up to a calculated value of 10^9 magnetic Janus particles (2 μm diameter) can be fabricated on a single 4" wafer, assuming 50% area coverage. The ferromagnetic particles were imaged using scanning electron microscopy (SEM) and light microscopy, as shown in **Figure 5-2**.

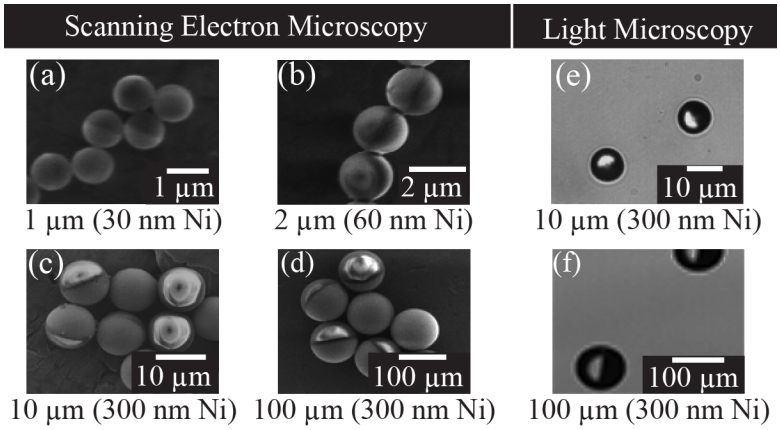

Figure 5-2. SEM (a-d) and light microscopy (e,f) images of magnetic Janus particles. The particle size and corresponding Ni coating thickness are stated below each figure.

5.4 Asynchronous Magnetic Bead Rotation (AMBR) Characterization

For the AMBR characterization experiments, the particle solutions were diluted to a concentration of 5000 particles/mL. For 2 μm particle characterizations, 10 μL of the particle solution was sandwiched between two 0-thickness glass slides, separated with a thin layer of white petroleum jelly (Kendall, Mansfield MA). Characterizations were conducted with a 100 X oil immersion objective. In contrast, the larger 10 μm particles were characterized using a 40 X objective with a Nunc LiveCell Array slide (Thermo Fisher Scientific, Waltham MA), which prevented particle translation. All rotation measurements were performed in a rotating magnetic field set-up on an Olympus IX71 inverted microscope with the corresponding objective. The ferromagnetic particles' average rotational rates were determined by focusing a low power laser on the particle of interest and measuring the scattered light intensity with a photodiode; the scattered light is modulated once per particle rotation due to the half coating Janus property.[16] The SPM particles' average rotational rate was determined through image analysis on ImageJ and MATLAB.

The particle rotates either synchronously or asynchronously with the external rotating magnetic field, depending on factors, such as the driving field frequency and the particle's magnetic properties.[14] Above the critical frequency, i.e., in the asynchronous regime, the average rotational rate of the magnetic particle, can be expressed as $\langle\dot{\theta}\rangle = \sqrt{\Omega^2 - \Omega_c^2}$,[14,24] where $\langle\dot{\theta}\rangle$ is the average rotation frequency of the magnetic bead (in radians per second), Ω is the driving frequency, and Ω_c is the critical frequency. The critical frequency at which the particle be- comes asynchronous is $\Omega_c = mB/\kappa\eta V$,[2,5,14] where m is the magnetic moment, B is the amplitude of the magnetic field, κ is the shape

factor, η is the dynamic viscosity, and V is the volume of the magnetic bead. The asynchronous rotational response provides information regarding the particle's magnetic behavior; subsequently, the magnetic moment of individual particles can be determined with

$$m = \left(\frac{\kappa \eta V}{B}\right) \Omega_c \qquad [2\text{-}1]$$

5.4.1 SQUID Characterization

For SQUID analysis, hysteresis curves of particle suspensions were obtained at a temperature below freezing (at 250 K) to eliminate the rotational degrees of freedom. A zero field-cooled and field cooled (ZFC/FC) analysis was performed at 300 Oe magnetic fields for the 2 μm SPM particles.

5.5 Results and Discussion

The evaporated magnetic layer was found not to contribute significantly to the variability in magnetic response and particle size. The magnetic variability due to the initial size distribution of the polystyrene spheres was estimated using [**Equation 5-1**]. The reported 1% coefficient of variation (CV) in diameter for NIST particles was calculated to affect the measured magnetic variability by up to 6% for the 2 μm ferromagnetic particles and 8% for the 10 μm ferromagnetic particles. Light microscopy image analysis shows that the CV in diameter for 10 μm ferromagnetic particles after coating is 1% (10.2 $\pm$ 0.12 μm), which is consistent with the reported CV in diameter of the NIST particles. This indicates that the variability in magnetic response and size predominantly arises from the size distribution of the initial particles.

The magnetic properties and uniformity of the 2 μm ferromagnetic particles were characterized by AMBR and with a SQUID. **Figure 5-3**(a) shows light microscopy

images of a 2 µm Janus particle rotating synchronously with a 5 Hz magnetic field. When the particle was placed in a rotating magnetic field at frequencies up to 1 kHz, the rotational behavior was ferromagnetic, as shown in **Figure 5-3**(b).[14] The magnetic particle-to-particle uniformity as well as the magnetic moment was estimated with [**Equation 5-1**].[14]

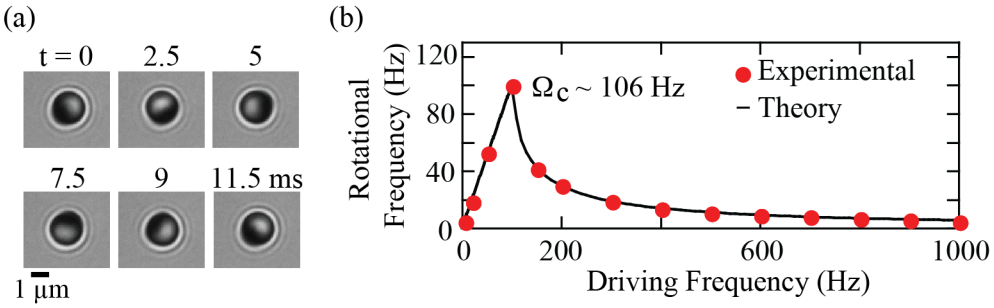

Figure 5-3. Characterization of the 2 µm ferromagnetic particles (60 nm Ni coating) with AMBR (a) Light microscopy image sequence of the 2 µm ferromagnetic particle rotating synchronously in a 5 Hz external rotating magnetic field. (b) Characteristic rotational response for a 2 µm ferromagnetic particle (experimental values are depicted by red circles), fitted to ferromagnetic particle rotational theory (black line)

The rotational response of 50 2 µm ferromagnetic particles was measured to have an average critical frequency of 116 $\pm$ 9.6 Hz, which corresponds to an 8% CV in the magnetic responsiveness. The magnetic moment of a single 2 µm ferromagnetic particle was calculated to be (1.83 $\pm$ 0.15) x 10^{-14} Am^2, provided η=1 mPa s, κ=6, and B=1 mT. From the SQUID analysis, the presence of coercivity (75 Oe) in hysteresis loop measurements also indicates that the particles are indeed ferromagnetic [**Figure 5-4**]. However, the magnetization saturated above 2000 Oe although the hysteresis loop closed at approximately 400 Oe, which may suggest a superparamagnetic contribution.[25] Assuming no particle aggregation during the SQUID measurements, a 2 µm ferromagnetic particle was calculated to have a magnetic moment of 5.22 x 10^{-14} Am^2

[Joules/Tesla], provided a saturation value of 1.4 x 10^{-12} Am^2; this closely agrees with the magnetic moment value estimated by AMBR.

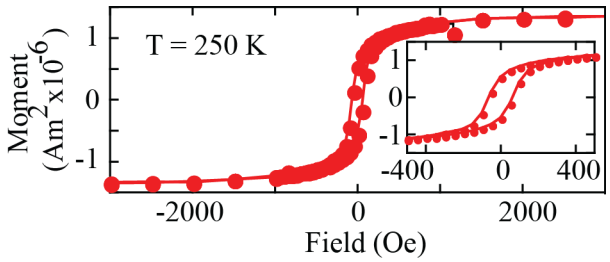

Figure 5-4. Characterization of the 2 μm ferromagnetic particles (60 nm Ni coating) with DC SQUID. Typical ferromagnetic hysteresis is apparent with 75 Oe coercivity.

The magnetic properties of 2 μm SPM particles were also investigated by AMBR and with a SQUID. The rotational behavior of the SPM particles does not agree with the ferromagnetic particle theory.[14] This suggests a nonpermanent magnetic dipole origin of magnetic torque. Furthermore, only 10% to 15% of the particles were observed to rotate. We speculate that this could arise from the variability in thin-film nucleation during deposition. At frequencies between 100 Hz and 1 kHz, the 2 μm SPM particles' rotational rates did not change significantly [**Figure 5-5**(a)]. This is a trait characteristic of an induced magnetic moment.[26-28] From the SQUID analysis, coercivity in hysteresis loop measurements was not observed [**Figure 5-5**(b)], which suggests that the particles are SPM. The SPM behavior was confirmed by the ZFC/FC curve [**Figure 5-5**(c)], as the blocking temperature, *Tb*, is approximately 120 K, a value well below our experimental conditions.[29] We thus observed a transition from ferromagnetic to SPM behavior by reducing the Ni layer thickness on the 2 μm particles from 60 to 5 nm. This indicates that the magnetic behavior of Janus particles can be tuned by selecting desired values for the magnetic layer thickness.

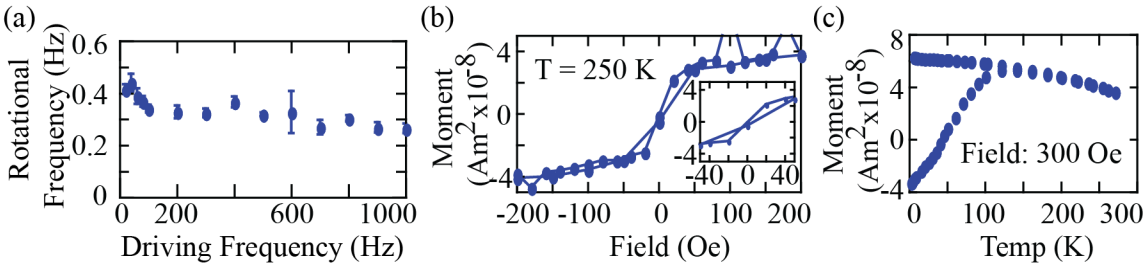

Figure 5-5. Characterization of the 2 µm SPM particles (5 nm Ni and 20 nm Au coating) with AMBR and DC SQUID (a) Characteristic rotational response for a 2 µm SPM particles; behavior does not conform to the ferromagnetic theory. (b) DC SQUID characterization; hysteresis is not apparent, suggesting SPM behavior. (c) ZFC/FC curve; the blocking temperature, T_b, is approximately 120 K. Note: For SQUID hysteresis curves, the connected lines are used to aid in visualization; they do not represent a data fit.

To further demonstrate magnetic tunability, additional experiments were performed on 10 µm ferromagnetic and 10 µm SPM particles. The magnetic properties and uniformity of the 10 µm ferromagnetic particles were characterized with a SQUID and by AMBR [**Figure 5-6** and **Figure 5-7**].[30]

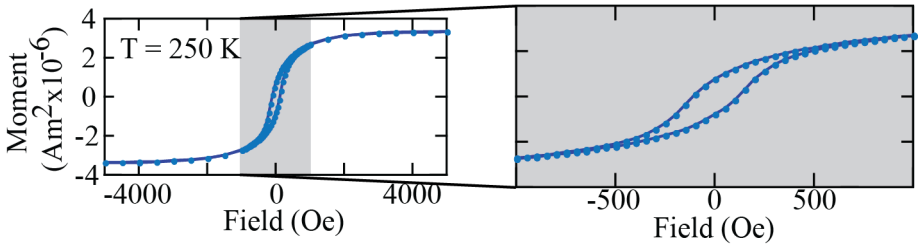

Figure 5-6. DC SQUID measurements for the 10 µm ferromagnetic particles (300 nm Ni coating). Typical ferromagnetic hysteresis is apparent, with 150 Oe coercivity. The magnetic moment of the sample, as determined by SQUID, is 4.22×10^{-12} Am^2. Note: The connected lines are used to aid in visualization; they do not represent a data fit.

From SQUID measurements, the average magnetic moment of a 10 µm ferromagnetic particle was calculated to be 4.22×10^{-12} Am^2, which is consistent with the value calculated with AMBR, $(2.31 \pm 0.09) \times 10^{-12}$ Am^2. In addition, the 10 µm ferromagnetic particles was calculated to have a 4% CV in magnetic responsiveness. For

comparison, commercially available 4 µm carboxylated ferromagnetic particles (Spherotech, Illinois), as measured by AMBR, were calculated to have a 26% CV in magnetic responsiveness. This level of non-uniformity is consistent with reported values.[11] Furthermore, the 10 µm SPM particles were characterized by AMBR, and their rotational response was found to behave similarly to the 2 µm SPM particles [**Figure 5-7**(c)].[30] Therefore, we have demonstrated that the magnetic behavior of the 10 µm particles can be tuned by selectively choosing Ni thicknesses above and below the thin-film SPM limit. This further suggests that this tunability can be extended toward the fabrication of magnetically uniform ferromagnetic or SPM particles of other sizes.

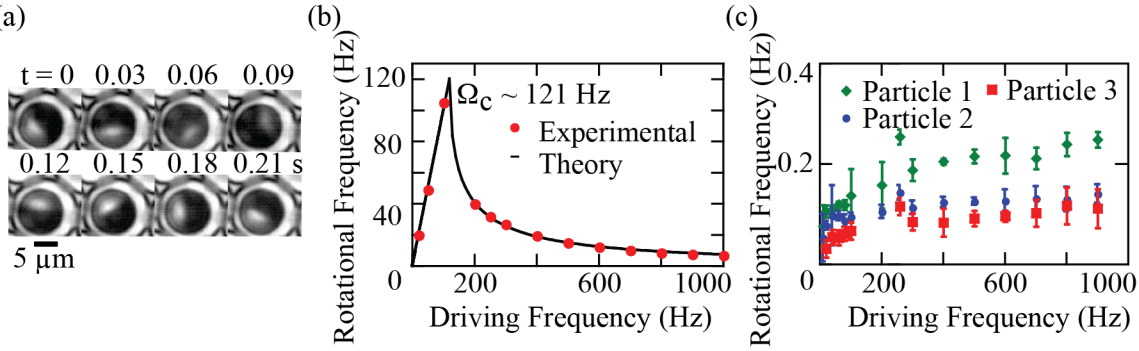

Figure 5-7. 10 µm magnetic Janus particle characterization by AMBR. (a) Light microscopy images of a 10 µm ferromagnetic particle (300 nm Ni coating) asynchronously rotating in a 1 kHz external rotating magnetic field. (b) Characteristic rotational response of a 10 µm ferromagnetic particle (experimental values are depicted by red circles), fitted to ferromagnetic particle rotational theory (black line). (c) Characteristic rotational response of three individual 10 µm SPM particles (5 nm Ni and 20 nm Au). The behavior does not correspond with ferromagnetic particle rotational theory.

5.6 Conclusion

In conclusion, we have fabricated Janus particles with greater particle-to-particle magnetic uniformity than those previously reported, by using a spin coating and thermal evaporation technique. This straightforward method allows the magnetic behavior and

moment to be tuned by varying the particle size and/or the thickness of the magnetic deposition layer. Such uniform magnetic particles, when functionalized, may have significant utility in biomedical and biophysical applications.

5.7 References

1. Saiyed, Z., Telang, S. & Ramchand, C. Application of magnetic techniques in the field of drug discovery and biomedicine. *BioMagnetic Research and Technology* **1**, 2 (2003).

2. Chambon, C., Clement, O., Le Blanche, A., Schouman-Claeys, E. & Frija, G. Superparamagnetic iron oxides as positive MR contrast agents: In vitro and in vivo evidence. *Magnetic Resonance Imaging* **11**, 509-519 (1993).

3. Dobson, J. Magnetic nanoparticles for drug delivery. *Drug Development Research* **67**, 55-60 (2006).

4. Ugelstad, J., Mørk, P.C., Schmid, R., Ellingsen, T. & Berge, A. Preparation and biochemical and biomedical applications of new monosized polymer particles. *Polymer International* **30**, 157-168 (1993).

5. Korneva, G. et al. Carbon Nanotubes Loaded with Magnetic Particles. *Nano Letters* **5**, 879-884 (2005).

6. Albrecht, M. et al. Magnetic multilayers on nanospheres. *Nat Mater* **4**, 203-206 (2005).

7. McNaughton, B.H. et al. Fabrication of Nanoparticles and Microspheres with Uniform Magnetic Half-Shells. *MRS Proceedings, 899E* **988**, (2006).

8. Smoukov, S.K., Gangwal, S., Marquez, M. & Velev, O.D. Reconfigurable responsive structures assembled from magnetic Janus particles. *Soft Matter* **5**, 1285–1292 (2009).

9. Roh, K.-H., Yoshida, M. & Lahann, J. Water-Stable Biphasic Nanocolloids with Potential Use as Anisotropic Imaging Probes. *Langmuir* **23**, 5683-5688 (2007).

10. Yuet, K.P., Hwang, D.K., Haghgooie, R. & Doyle, P.S. Multifunctional Superparamagnetic Janus Particles. *Langmuir* **26**, 4281-4287 (2010).

11. Häfeli, U.O., Lobedann, M.A., Steingroewer, J., Moore, L.R. & Riffle, J. Optical method for measurement of magnetophoretic mobility of individual magnetic microspheres in defined magnetic field. *Journal of Magnetism and Magnetic Materials* **293**, 224-239 (2005).

12. Ferreira, H.A., Graham, D.L., Freitas, P.P. & Cabral, J.M.S. Biodetection using magnetically labeled biomolecules and arrays of spin valve sensors (invited). *J. Appl. Phys.* **93**, 7281 (2003).

13. Shen, W., Liu, X., Mazumdar, D. & Xiao, G. In situ detection of single micron-sized magnetic beads using magnetic tunnel junction sensors. *Appl. Phys. Lett.* **86**, 253901 (2005).

14. McNaughton, B.H., Kehbein, K.A., Anker, J.N. & Kopelman, R. Sudden Breakdown in Linear Response of a Rotationally Driven Magnetic Microparticle and Application to Physical and Chemical Microsensing. *The Journal of Physical Chemistry B* **110**, 18958-18964 (2006).

15. McNaughton, B.H., Agayan, R.R., Wang, J.X. & Kopelman, R. Physiochemical microparticle sensors based on nonlinear magnetic oscillations. *Sensors and Actuators B: Chemical* **121**, 330-340 (2007).

16. Kinnunen, P., Sinn, I., McNaughton, B.H. & Kopelman, R. High Frequency Asynchronous Magnetic Bead Rotation for Improved Biosensors. *Applied Physics Letters* **97**, 223701 (2010).

17. McNaughton, B.H. et al. Compact sensor for measuring nonlinear rotational dynamics of driven magnetic microspheres with biomedical applications. *Journal of Magnetism and Magnetic Materials* **321**, 1648-1652 (2009).

18. McNaughton, B.H., Agayan, R.R., Clarke, R., Smith, R.G. & Kopelman, R. Single bacterial cell detection with nonlinear rotational frequency shifts of driven magnetic microspheres. *Appl. Phys. Lett.* **91**, 224105 (2007).

19. Hecht, A., Kinnunen, P., McNaughton, B.H. & Kopelman, R. Label-acquired magnetorotation for biosensing: An asynchronous rotation assay. *Journal of Magnetism and Magnetic Materials* **323**, 272-278 (2011).

20. Kinnunen, P. et al. Monitoring the growth and drug susceptibility of individual bacteria using asynchronous magnetic bead rotation sensors. *Biosensors and Bioelectronics* **26**, 2751-2755 (2011).

21. Browning, V.M. Potential Department of Defense (DOD) applications of magnetic carriers. *European Cells and Materials* **3**, 5–6 (2002).

22. Singamaneni, S. & Bliznyuk, V. Fabrication of Ni nanoparticles and their size-selective self-assembly into chains under external magnetic field. *Applied Physics Letters* **87**, 162511 (2005).

23. Takei, H. & Shimizu, N. Gradient Sensitive Microscopic Probes Prepared by Gold Evaporation and Chemisorption on Latex Spheres. *Langmuir* **13**, 1865-1868 (1997).

24. Cēbers, A. & Ozols, M. Dynamics of an active magnetic particle in a rotating magnetic field. *Phys. Rev. E* **73**, 021505 (2006).

25. Hwang, J.I. et al. X-ray magnetic circular dichroism characterization of GaN/ GaMnN digital ferromagnetic heterostructure. *Applied Physics Letters* **91**, 072507 (2007).

26. Fannin, P.C. et al. Investigation of the complex susceptibility of magnetic beads containing maghemite nanoparticles. *Journal of Magnetism and Magnetic Materials* **303**, 147-152 (2006).

27. Janssen, X.J.A., Schellekens, A.J., van Ommering, K., van IJzendoorn, L.J. & Prins, M.W.J. Controlled torque on superparamagnetic beads for functional biosensors. *Biosensors and Bioelectronics* **24**, 1937-1941 (2009).

28. Biswal, S.L. & Gast, A.P. Mechanics of semiflexible chains formed by poly(ethylene glycol)-linked paramagnetic particles. *Phys. Rev. E* **68**, 021402 (2003).

29. Liu, Y., Shindō, D. & Sellmyer, D.J. *Handbook of advanced magnetic materials*. (Springer Science+Business Media, Inc.: 2005).

CHAPTER 6:

Conclusions and Future Work

We have developed a novel platform that integrates the sensitivity and robustness of AMBR and the high-throughput, low volumes, and long-term capability of microfluidics [Chapter 1]. The integrated AMBR microfluidic biosensor platform is widely applicable for biomedical tests, such as for cell growth assays and viscosity-based assays. In this dissertation, we demonstrated proof-of-concept studies delineating the potential of the AMBR microfluidic platform for clinical antimicrobial susceptibility testing (AST). Naturally, there is still a need to conduct comprehensive examinations across different bacterial species and antibiotic classes in order to fully validate the platform for AST applications. While shown to be highly promising, nonetheless, the AMBR microfluidic platform is still at its juvenile development stage; significant advancements towards increasing throughput, reducing cost, and simplifying protocols are required to bring the AMBR microfluidic platform closer towards clinical implementation.

In Chapters 2-5, we monitor bacterial growth and drug susceptibility with the AMBR microfluidic platform, using three approaches (1) single bacterium approach (bead size is on the same order of magnitude as bacterium), (2) small bacteria population approach (bead is larger and has greater surface area), and (3) the viscosity approach.

When particle sizes are on the same order of magnitude as that of a single bacterium, the AMBR sensor possesses its highest sensitivity; in fact, single bacterium elongation and division events can be easily detected [Chapter 2]. Although the single bacterium growth approach can be applied towards AST applications, the system has critical limitations: (1) clonal bacteria are phenotypically heterogeneous, (2) the sampling size may not be representative of the population, (3) the environment is not representative, as bacteria are generally found in colonies in physiological conditions, and (4) the system is low throughput even if AMBR sensors are used in parallel. To address these issues, larger magnetic beads were used to detect bacterial growth, as the larger surface area enabled many bacteria to bind to one bead [Chapter 3]. Compared to the approach using a magnetic bead size on the order of magnitude as the bacteria, the sensitivity of the large bead approach is reduced. Nevertheless, the large-bead system is not subject to the inherent heterogeneity limitations and provides a more representative sampling, and higher throughput; therefore, this approach is more amenable for AST applications. Another approach to monitor bacterial growth is the viscosity-based method, which is a sensitive, label-free technique that does not require any *a priori* knowledge of the bacterial species [Chapter 4]. In this dissertation, we have demonstrated proof-of-concept studies for bacterial growth and AST studies with the above three unique methods using the AMBR microfluidic platform.

There are a variety of advancements that can be made to improve further the sensitivity and robustness of the AMBR microfluidic platform; a few possible advancements are described below. In the work described in Chapter 5, we fabricated magnetically uniform and tunable Janus particles, which are morphologically uniform as

well. Unlike the use of commercial particles that allows for only qualitative measurements, the use of magnetically uniform particles enables the AMBR system to provide quantitative measurements. When these magnetically uniform particles are exposed to identical magnetic fields and environmental conditions, these magnetic particles should all rotate at the same frequency. With this technique, the bead's rotational period at any given time would provide insight into the system parameters; as a result, there is no need to monitor the particle's rotation; for instance, if the values of the magnetic moment, field strength, bead volume, and shape factor are known, it is possible to calculate the solution viscosity. After a given amount of time, if the bead's rotational rate is different and all bead and field parameters remained constant, the change in solution viscosity can be calculated. An application for the use of such magnetically uniform magnetic beads is described below.

The work described in this dissertation is innovative in several ways: (i) previous work with beads rotating in a magnetic field was based on *synchronous* rotation; in contrast, the method here is based on *asynchronous* rotation, with the unique advantages it offers; (ii) the AMBR microfluidic biosensor platform provides the most rapid, high-resolution clinical technique for monitoring bacterial growth that we are aware of, and (iii) we have demonstrated fundamental AMBR principles involved in monitoring viscosity and volume changes associated with bacterial growth – at both the single cell and small population level.

In short, our AMBR system has the following capabilities and advantages:

1. Enables antimicrobial susceptibility testing (AST) without *a priori* knowledge of the bacterial species;

2. Short measurement times to detect microbial growth, within a fraction of a bacteria's doubling time;
3. Sensitivity towards detecting small changes in the viscosity of the medium;
4. Seamless synergism with state-of-the-art magnetic bead cell separation/isolation;
5. Integration with non-microscopy techniques.

Underlying these capabilities is the innovation of rotating the "micromotor" continuously and asynchronously and of integrating the AMBR sensor with a microfluidic droplet platform that enable for long-duration studies and higher-throughputs. Overall, we have demonstrated comprehensive proof-of-concept studies utilizing this AMBR microfluidic platform for bacterial growth assays, specifically for AST applications. It is crucial to remember that the basis of this asynchronous magnetorotation sensor lies in monitoring changes over time; *any changes or variations that are not on the time-scale of the measurement, such as external vibrations or AMBR reorientation and translation, are of little consequence.*

6.1 AMBR sensors in Tubing

Currently, the AMBR microfluidic platform is fabricated in a clean room setting; as a result, the cost and the skill required to fabricate the devices are high. Nevertheless, the primary goal of the microfluidic platform is to form small volume water in oil (w/o) droplets rapidly and at high droplet densities. Therefore, an inexpensive and user-friendly system that can form these w/o microfluidic droplets would be beneficial. Early proof-of-concept demonstrations indicate the possibility of forming small volume droplets within the lumen of a section of Teflon tubing. Furthermore, to integrate the system with AMBR, magnetic beads can be included in the initial aqueous phase [**Figure 6-0-1**]. In order to

ensure that each droplet has an AMBR sensor, a complex that comprises of many magnetic beads would be used. Visualization is straightforward using this tubing technique, as the curvature of the tube system does not interfere. In fact, the magnetic bead complexes can be visualized simply by submerging the tubing in a solution that has an equal index of refraction to the tubing material; in preliminary experiments, the PTFE tubings were submerged in water.

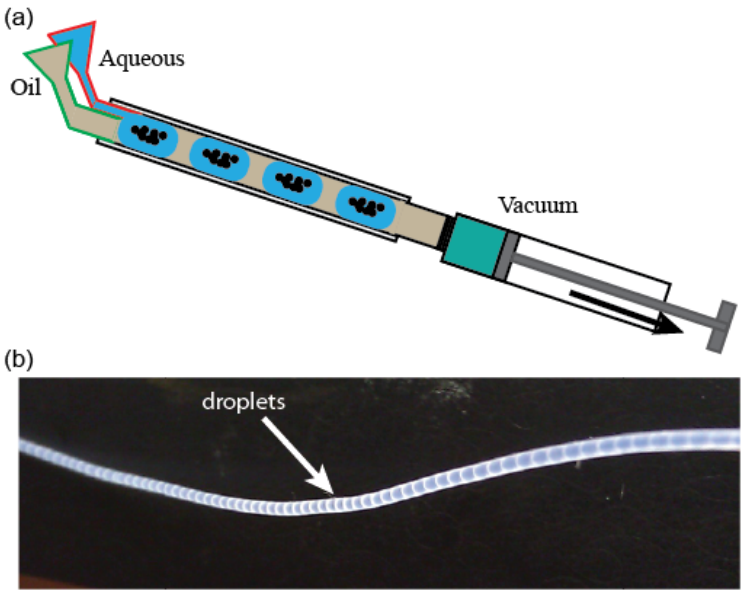

Figure 6-0-1. (a) Schematic of AMBR droplet formation in tubing. (b) Image of droplets confined within the lumen of a 100 μm diameter Teflon tubing.

We have thus demonstrated a low-cost, user-friendly system that can encapsulate, isolate, and array AMBR sensors in small volume w/o droplets. As mentioned earlier, this tubing platform utilizes the recently reported group rotation approach.[1] The group approach is beneficial, as it ensures that every droplet will have an AMBR sensor (i.e. AMBR group complex), and the magnetic groups can be visualized in a simple and straightforward manner.

6.2 Binary AMBR System for Identification and Detection

Magnetically uniform particles would enable quantitative measurements to be made. Commercial magnetic particles are inherently heterogeneous in magnetic content and bead volume; as a result, applications were limited to measuring relative changes in the magnetic bead's rotational rate. When 4 out of 5 of the listed parameters of the magnetic bead and environment are known: magnetic moment, volume, field strength, shape factor, and environmental property, naturally, the unknown value can be calculated. Therefore, a single rotational measurement, on the time-scale of seconds to minutes, is sufficient to determine whether the result is positive ("1") or negative ("0"). Therefore, we present a binary AMBR system that can be applied towards a variety of biomedical applications, such as bacterial detection and identification assays.

For bacterial detection and identification assays, the uniform magnetic beads must be functionalized with antibodies that bind their target organisms. This system can be scaled-up such that multiple, different bacterial species can be detected and identified. For instance, magnetic beads can be fabricated such that different batches of magnetic beads will have different magnetic moments; therefore, each magnetic bead batch would have a unique baseline rotational frequency. By changing the evaporated material or the magnetic layer thickness, the magnetic moment of the bead can be adjusted.[2,3] Each batch of magnetic beads, i.e. beads with distinct magnetic moments, can be linked to antibodies against different bacterial species. Simply, the magnetic bead behaves essentially like a barcode.

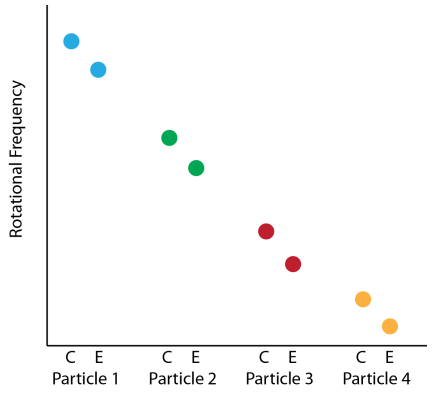

Figure 6-0-2. Schematic of the rotational response of four batches of magnetic beads (Particle 1, 2, 3, and 4). Each particle type has a unique rotational frequency (i.e. control conditions [C]). Upon bacterial binding, the rotational frequency will shift [E]. As a result, a measurable shift indicates the presence of the target bacterial species.

The number of unique magnetic bead batches is equivalent to the number of bacterial species that must be detected. For instance, to differentiate between four bacterial species, four identically sized magnetic particles, each of which possess a different magnetic moments, would be used. The baseline rotational frequencies of each AMBR sensor must be sufficiently different; this ensures that when bacteria do bind to the magnetic bead (positive result), the resultant rotational frequency does not overlap with the baseline rotational frequency of any other control (i.e. bare) particle [**Figure 6-0-2**]. As a result, this system could be naturally extended for detection and identification of bacterial infections in co-infected samples.

6.3 Single Cell Analysis

Traditional bulk cellular analysis measurements provide averaged information of a whole sample; these averaged results mask the variance and responses of individual bacteria. Tools that provide information about cellular behavior at the single-cell level would provide an understanding of the diversity and heterogeneity within genetically identical populations. This information, for instance, may provide researchers with insight into

possible mechanisms of cancer cell initiation, progression, metastasis, and therapeutic responses.4 Advancements towards understanding how cells behave at the single cell level have tremendous impact, as it helps accelerate fundamental biological research and the development of clinical diagnostic tools.4

The single bacterium growth method, which was described in Chapter 2, is a novel platform that enables heterogeneity studies in isogenic bacterial populations. With this platform, fundamental growth patterns at a single-cell level can be identified with high sensitivity and at high-throughput. The AMBR microfluidic platform can be used to encapsulate single bacterium – magnetic bead complexes in nanoliter droplets and densely array these droplets within a confined chamber. This close-packing not only improves visualization capabilities, but also enables environmental conditions, such as temperature, nutrients, and toxins, to be exposed uniformly to the droplet ensemble. With this platform, the diverse growth patterns of a large number of individual cells can be rapidly determined.

6.4 References

1. Kinnunen, P. *Asynchronous Magnetic Bead Rotation (AMBR) for Biosensors*. (University of Michigan, Ph.D. Thesis: 2011).

2. Sinn, I. *et al.* Magnetically uniform and tunable Janus particles. *Appl. Phys. Lett.* **98**, 024101 (2011).

3. Korneva, G. *et al.* Carbon Nanotubes Loaded with Magnetic Particles. *Nano Letters* **5**, 879-884 (2005).

4. Wang D. *et al.* Single cell analysis: the new frontier in 'omics'. *Trends in Biotechnology* **28***,* 281-290 (2010).